^{90}Nb: potential radionuclide for application in *immuno*-PET. Development of appropriate production strategy and first *in vivo* evaluation of ^{90}Nb-labeled monoclonal antibody.

zur Erlangung des Grades
„Doktor der Naturwissenschaften“
im Promotionsfach Chemie

am Fachbereich Chemie, Pharmazie und Geowissenschaften
der Johannes Gutenberg-Universität Mainz

Valery Radchenko
geb. in Penzenskaya obl.
Mainz 2013

To my mother, my wife and my son

Abstract

Nuclear medicine is a modern and highly effective tool for the detection and treatment of oncological disease. Molecular imaging based on radiotracers includes single photon emission tomography (SPECT) and positron emission tomography (PET), which provide non-invasive tumor visualization on nano- and picomolar level, respectively.

Currently, many novel tracers for more precise discovery of small tumors and metastases have been introduced and are under investigation. Many of them are protein-based biomolecules which nature herself produces as antigens for the eradication of tumor cells. Antibodies and antibody fragments play an important role in tumor diagnostis and treatment. PET imaging with antibodies and antibody fragments is called *immuno*-PET. The main issue that needs to be addressed is that appropriate radiotracers with half-lives related to the half-lives of biomolecules are needed.

The development of novel radiotracers is a multistep, complicated task. This task includes the evaluation of production, separation and labeling strategy for chosen radionuclide. Finally, the biomolecule-radionuclide complex should be stable in time. An equally important factor is the economic suitability of the production strategy, which will lead to a key decision for future application of the developed radionuclide.

In recent work, ^{90}Nb has been proposed as a potential candidate for application in *immuno*-PET. Its half-life of 14.6 hours is suitable for application with antibody fragments and some intact antibodies. ^{90}Nb has a relatively high positron branching of 53% and an optimal energy of β^+ emission of 0.35 MeV that can provide high quality of imaging with low dose of used radionuclide.

First proof-of-principle studies have shown that ^{90}Nb: i) can be produced in sufficient amount and purity by proton bombardment of natural zirconium target ii) can be isolated from target material with appropriate radiochemical purity iii) may be used for labeling of monoclonal antibody (Rituximab) iv) provides high *in vitro* stability. An alternative rapid separation strategy was developed, which provided a source of ^{90}Nb within one hour, with appropriated radiochemical and radionuclidic purity for subsequent labeling of biomolecules. Finally, for the first time ^{90}Nb labeled biomolecules were investigated *in vivo*. Further, experiments on searching of optimal bifunctional chelating (BFC) agents were conducted. Several common BFC were examined on complex formation with Nb^V. Desferrioxamine (Df) was found to be the most appropriate chelator for ^{90}Nb. The monoclonal antibody bevacizumab (Avastin®) was labeled with ^{90}Nb and biodistribution study and PET imaging was conducted. All these results proved that ^{90}Nb is a potential radionuclide for *immuno*-PET, and may even be further commercially applied for clinical usage.

Kurzzusammenfassung

Die Nuklearmedizin ist ein modernes und effektives Werkzeug zur Erkennung und Behandlung von onkologischen Erkrankungen. Molekulare Bildgebung, die auf dem Einsatz von Radiopharmaka basiert, beinhaltet die Einzel-Photonen-Emissions-Tomographie (SPECT) und Positronenemissionstomographie (PET) und ermöglicht die nicht-invasive Visualisierung von Tumoren auf nano-und picomolarer Ebene.

Derzeit werden viele neue Tracer für die genauere Lokalisierung von kleinen Tumoren und Metastasen eingeführt und hinsichtlich ihrer Eignung untersucht. Die meisten von ihnen sind Protein-basierte Biomoleküle, die die Natur selbst als Antigene für die Tumorzellen produziert. Dabei spielen Antikörper und Antikörper-Fragmente eine wichtige Rolle in der Tumor-Diagnostik und Behandlung. Die PET-Bildgebung mit Antikörpern und Antikörperfragmenten bezeichnet man als *immuno*-PET. Ein wichtiger Aspekt hierbei ist, dass entsprechende Radiopharmaka benötigt werden, deren Halbwertszeit mit der Halbwertszeit der Biomoleküle korreliert ist.

In neueren Arbeiten wird ^{90}Nb als potenzieller Kandidat für die Anwendung in der *immuno*-PET vorgeschlagen. Seine Halbwertszeit von 14,6 Stunden ist geeignet für die Anwendung mit Antikörperfragmenten und einige intakten Antikörpern. ^{90}Nb hat eine relativ hohen Anteil an Positronenemission von 53% und eine optimale Energie für die β^+-Emission von 0,35 MeV, die sowohl eine hohe Qualität der Bildgebung als auch eine niedrige Aktivitätsmenge des Radionuklids ermöglicht.

Ersten grundlegende Untersuchungen zeigten: i) dass ^{90}Nb in ausreichender Menge und Reinheit durch Protonen-Bombardierung des natürlichen Zirkonium Targets produziert, ii) aus dem Targetmaterial in entsprechender radiochemischer Reinheit isoliert und iii) zur Markierung des monoklonalen Antikörpers (Rituximab) verwendet werden kann und iv) dieser ^{90}Nb-markierte mAb eine hohe *in vitro* Stabilität besitzt. Desweiteren wurde eine alternative und schnelle Abtrennungsmethode entwickelt, die es erlaubt ^{90}Nb, mit einer geeigneten radiochemischen und radionuklidischen Reinheit für eine anschließende Markierung von Biomolekülen in einer Stunde zu aufzureinigen. Schließlich wurden erstmals ^{90}Nb-markierte Biomolekülen *in vivo* untersucht. Desweiteren wurden auch Experimente durchgeführt, um den optimalen bifunktionellen Chelatbildner (BFC) für ^{90}Niob zu finden. Mehrere BFC wurden hinsichtlich Komplexbildung mit Nb^V untersucht. Desferrioxamin (Df) erwies sich als geeignetster Chelator für ^{90}Nb. Der monoklonale Antikörper Bevacizumab (Avastin®) wurde mit ^{90}Nb markiert und eine Biodistributionsstudie und eine PET-Untersuchung durchgeführt. Alle diese Ergebnisse zeigten, dass ^{90}Nb ein vielversprechendes Radionuklid für die Immuno-PET ist, welches sogar für weitere kommerzielle Anwendungen in der klinischen Routine geeignet zu sein scheint.

Contents

1. Introduction

Cancer today has the leading position in death cases on disease lists all over the world [1]. Statistical data showed that the global burden of cancer has more than doubled during the past 30 years [2]. In 2008, it was estimated that there were over 12 million new cases of cancer diagnosed, 7 million deaths from cancer and 25 million persons alive with cancer. The continued growth and ageing of the world's population will greatly affect the cancer burden. By 2030, it could be expected that there will be 27 million incident cases of cancer, 17 million cancer deaths annually and 75 million persons alive with cancer within five years of diagnosis.

An important factor is also the survival percentage of cancer patients which is also increasing year by year thanks to progress of treatment strategies [3]. The improvement in survival reflects both progress in diagnosing certain cancers at an earlier stage and improvements in treatment. In the US, the 5-year relative survival rate for all cancers diagnosed between 2001 and 2007 is 67%, up from 49% in 1975-1977 [4]. However, rapid cancer evolution gives an urgent need for novel more effective treatment procedures.

There are currently two fields for cancer treatment: diagnosis and therapy. Diagnosis is very important part of tumor handling due to estimation of tumor location and tumor size which allow for further therapy planning and performing with minimal amount of healthy tissue being affecting. Molecular imaging is recently the most convenient technique for precise tumor visualization [5].

1.1 Molecular imaging

The main advantage of molecular imaging (MI) is *in vivo* visualization and quantification of biological processes on a cellular and subcellular level in living subjects [6, 7]. This means that processes can be detected online and kinetics can be evaluated at different time points. This is not achievable by other techniques such as microscopy methods (histopathological and cytological), which can require chemical fixation of removed tissues and involve the observation of biological samples under conditions which are not physiological.

There are three components required for the MI techniques to provide high contrast image of the selected object: i) a specific "sensor" probe which allows visualization of targeted molecules ii) a selective targeting molecule which has maximal capacity to the targeting vector iii) the formation of a stable complex between the specific probe and the target molecule.

Several MI techniques based on various mechanisms have been evaluated for tumor diagnosis, over the past decades [8-11]:

- *Optical imaging (OI)*. Light generated from within an intact organism as a result of a biologic reaction or physical process can be used to produce an image. Optical techniques exploit absorption, emission, reflectance, scattering and fluorescense as the source of contrast, but it is fluorescence and luminescence that primarily support *in vivo* studies.
- *Ultrasound (US).* Ultrasound produces sound waves that are beamed into the body causing return echoes that are recorded to "visualize" structures beneath the skin. The ability to measure different echoes reflected from a variety of tissues allows a shadow picture to be constructed. The technology is especially accurate at seeing the interface between solid and fluid filled spaces.
- *Computed Tomography (CT)* that uses special x-ray equipment to obtain cross-sectional pictures of the body.
- *Magnetic resonance Imaging (MRI)* uses the magnetic properties of hydrogen and its interaction with both a large external magnetic field and radio waves.
- Single photon emission tomography (SPECT) and Positron emission tomography (PET) utilize radioactive probes which emit photons and positrons respectively as the radiotracer.

There are also several combined imaging techniques are available, such as PET/MRI, PET/SPECT and most commonly PET/CT [12, 13]. The main goal of combined imaging techniques is using the advantage of each technique while “masking” the disadvantages of the other technique.

Several important criteria relevant to tumor imaging are required for molecular imaging techniques:

i) spatial resolution, ii) penetration depth iii) target specific imaging iv) imaging time v) clinical translation and vi) cost of the procedure

In Figure 1 a comparison of the most common molecular imaging techniques is presented.

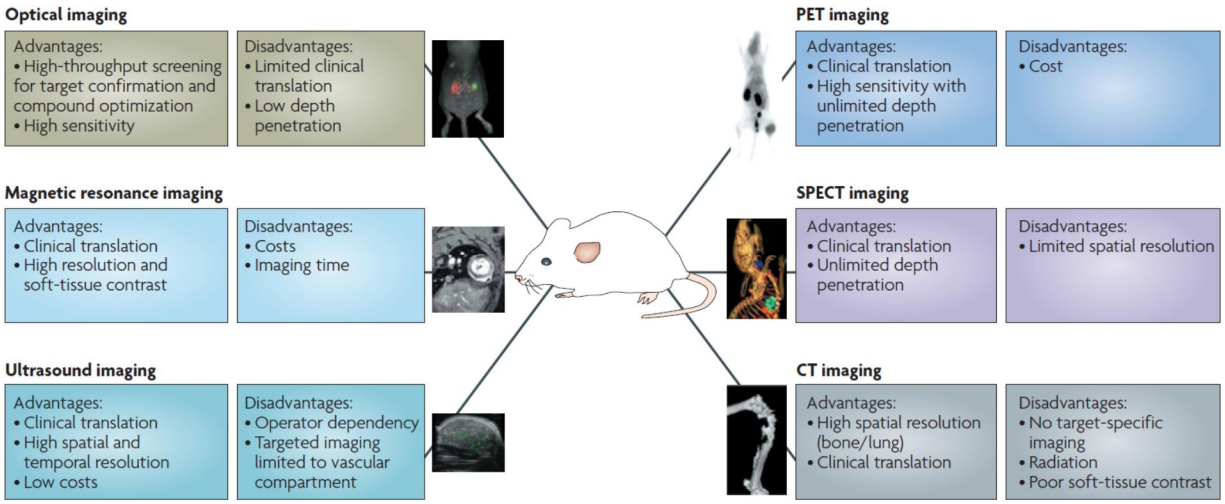

Figure 1: Advantages and limitations of most used molecular imaging techniques [5].

Currently, there is no imaging technique which can be ideally suitable for tumor visualization. Each technique has as advantages as well disadvantages as can be seen in Figure 1. However, among these imaging modalities PET and SPECT agents could provide target specific information as well as function, pathway activities, and cell migration in the intact organism. Furthermore, the radiotracer could noninvasively assess diseases treatment endpoints which used to rely almost exclusively on biopsies and histopathological assays. Finally, PET has higher spatial resolution in comparison to SPECT, thus allowing for more precise tumor localization with a lower dose of injected compound [13].

Two major applications of molecular imaging nowadays in cancer care can be noted.

Personalized medicine is new model of world medicine that proposes the customization of healthcare - with medical decisions, practices, and/or products being tailored to the individual patient information (such as the use of genetic or other data) [14, 15]. This practically means that each patient will be provided with the individual treatment plan dependent on his/her organism features.

In the personalized medicine model of cancer care, molecular imaging will play key role. Molecular imaging can provide information on tumor type, location, size for each individual patient. Also by MI, drug response of each single patient can be measured. Based on this data, a therapy program can be planned, tailored to needs of each patient with minimal injury to other healthy tissues.

The advantage of radioactive probes is the realization of the Theranostic concept [16-18]. The key idea of this concept is that each patient will undergo scanning with a drug or imaging agent coupled to a diagnostic radionuclide which provides information about his/her response to the drug, as well as tumor

uptake dose. Furthermore an individual therapy program based on these data can be prepared in each particular case. Therapy can then be performed by exchanging the diagnostic radionuclide with a therapeutic radionuclide bearing the same drug or imaging agent which will deliver in advance calculated dose of therapeutic radionuclide to the tumor with minimal effect on healthy tissues.

After therapy, additional scanning with a diagnostic radionuclide should be performed to obtained information about therapy response and future treatment prognosis. Theranostic in contrast with cancer chemotherapy, which in evolution from non-specific cytotoxic drugs damage tumor as well as normal cells, turns to more specific agents and immunotherapy approaches.

Another important application of molecular imaging is novel drug investigation, which allows for a dramatically reduced evaluation period, from several decades to several years [19, 20]. The drug development process is a long term, risky and costly process as can be seen in Figure 2.

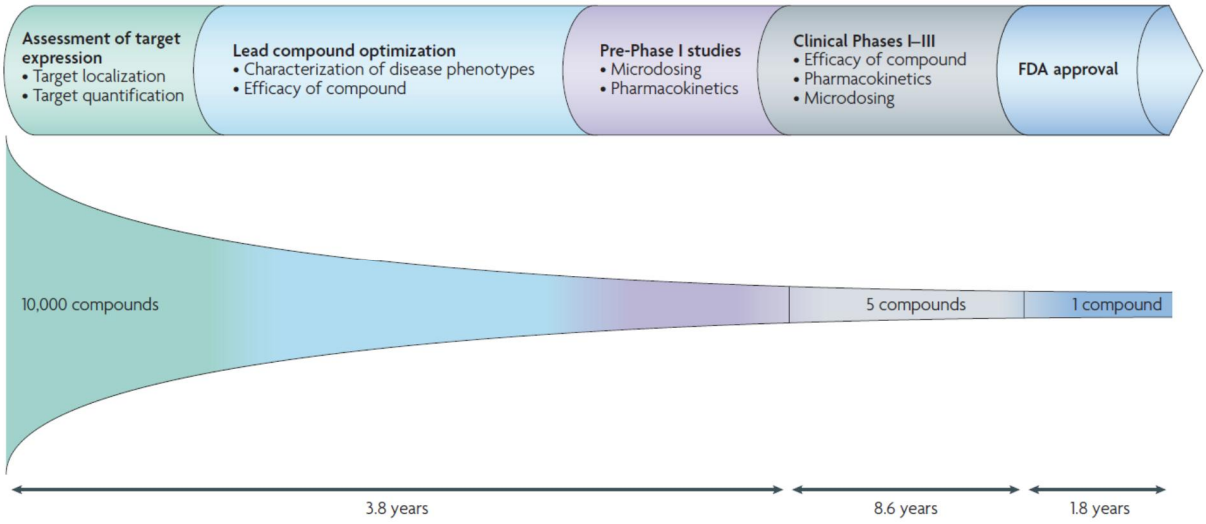

Figure 2: Time scale and procedures for novel drug development [5].

Although the specifics and duration of each step depends on the target indication as well as the drug class, in general, clinical development (from investigational new drug (IND) filing to regulatory approval) takes more than decade. Attrition rates are high, statistically from 10.000 compounds just one will be FDA approved. Moreover, despite dramatically increased investment, the rate of introduction of novel drugs has remained relatively constant over the past 30 years, with only two to three agents in new drug classes per year eventually making it to the market. Indeed, the estimated cost of bringing a new potential drug

to the end of Phase III trials has increased approximately 2.5-fold between 1991 and 2001, from US$318 million to $802 million [21]. Assuming a similar cost growth rate, the costs for a new approved drug in 2013 would be $1.9 billion. As pivotal trials involve the greatest time, patient exposure and cost , new strategies that aid the early selection of promising candidates to move to pivotal trials, or termination of candidates that are unlikely to be successful, could significantly improve the overall drug development process. Molecular imaging applied in the initial stages of drug development can provide evidence of biological activity, confirm on-target drug effects and identify patients who are more likely to benefit. So, there are considerable expectations that investments in molecular imaging technology will enhance drug development.

1.2 Positron emission tomography (PET)

Positron emission tomography is non-invasive molecular imaging technique which provides *in vivo* biochemical and physiological process quantification at picomolar (10^{-12} M) level of concentrations.

PET is widely involved in routine clinical routine use, in fields such as cancer diagnosis and management, cardiology and cardiac surgery, neurology and psychiatry [22].

PET imaging is primary based mostly on two components: the positron emitting radionuclide, which allows visualization of the studied object, and the targeting molecule, which provides connection of the radionuclide with the target (in the case of cancer, with the tumor cell). The imaging principle is based on the annihilation of a positron which is emitted by neutron-deficient radionuclides (Figure 3). After its emission, the positron travels a certain distance (typically 0.5 -2.4 mm) before meeting an electron. Due to the fact that the positron is an antiparticle of the electron after collision they briefly (10^{-7} s) form a positronium particle and further annihilate, with the emission of two gamma quanta which fly in opposite directions (at an angle of 180°) with an energy of 511 KeV of each. These two gamma quanta can be registered by detectors and the point of annihilation can be later reconstructed by computed modulation.

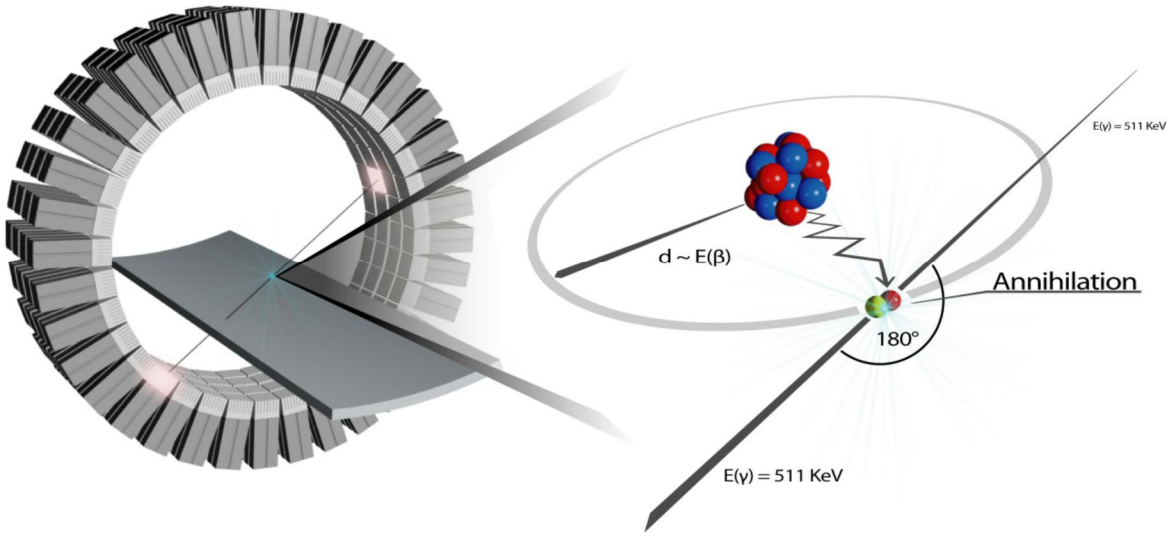

Figure 3: Schematically installation of positron emission tomography (PET)[23].

There is a number of positron emitting radionuclides which is used in the daily clinical practice (Table 1). Several crucial factors and characteristics apply to radionuclide candidates for PET imaging. The most important ones are: i) a physical half-life paralleling the biological half-life of the labeled molecule, ii) a high positron branching with no or weak accompanying radiation (β^-, γ) to offer high-sensitive PET imaging while reducing the radiation burden of the patient, iii) a preferably low β^+-energy to allow high-resolution PET imaging; and iv) the availability of the radionuclide, i. e. an efficient production and radiochemical separation route.

Table 1: Several common radionuclides for clinical PET (ordered by half-lives) [24, 25].

Radionuclide	$T_{1/2,}$ min	β^+ yield, %	Mean β^+ energy, MeV	Max β^+ energy, MeV	Other accompanying emissions
^{18}F	109.8	96.7	0.249	0.634	AE, XR*
^{68}Ga	67.7	88.9	0.830	1.899	AE, CE, XR, γ
^{11}C	20.4	99.8	0.386	0.960	AE, XR
^{13}N	10.0	99.8	0.482	1.199	AE, XR
^{15}O	2.04	99.9	0.735	1.732	AE, XR

** AE: Auger electrons, CE: Conversion electrons, XR: X-rays, γ: γ-rays*

More than 90% of the current clinical PET scans in oncology are performed with 2-deoxy-2-(^{18}F)fluoro-D-glucose (^{18}F-FDG) which is a radiolabelled sugar (glucose) molecule [26]. Imaging with ^{18}F-FDG PET is used to determine sites of abnormal glucose metabolism and can be used to characterize and localize many types of tumors. However, not all tumors show high ^{18}F-FDG uptake and high glucose use is not a process specific to cancers; in particular, inflammatory processes can give rise to false-positive FDG-PET scans. In addition, although ^{18}F-FDG uptake can correlate with the aggressiveness of some tumors, it reveals little about the molecular phenotype of the tumor. Therefore, more tumor specific molecules have been investigated and are currently under investigation.

Peptides are short chains of amino acid monomers linked by peptide (amide) bonds containing approximately 50 amino acids or less. The biological action of peptides is mediated upon binding with high affinity to specific receptors [27, 28]. Many of these receptors are massively overexpressed in numerous cancers, compared to their relatively low density in physiological organs. This became the molecular basis for the development of radiolabelled peptides as radiopharmaceuticals for tumor imaging and therapy.

One of common example of peptide-based radiopharmaceuticals is the somatostatin analogue DOTA^{0}-Phe^{1}-Tyr^{3}-octreotide (DOTATOC) labeled with ^{68}Ga (Figure 4) or ^{90}Y for endocrine tumor diagnosis and therapy, respectively [29].

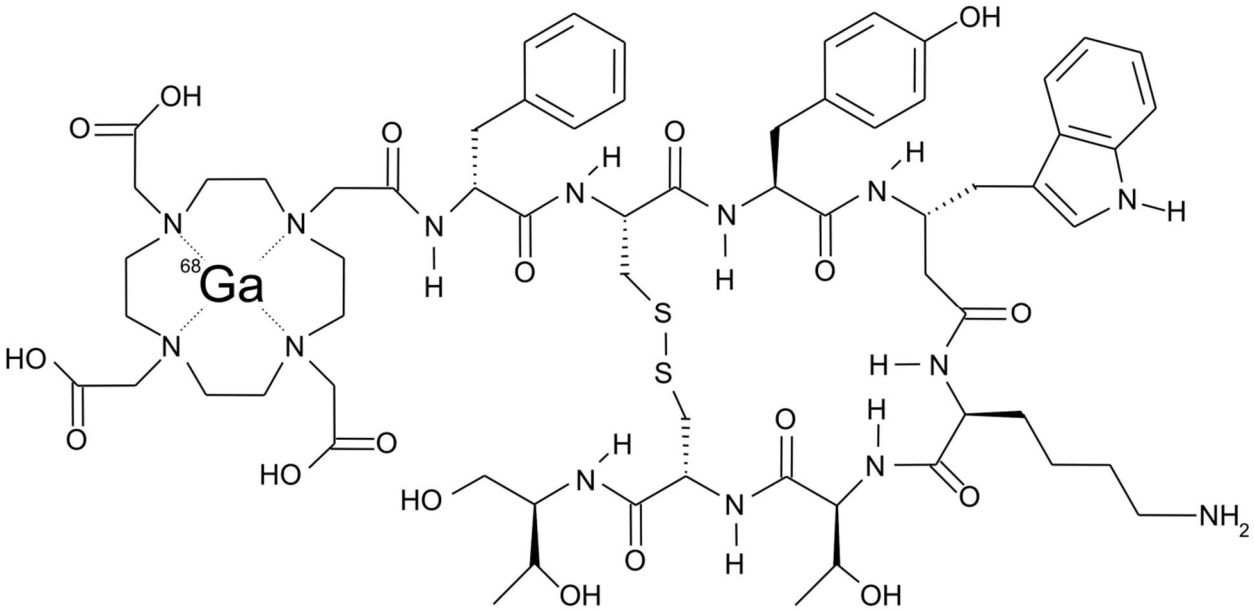

Figure 4: Chemical structure of ^{68}Ga-DOTA(0)-Phe(1)-Tyr(3)-octreotide.

Another group of biomolecules applied for specific tumor diagnosis are antibodies and their engineered fragments. This direction of molecular imaging called *immuno*-PET.

1.2.1 *Immuno*-PET

Immuno-PET is a branch of PET imaging which rapidly evolving in the last decade, and is based on the labeling of biomolecules, such as antibodies and antibody fragments, with positron emission radionuclides for selective tumor imaging [30-32]. Antibodies are large Y-shaped proteins. They are produced by the immune system to identify and neutralize foreign objects like bacteria and viruses. A variety of antibodies and antibody fragments (Figure 5) for tumor targeting is currently under preclinical investigation. Although a rather low number of all developed antibodies manage to make it to the clinic

worldwide, more than 20 different antibodies are approved by the US Food and Drug Administration today [33].

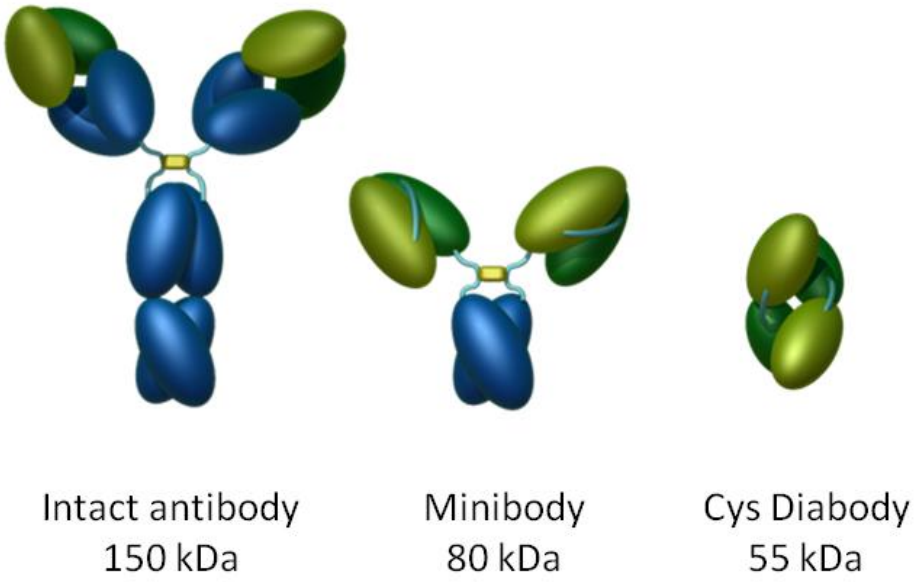

Figure 5: Domain composition of engineered fragments compared with intact antibody (adopted from [32]).

Those targeting vectors enable a very precise visualization of tumors at earlier stages and at later stages, and metastases can be comprehensively detected. Standard PET radionuclides such as ^{18}F ($T_{1/2}$ = 110 min), ^{15}O ($T_{1/2}$ = 2.04 min) and ^{11}C ($T_{1/2}$ = 20.4 min) are practically useless for applications in *immuno*-PET because of the slow pharmacokinetics of monoclonal antibodies and antibody fragments, which can last for several days (unless pretargeting concepts are established).

Consequently, positron-emitting radionuclides should be chosen according to the biological half-life of the biomolecules (Table 2). Recently, several radioisotopes with long half-lives have become commercially available and have been introduced in the clinic such as ^{89}Zr ($T_{1/2}$ = 78.4 h) [34, 35] and ^{124}I ($T_{1/2}$ = 100.2 h) [36].

For engineered antibody fragments the molecular weight is lower and correspondingly, the kinetics for tumor accumulation is faster. Thus, radionuclides with long half-lives would create an extra dose burden for patients. Therefore, nuclides with intermediate half-lives (from several hours up to one day) would better correlate with the time necessary for achieving optimal imaging conditions.

Accordingly, positron emitters such as ^{64}Cu ($T_{1/2}$ = 12.7 h) [37, 38], ^{86}Y ($T_{1/2}$ = 14.7 h) [39, 40] and ^{76}Br ($T_{1/2}$ = 16.2 h) [41] have been investigated, with ^{86}Y and ^{64}Cu becoming used even for human application.

Table 2: Several promising radionuclides for application in immuno-PET [24, 25].

Radionuclide	$T_{1/2}$, h	β^+ yield, %	Mean β^+ energy, MeV	Max. β^+ energy, MeV	Other emissions
^{64}Cu	12.7	17.6	0.278	0.653	β^-, AE, XR*
^{86}Y	14.7	31.9	0.213	3.141	AE, CE, XR, γ
^{90}Nb	14.6	53.0	0.340	1.500	AE, CE, XR, γ
^{76}Br	16.2	55.0	0.641	3.941	AE, XR, γ
^{89}Zr	78.4	22.4	0.396	0.902	AE, XR, γ
^{124}I	100.2	22.7	0.187	2.138	AE, CE, XR, γ

AE: Auger electrons, CE: conversion electrons, XR: X-rays, γ: γ-rays

Development and industrial translation of novel radionuclides for molecular imaging is a always complicated multistep procedure, involving several scientific fields such as nuclear physics (for development of production strategy), material construction (for target design), nuclear and inorganic chemistry (for target separation), organic chemistry and biochemistry (for evaluation of labeling procedure) [42]. An Important factor for future clinical application of novel radionuclide is also its cost.
Several important requirements should be met for the production of non-standard PET radionuclides for further commercial application and clinical translation [43, 44]:

- Decay characteristics
- Cost effective production strategy by small or intermediate cyclotrons preferably from not enriched target materials, or by use of radionuclide generator system
- Cost-effective, fast separation strategies which allow remote and automated separation processes
- Simple and fast labeling procedures, which include conjugation via the appropriate bifunctional chelator for metallic radionuclides

In some cases, due to the uniqueness of the radionuclides (decay characteristic, matching with diagnostic or therapeutic analogue, radionuclide generator system availability) some of above criteria can be disregarded.

1.3 Production of non-standard PET radionuclides

There are several ways for production of neutron-deficient radionuclides, by irradiation with protons, deuterons, ^{3}He and α particle [45, 46]. In Figure 6 different routes for production of ^{124}I are presented.
Due to the limited number of ^{3}He and α particle accelerators and also to the low production yield by these reactions, currently the most common method is irradiation with protons at small cyclotrons with low energy (up to 20 MeV) as well as generator -based systems [47, 48]. Thus the production of radionuclides is "in house" i.e. at small cyclotrons available near clinics and by generator systems providing cyclotron-independent source of radionuclides. Several important parameters characterize targets for cyclotron production of non-standard PET radionuclides, such as:
Target material. Different material states for irradiation can be applied; most widely used and the safest is the application of a solid target. A solid target is also usually easier for preparation. However, in several cases the application of a gas and liquid target is necessary, and provides a more effective production yield. An important factor is also the natural abundance of the target material. For example, for production of ^{64}Cu, the irradiation with protons and deuterons is most convenient production strategy (^{64}Ni (p, n)^{64}Cu or ^{64}Ni(d, 2n)^{64}Cu). However, the natural isotopic composition of Ni is 0.93% in ^{64}Ni, for the isotopes values are ^{58}Ni (68.07%), ^{60}Ni (26.2%), ^{61}Ni (1.139%) and ^{62}Ni (3.63%) [23]. Therefore, during proton bombardment of natural Ni target, other reactions ^{58}Ni(p, n)^{58}Cu, ^{60}Ni(p, n)^{60}Cu will be occur as well. This will produce strong contamination of final ^{64}Cu product with other Cu radioisotopes which can

create additional dose burden for the patients and personnel and sufficiently decrease quality of imaging. To reduce contamination of other Cu radioisotopes enriched on ^{64}Ni (up to 99.9%) can be applied. This will reduce coproduction of other radionuclides but will also increase the production cost due to the high cost of the enriched material. Another example of natural abundance of target material can be found with the production of ^{89}Zr, whereas target material for ^{89}Y(p, n)^{89}Zr, a natural yttrium target with 100% of natural abundance can be applied without significant contamination with other Zr radioisotopes.

Irradiation parameters. Several important characteristics are applied for the determination of optimal irradiation parameters. First, a nuclear reaction is characterized by a cross section, a geometrical quantity given in barn (10^{-24}cm^2), describing the probability that a particle, with a beam intensity of 1 particle per 1 cm^2, and an incident on 1 target nucleus will lead to a specific physical process, where the incident particle, target nucleus, reaction channel and the final nucleus are exactly specified.

Other parameters affecting the production yields of radionuclides are: i) Energy of protons or deuterons, usually in MeV ii) proton beam intensity, usually in μA and iii) time of irradiation, usually in hours. Finally, determination of optimal parameters provide thickness of target material: A thin target has a thickness so small that the reaction cross section can be considered as constant through the whole target. This is equivalent to the energy loss being negligible when compared to the energy range needed to see significant changes in the reaction cross section. A thick target has its thickness comparable or larger than the range of the incident particle in the target material. The production yield can be then presented as the amount of activity (MBq) that can be produced at a defined energy per one μA for 1 hour irradiation time.

In Figure 6, a graph showing the dependence of the cross section on proton energy is presented for reactions of ^{124}Te(p, n)^{124}I and ^{124}Te(p, 2n)^{123}I [49]. For a thin target, the maximal production yield for ^{124}I will occur at an energy range of 10 to 15 MeV, however starting from approx. 12 MeV, a coproduction of ^{123}I will be observed. Therefore an optimal decision will be to perform the irradiation at a range of up to 12 Mev to prevent contamination of ^{124}I.

There are also some limitations for irradiation parameters, depending on the target material. Some cyclotrons can apply proton intensity up to several hundred μA, thus providing the opportunity to produce a high amount of activity for a shorter irradiation time. However, the melting point of the target material should be taken into account. An increase in current will create additional heating on the target surface, which a cooling system is called to reduce. Some target materials have a melting point below several hundred C°, which can limit production yield or increase irradiation time by restriction of proton intensity.

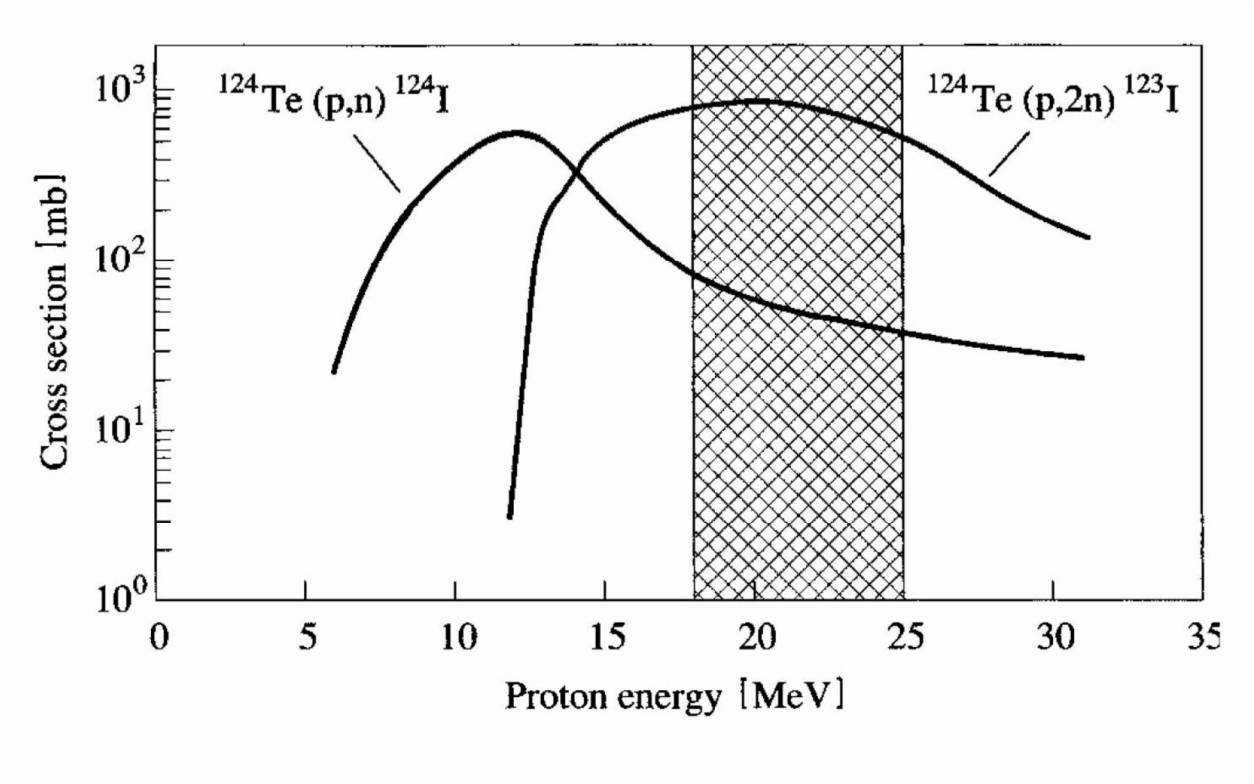

Figure 6: Cross section for production of ^{124}I and ^{123}I via proton irradiation of ^{124}Te [49].

Generator based systems are a source of PET radionulicdes independent from a cyclotron. The principle idea is that the parent radionuclide (with a "long" half-life) fixed onto a matrix, decays to the daughter PET radionuclide with a short or intermediate half-life, which can be eluted from the matrix and applied for imaging. The parent radionuclide is usually produced by long-term proton irradiation with intermediate (up to 30 Mev) and high energies (up to 100 MeV). For example, for the ^{44}Ti/^{44}Sc generator system the most convenient way to produce the parent ^{44}Ti ($T_{1/2}$ = 60 a) is the ^{45}Sc(p,2n)^{44}Ti reaction, with a maximum cross section at 22 – 25 MeV and an estimated production yield of ^{44}Ti is 2 – 3 kBq/µAh [50]. This practically means that to obtain generator relevant activity of parent radionuclide of several hundred MBq, the irradiation should be performed at a proton energy of approx. 30 MeV with a current of 10-30 µA (which cannot be increased, due to thermal instability of the target material) for several hundred hours (one week). In this way, a long-term source of ^{44}Sc can be produced [51, 52]. Unfortunately there are not so many generator systems relevant for the purposes of *immuno*-PET, which is mostly the short half-lives of the produced radionuclides (less than 1 hour).

In table 3 several (relevant to *immuno*-PET) generator systems are presented.

Table 3: Relevant to immuno-PET radionuclide generator systems [24, 25].

Generator system	Parent $T_{1/2}$	Daughter $T_{1/2}$	β^+ yield, %	Mean. β+ energy, MeV	Max. β+ energy, MeV	Other irradiation
$^{68}Ge/^{68}Ga$	270.8 d	67.7 min	88.9	0.830	1.899	AE, CE, XR*, γ
$^{44}Ti/^{44}Sc$	60.0 a	3.97 h	94.0	0.632	1.473	AE, CE, XR*, γ
$^{86}Zr/^{86}Y$	16.5 h	14.6 h	31.9	0.213	3.141	AE, CE, XR*, γ
$^{72}Se/^{72}As$	8.4 d	26.0 h	87.8	1.026	3.334	AE, CE, XR*, γ

AE: Auger electrons, CE: conversion electrons, XR: X-rays, γ: γ-rays

1.4 Separation and purification of non-standard PET radionuclides

After irradiation the radionuclide should be separated from the target material. A variety of standard separation techniques can be applied [53-55]. An important distinctive feature of radiochemical separation is that a micro amount of product in the no-carrier added state should be isolated from a macro amount of target material. Practically, this means that grams/milligrams of target material should be reduced in final fractions to the level of no-carrier added product radionuclide, usually nanograms (10^{-9} g).

The aim of the separation strategy is not just to isolate target material, but also to provide isolation of other simultaneously produced radionuclides and provide a source of final radionuclide appropriate for future labeling procedures.

Therefore, combinations of several separation techniques are usually applied [56]. During the first step of separation, a crude separation of the target material is performed. During the second step, a gentle separation follows, allowing additional separation and preconditioning of the radionuclide for further labeling.

Target dissolution. Dissolution of the target material is a very important step, which defines the success of the separation. Depending on the target material, there is some limitation to the dissolution procedure [57]. In the case of a solid target material, usually aggressive acids such as hydrofluoric, hydrochloric, nitric or even sometimes their mixtures should be applied. Main demands for dissolution procedure are: short dissolution time, fully dissolution, not precipitation formation and possibility of automation and remote control. In case of enriched target material very important take into account necessity recovery of the material after each separation. Important also possibly decrease losses of target material during the dissolution and separation. Usually, enriched target material is a powder of salt or oxide of element and some difficulties with target design to provide sufficient cooling during irradiation and later handling of the material should be solved. Sometimes for good thermo conductivity of the target during irradiation electroplating strategy can be applied. Thin layer of enriched target material is coated by electrolysis surface of base plate with good thermo conductivity and different chemical proprieties. Later, after irradiation dissolution procedure should be chosen that thin layer of target material will dissolve while base plate remains unsolved.

Crude separation. Usually crude separation step allow isolation of bulk amount of the target material [58]. In case grams amount of target material wet separation techniques such as precipitation and extraction and chromatographically techniques are applied. In case of precipitation important find a reagent which allows precipitation of bulk amount of target while no carrier added product will remain into solution. In case of extraction appropriate extractant should be selected to no carrier product move to the organic phase while macro amount of target remain into the aqueous phase. Often precipitation and extraction steps repeated several times to obtain more fully target isolation. In some cases when the mass of target material limited of several grams ion exchange chromatography can be applied and more preferable. Chromatographically methods usually, can provide more accurate and selective separation in compare with wet chemistry methods. However, appropriate conditions to remain product on the ion exchange matrix and target material passed through should be selected. Sometimes opposite way conditions just possible to separate no-carrier added product from irradiated target material, then target material remains on the matrix and product passed through. However disadvantage of this strategy that appropriate amount of exchange matrix with capacity for whole target material to avoid breakthrough should be taken.

Gentle separation. By the second separation step additional separation from the target material and other coproduced no-carrier-added radionuclides should be performed. Also final product should be

presented in appropriate for further labeling condition (volume, media and purity). The second step should remove all tracers of aggressive medias which is not comparable with an animal or human application.

Usually for the final separation step ion exchange chromatography are applied. There is variety of the ion exchange matrix and medias which can be applied for final step. However important is also to adopt second separation strategy from solution obtained after first step, the best option will be direct application of solution from the first step to the second without additional modification. Due to low concentration of target material there is not so important which component will be absorbed on the column and which will be eluted, however more preferably to obtain follow preconditioning of product that product retain on the column and tracers of target material are passed through.

Generator based systems. All above described in this chapter procedure are applicable also and for isolation of parent generator radionuclide from irradiated target material. After purification parent radionuclide should be fixed on the matrix (can be solid or liquid) and condition for elution of daughter radionuclide while keeping parent radionuclide on the matrix should be identified [59]. Several crucial parameters should be fulfilled to successful generator application: i) minimal breakthrough of parent radionuclide. ii) maximal elution of daughter radionuclide iii) eluate contained final product should be in appropriate for radiopharmaceutical application conditions (pH, volume, concentration, media), otherwise post-processing procedure to modify final fraction should be evaluated. iv) daughter radionuclide in the final fraction should be in appropriate condition to further form complex with ligand or be attached to the molecule.

Separation automation and remote control. Important factor which should be taken into account while developing of production and separation procedure is further automation of process [60, 61]. Due to radioactivity for daily clinical application essential term is automation system with remote control to reduce dose burden on the personal. Wet separation techniques such as precipitation and extraction are usually more unprofitable due their bulky performance and necessity precise separation of two phases. Column-based chromatographic methods are more preferable for automation and provide less loss during the automation.

From one hand multiplicity of separation steps provide higher purity of final product but from other hand increase the losses of product especially by automation process (by valves and tubes). Therefore minimal number of separation steps provided maximal decontamination yield are preferable.

The systems automation can be as semi-automated for example by manually regulated inert flow gas pressure or fully automated were all parameters can be programmed and regulation performed automatically (Figure 7).

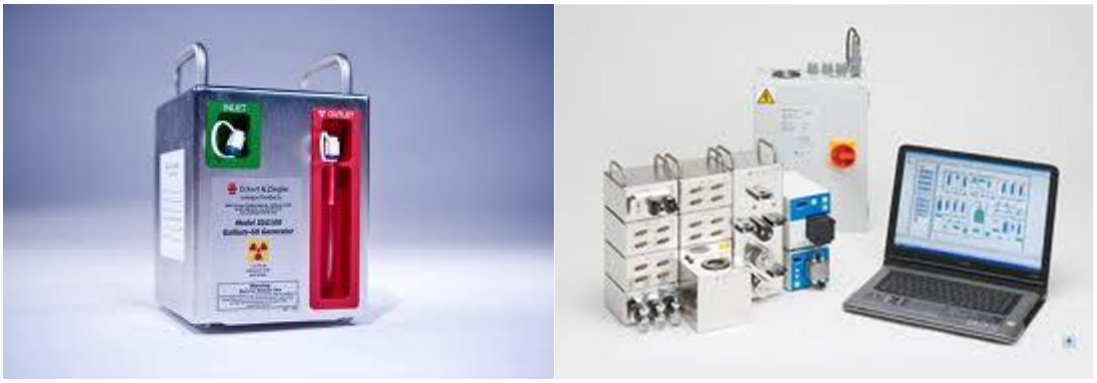

Figure 7: $^{68}Ge/^{68}Ga$ generator (left) and universal automated kit Modular-Lab (right) commercially available by Eckert and Ziegler GmbH (http://www.ezag.com/).

1.5 Labeling strategies of biomolecules for non-standard PET radionuclides

Several strategies involved for coupling radionuclide to the target molecules [62, 63]. For the all strategies several important criteria should be fulfilled.

- Connection between radionuclide and targeting molecule should be stable in living subjects
- Each molecule should contain maximal amount of radionuclide
- Attached radionuclide should not sufficient change the proprieties of the targeting molecule
- Labeling conditions (pH, temperature, media) should be comparable with the targeting molecule

Two main conjugation strategies to attach radionuclides to the targeting molecules can be noted: direct strategy where radionuclide attached to the molecule by exchange of one atom or via linker and the second strategy is by using bifunctional chelator, compound which from one side formed strong complex with radionuclides and from other side can provide a connection formation with targeting molecule.

1.5.1 Direct labeling

Direct labeling is an advantage for organogen and halogens, radioisotopes of these elements can be exchanged by one of the presented atoms in molecule which should be analogue of radionuclide or via linker attached to the labeling molecule [64-66]. Common non-standard nonmetal radionuclides for *immuno*-PET which can be applied for direct labeling are ^{124}I, ^{76}Br and ^{72,74}As.

On the Figure 8 example of labeling for arsenic isotopes via SATA modification are presented [67]. There is also strategy which allow attach *As directly via sulfur bound of antibody, however this can sufficiently change structure and influence on further behavior of biomolecules.

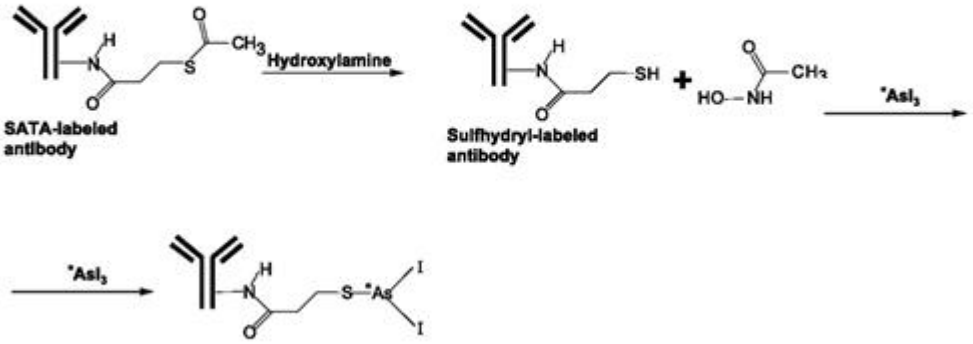

Figure 8: Reaction scheme for the labeling of SATA-modified antibody with radioactive arsenic isotopes [67].

Main advantage of direct labeling strategy is possibility to develop one-step labeling procedure which allows rapid preparation of radiopharmaceticals. Another advantage is that the bond formed between radionuclides and proteins are usually very strong and resistant for transchelation. Further cost and complicity of preparation and purification of bifunctional chelators can be avoided.

Biomolecules such as antibody, antibody fragments and peptides provide several opportunities to attach radionuclides or linkers (Figure 9) [68, 69]:

i) Primary amines ($-NH_2$) are found on lysine residues and the N-terminus. These are abundant and distributed over the entire antibody.

ii) Sulfhydryl groups (–SH) are found on cysteine residues and are formed by selectively reducing disulfide bonds in the hinge region of the antibody.

iii) Carbohydrate residues containing *cis*-diols can be oxidized (–CHO) to create active aldehydes. These are localized to the Fc region on antibodies and are more abundant on polyclonal antibodies.

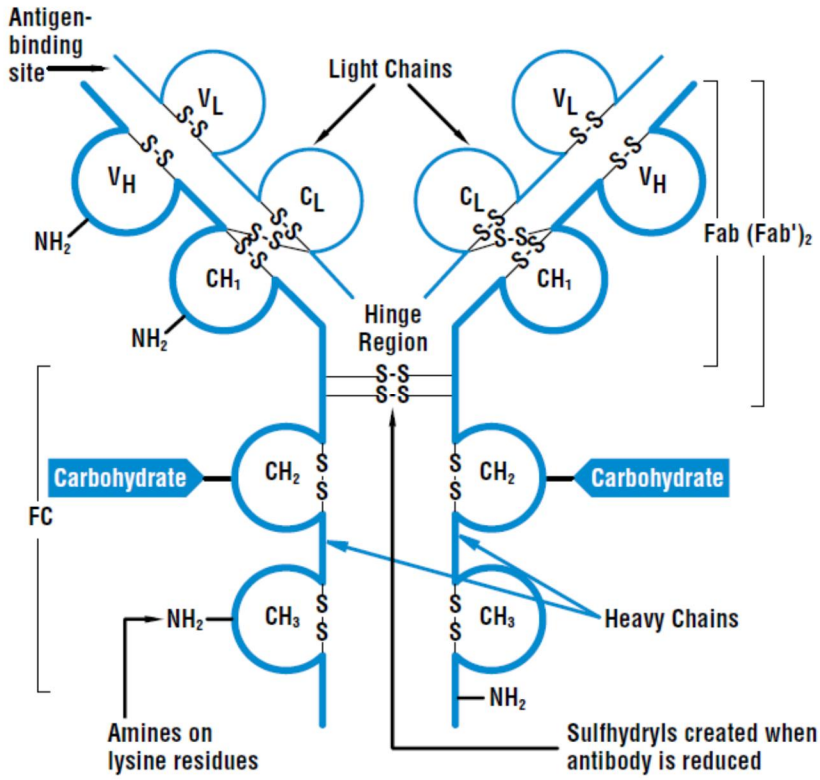

Figure 9: Available groups on antibody for attachments of radionuclides or linkers [68].

1.5.2 Indirect labeling (via bifunctional chelators)

Indirect labeling strategy involved additional step of using bifunctional chelator (BFC) (Figure 10). Indirect labeling of biomolecules is very common for metallic radionuclides, due their foreign to biomolecules nature they should be first "packed" into bifunctional chelate which can be later attached to the biomolecules [70-73]. There is can be different order dependence from labeling strategy, where BFC first

attached to the biomolecule and then radiolabeling are preformed, or BFC first labeled with radionuclide and later attached to the biomolecules.

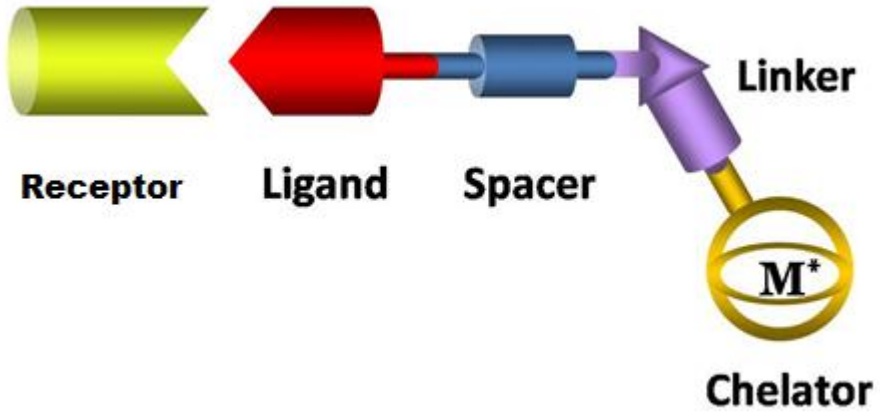

Figure 10: Schematic structure of radiolabeling via BFC bioconjugate (adopted from presentation of Prof. Dr. F. Roesch).

Indeed, both the formation of a kinetically inert metal chelate and the stable covalent attachment of the chelator moiety to the biomolecule are essential to the creation of an effective radiopharmaceutical. To this end, a wide variety of metal-chelating molecules have been synthesized, studied, and, in many cases, made bifunctional to facilitate their conjugation to a biomolecular vector (Figure 11).

Usually, BFC can be divided by two broad classes: Macrocyclic chelators (DOTA, NOTA or TETA) and acyclic chelators (DTPA, EDTA or DFO) [74]. Each has its own unique set of advantages: while macrocyclic chelators typically offer greater kinetic stability, acyclic chelators usually have faster rates of metal binding. Generally, transition metal chelators offer at least four (and usually six or more) coordinating atoms, arrayed in a configuration that suits the preferred geometry of the oxidation state and d-orbital electron configuration of the metal in question.

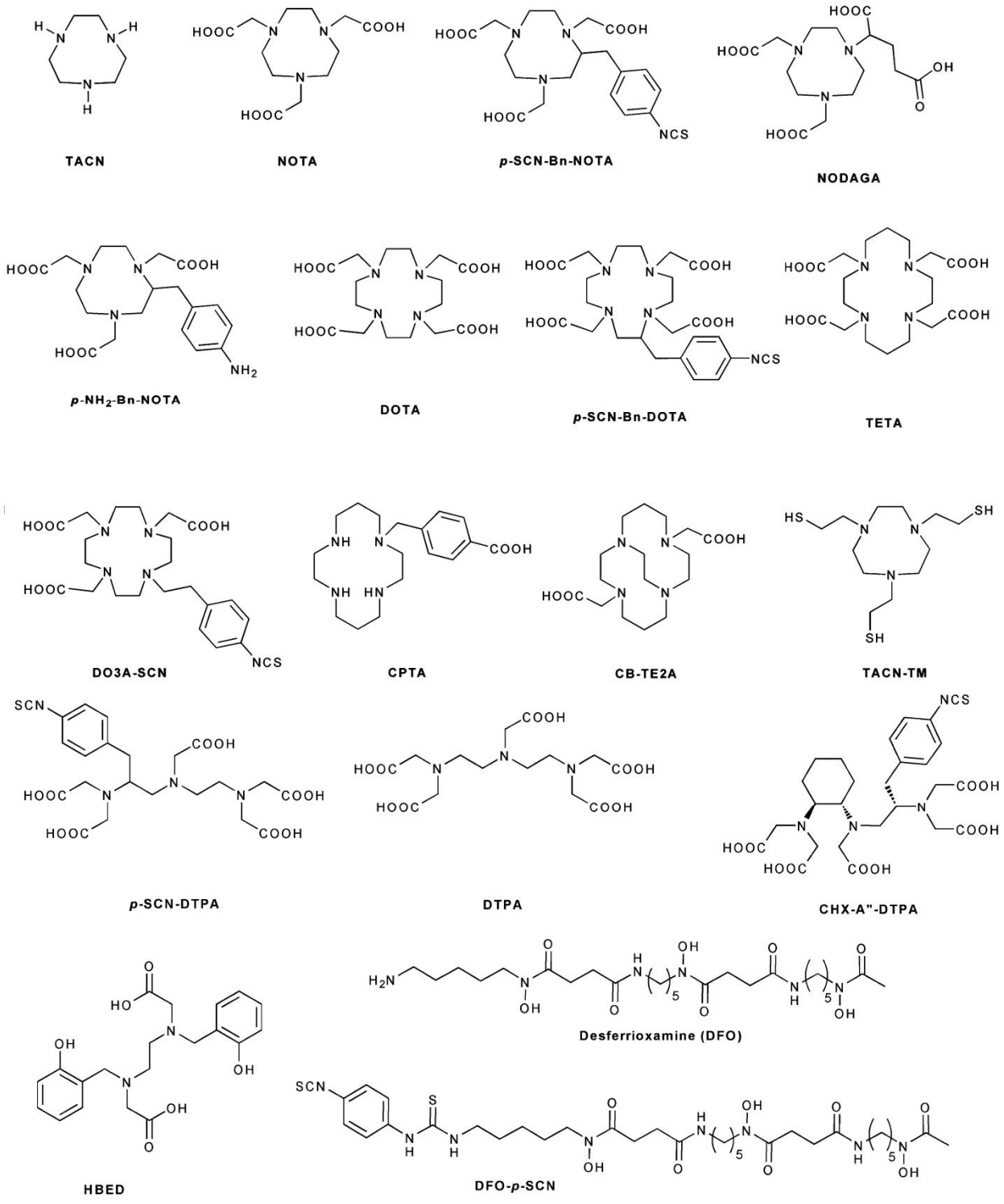

Figure 11: Several common bifunctional chelators for metallic radionuclides [62].

Before choosing appropriate BFC, several important criteria should be taken into account:

- BFC should provide appropriate amount of donor groups for complexation of radiometal
- In case of macrocyclic BFC ionic radius of radiometal should correlate with internal sphere of BFC
- In case of BFC first attached to the biomolecule and then labeled with radiometal, condition for the labeling such as temperature and pH should be suitable for biomolecules
- Time for conjugation of BFC to biomolecules and labeling should be related with the half-life of radionuclide

To couple BFC to the biomolecules using a linker are required. As described above biomolecules cannot provide wide spectrum of spacers. Therefore, linker should be aimed for one of available spacers. Most common spacer is primary amine bond which can provide lasting connection while minimal biomolecule structure changes. Currently, very often applied linker is *p*-isothiocyanatobenzyl (p-Bz-SCN) which can be coupled to DFC (DOTA or DFO) and to other side to -NH_2 group of biomolecules.

1.6 References

1. Global status report on noncommunicable diseases 2010. *World Health Organization* 2011; Geneva
2. Boyle, P., Levin, B. World Cancer Report 2008 *IARC Non serial Publication* 2008; Lyon
3. AACR Cancer Progress Report 2012. *Clin Cancer Res* 2012; 18; 1-100.
4. Siegel, R., DeSantis, C., Virgo, K., Stein, K., Mariotto, A., Smith, T., Cooper, D., Gansler, T., Lerro C., Fedewa, S., Lin, C., Leach, C., Cannady,S. R., Cho, H., Scoppa, S., Hachey, M., Kirch,R., Jemal, A., Ward, E. Cancer treatment and survivorship statistics 2012. *Canc J Clin* 2012; 62(4); 220-241.
5. Willmann, J. K., van Bruggen, N., Dinkelborg, L. M., Gambhir, S. S. Molecular imaging in drug development. *Nat Rev Drug Discov* 2008; 7(7); 591-607.
6. Dzik-Jurasz, A. S. K. Molecular imaging *in vivo*: an introduction. *Brit J Rad* 2003; 76; 98-109.
7. Fass, L. Imaging and cancer: A review. *Mol Oncol* 2008; 2(2); 115-152.
8. Margolis, D. J., Hoffman, J. M., Herfkens, R. J., Jeffrey, R. B., Quon, A., Gambhir, S. S. Molecular imaging techniques in body imaging. *Radiology* 2007; 245(2); 333-356.

9. Meng, Q., Li, Z. Molecular Imaging Probes for Diagnosis and Therapy Evaluation of Breast Cancer. *Int J Biomed Img* 2013, Article ID 230487, 14 pages.

10. Bonekamp, D., Hammoud, D. A., Pomper, M. G. Molecular Imaging, Techniques and Current Clinical Applications *App Radiol* 2010; 39(5); 10-21.

11. Culver, J., Akers, W., Achilefu, S. Multimodality molecular imaging with combined optical and SPECT/PET modalities. *J Nucl Med* 2008; 49(2); 169-172.

12. Cherry, S. R. Multimodality imaging: beyond PET/CT and SPECT/CT. *Semin Nucl Med* 2009; 39(5); 348-353.

13. Mc Ardle, B. A., Dowsley, T. F., deKemp, R. A., Wells, G. A., Beanlands, R. S. Does rubidium-82 PET have superior accuracy to SPECT perfusion imaging for the diagnosis of obstructive coronary disease?: A systematic review and meta-analysis. *J Am Coll Cardiol* 2012; 60(18); 1828-1837.

14. Kircher, M. F., Hricak, H., Larson, S. M. Molecular imaging for personalized cancer care. *Mol Oncol* 2012; 6(2); 182-195.

15. Hricak, H. Oncologic imaging: a guiding hand of personalized cancer care. *Radiology* 2011; 259(3); 633-640.

16. Alberti, C. From molecular imaging in preclinical/clinical oncology to theranostic applications in targeted tumor therapy. *Eur Rev Med Pharmacol Sci* 2012; 16(14); 1925-1933.

17. Rösch, F., Baum, R. P. Generator-based PET radiopharmaceuticals for molecular imaging of tumours: on the way to THERANOSTICS. *Dalton Trans* 2011; 40; 6104-6111.

18. Baum, R. P., Kulkarni H. R. THERANOSTICS: From Molecular Imaging Using Ga-68 Labeled Tracers and PET/CT to Personalized Radionuclide Therapy - The Bad Berka Experience. *Theranostics* 2012; 2(5); 437–447.

19. Willmann, J. K., van Bruggen, N., Dinkelborg, L. M., Gambhir, S. S. Molecular imaging in drug development. *Nat Rev Drug Discov* 2008; 7(7); 591-607.

20. Matthews, P. M., Rabiner, E. A., Passchier, J., Gunn, R. N. Positron emission tomography molecular imaging for drug development. *Br J Clin Pharmacol* 2012; 73(2); 175-186.

21. Di Masi, J. A., Hansen, R. W., Grabowski, H. G. The price of innovation: new estimates of drug development costs. *J Health Econ* 2003; 22; 151–185.

22. Valk, P.E., Bailey, D. L., Townsend, D. W., Maisey M. N. Positron Emission Tomography: Basic Science and Clinical Practice. *New York: Springer-Verlag* 2004; 884 pages.

23. Moderegger, D. Radiolabeling of defined polymer architectures with fluorine-18 and iodine-131 for *ex vivo* and *in vivo* evaluation: Visualization of structure-property relationships. PhD thesis, *University of Mainz*, 2012.

24. Interactive Chart of Nuclides. *National Nuclear Data Center, Brookhaven National Laboratory*; *available online: http://www.nndc.bnl.gov/chart/*

25. The Berkley Laboratory Isotopes Projects. *Ernest O. Lawrence Berkeley National Laboratory*; *available online: http:///ie.lbl.gov/education/isotopes.htm*

26. Ross, T. L., Wester, H. J. 42 ^{18}F: Labeling Chemistry and Labeled Compounds. In *Handbook of Nuclear Chemistry*; Vértes A, Nagy S, Klencár Z, Lovas R, Rösch F, Eds.; Springer Heidelberg, 2011; 4; 2021-2071.

27. Fani, M., Maecke H. R. Radiopharmaceutical development of radiolabelled peptides. Eur J Nucl Med Mol Imaging 2012; 39(1); 11-30.

28. Ambrosini, V., Fani, M., Fanti, S., Forrer, F., Maecke, H. R. Radiopeptide imaging and therapy in Europe. *J Nucl Med* 2011; 52(2); 42-55.

29. de Jong, M., Breeman, W. A., Kwekkeboom, D. J., Valkema, R., Krenning, E. P. Tumor imaging and therapy using radiolabeled somatostatin analogues. *Ac Chem Res* 2009; 42(7); 873-880.

30. van Dongen, G. A., Vosjan, M. J. Immuno-positron emission tomography: shedding light on clinical antibody therapy. *Cancer Biother Radiopharm* 2010; 25(4); 375-85.

31. Marik, J., Junutula, J. R. Emerging role of immuno-PET in receptor targeted cancer therapy. *Curr Drug Deliv* 2011; 8(1); 70-78.

32. Wu, A. M. Antibodies and antimatter: the resurgence of immuno-PET. *J Nucl Med* 2009; 50(1); 2-5.

33. U. S. Food and Drug Administration, U. S. Department of Health and Human Services. [Website] *Available, from: http://www.fda.gov*

34. Vugts, D. J., van Dongen, G. A. M. S. ^{89}Zr-labeled compounds for PET imaging guided personalized therapy. *Drug Discovery Today: Technologies* 2011; 8(2); 53-61

35. Holland, J. P., Sheh, Y., Lewis J. S. Standardized methods for the production of high specific-activity zirconium-89. *Nucl Med Biol* 2009; 36(7); 729–739.

36. Belov, V. V., Bonab, A. A., Fischman, A. J., Heartlein, M., Calias, P., Papisov, M. I. Iodine-124 as a label for pharmacological PET imaging. *Mol Pharm* 2011; 8(3); 736-747.

37. Anderson, C. J., Ferdani, R. Copper-64 radiopharmaceuticals for PET imaging of cancer: advances in preclinical and clinical research. *Cancer Biother Radiopharm* 2009; 4(4); 379-393

38. Shokeen, M., Anderson, C. J. Molecular imaging of cancer with copper-64 radiopharmaceuticals and positron emission tomography (PET). *Ac Chem Res* 2009; 42(7); 832-841.

39. Rösch, F., Herzog, H., Stolz, B., Brockmann, J., Köhle, M., Mühlensiepen, H., Marbach, P., Müller-Gärtner, H. W. Uptake kinetics of the somatostatin receptor ligand [^{86}Y]DOTA-Dphe^{1}-Tyr^{3}-octreotide ([^{86}Y]SMT 487) using positron emission tomography in non-human primates and calculation of radiation doses of the ^{90}Y-labelled analogue. *Eur J Nucl Med* 1999; 26; 358-366.

40. Nayak, T. K., Brechbiel, M. W. ^{86}Y based PET radiopharmaceuticals: radiochemistry and biological applications. *Med Chem* 2011; 7(5); 380-388.

41. Rossin, R., Berndorff, D., Friebe, M., Dinkelborg, L. M., Welch, M. J. Small-animal PET of tumor angiogenesis using a (76)Br-labeled human recombinant antibody fragment to the ED-B domain of fibronectin. *J Nucl Med* 2007; 48(7); 1172-1179.

42. Serdons, K., Verbruggen, A., Bormans, G. M. Developing new molecular imaging probes for PET. *Methods* 2009; 48(2); 104-111.

43. Qaim S. M. Development of novel positron emitters for medical applications: nuclear and radiochemical aspects. *Radiochimica Acta* 2011; 99(10); 611-625.

44. Welch, M. J., Laforest, R., Lewis, J. S. Production of non-standard PET radionuclides and the application of radiopharmaceuticals labeled with these nuclides. *Ernst Schering Res Found Workshop* 2007; (62); 159-181.

45. Cyclotron produced radionuclides: physical characteristics and production methods. Technical reports series No. 468, *International Atomic Energy Agency, Vienna,* 2009.

46. Qaim, S. M. Recent Advances in Nuclear Data Research for Medical Applications. *J Korean Phys Soc* 2011; 59; 1965-1970.

47. Rösch, F., Knapp F. F. Radionuclide Generators. Handbook of Nuclear Chemistry Vértes A, Nagy S, Klencár Z, Lovas R, Rösch F, Eds.; Springer Heidelberg, 2011; 4; 1935-1976.

48. Qaim, S. M. Decay data and production yields of some non-standard positron emitters used in PET. *Q J Nucl Med Mol Imaging* 2008; 52(2); 111-120.

49. Scholten, B., Kovács, Z., Tárkányi, F., Qaim, S. M. Excitation functions of ^{124}Te(p,xn)^{124,123}I reactions from 6 to 31 MeV with special reference to the production of ^{124}I at a small cyclotron. *App Rad Isot* 1995; 46; 255.

50. Alenitzky, Yu. G., Novgorodov, A. F., Skripnik, A. V., Filosofov, D. V., Skripnik, A. V., Kaplun, V. G., Suzikov, A. G., Eliseev,I. A., Rösch, F.: ^{44}Ti: Investigation of target preparation, irradiation and yields in the ^{45}Sc(*p, 2n*) process. In: Annual Report. Institute of Nuclear Chemistry, University of Mainz 2005, *http://www.kernchemie.uni-mainz.de/Dateien/b3_05.pdf*

51. Filosofov, D. V., Loktionova, N. S., Rösch, F. A ^{44}Ti/^{44}Sc radionuclide generator for potential application of ^{44}Sc-based PET-radiopharmaceuticals. *Radiochim Acta* 2010; 98(3); 149-156.

52. Roesch, F. Scandium-44: benefits of a long-lived PET radionuclide available from the ^{44}Ti/^{44}Sc generator system. *Curr Radiopharm* 2012; 5(3); 187-201.

53. Nemeth, Z., Varga K. Radiochemical Techniques. Radiochemistry V. 1 Ed. Sandor Nagy, Hungary 2007; 197-230.

54. Novgorodov, A. F., Roesch, F. Korolev, N. A. Radiochemical Separations by Thermochromatography Handbook of Nuclear Chemistry Vértes A, Nagy S, Klencár Z, Lovas R, Rösch F, Eds.; Springer Heidelberg, 2011; 2429-2459.

55. Skarnemark, G. Solvent Extraction and Ion Exchange in RadiochemistryHandbook of Nuclear Chemistry Vértes A, Nagy S, Klencár Z, Lovas R, Rösch F, Eds.; Springer Heidelberg, 2011; 2403-2429.

56. Jahn, M., Radchenko, V., Filosofov, D., Hauser, H., Eisenhut, M., Jennewein, M., Rösch, F. Separation and purification of no carrier added arsenic from bulk amounts of germanium being adequate to radiopharmaceutical labeling chemistry. *Radiochim Acta* 2010; 98(12); 807-812.

57. Cyclotron Produced Radionuclides: Principles and Practice. Chapter 7: Target processing and material recovery. International Atomic Energy Agency; Technical Reports Series No. 465, Vienna, 2008; 155-199.

58. Radchenko, V., Filosofov, D. V., Bochko, O. K., Lebedev, N. A., Rakhimov, A., Aksenov, N. V., Bozhikov, G. A., Roesch, F.: Rapid strategy for separation of nocarrier- added ^{90}Nb from zirconium target for application in *immuno*-PET. In preparation for submission to *Radiochim Acta* (2013).

59. Zhernosekov, K. P., Filosofov, D. V., Baum, R. P., Aschoff, P., Bihl, H., Razbash, A. A., Jahn, M., Jennewein, M., Rösch, F. Processing of generator-produced ^{68}Ga for medical application. *J Nucl Med* 2007; 48(10); 1741-1748.

60. Radioisotope handling facilities and automation of radioisotope production. IAEA-TECDOC-1430; International Atomic Energy Agency; 2004; Vienna.

61. Decristoforo, C., Knopp, R., von Guggenberg, E., Rupprich, M., Dreger, T., Hess, A., Virgolini, I., Haubner, R. A fully automated synthesis for the preparation of ^{68}Ga-labelled peptides. *Nucl Med Commun* 2007; 28(11); 870-875.

62. Zeglis, B. M., Lewis, J. S. A practical guide to the construction of radiometallated bioconjugates for positron emission tomography. *Dalton Trans* 2011; 40(23); 6168-6195.

63. Tolmachev, V. Choice of radionuclides and radiolabelling techniques. Torgny Stigbrand, Jörgen Carlsson, Gregory P. Adams, *Targeted Radionuclide Tumor Therapy, Springer Hedielberg* 2008; 145-174.

64. Griffiths, G. L., Goldenberg, D. M., Knapp, F. F. Jr., Callahan, A. P., Chang, C. H., Hansen, H. J. Direct radiolabeling of monoclonal antibodies with generator-produced rhenium-188 for radioimmunotherapy: labeling and animal biodistribution studies. *Cancer Res* 1991; 51(17); 4594-4602.

65. Eisenhut, M., Mier, W. Radioiodination Chemistry and Radioiodinated compounds Handbook of Nuclear Chemistry Vértes A, Nagy S, Klencár Z, Lovas R, Rösch F, Eds.; Springer Heidelberg, 2011; Vol. 4; 2121-2141.

66. Bruskin, A., Sivaev, I., Persson, M., Lundqvist, H., Carlsson, J., Sjöberg, S., Tolmachev, V. Radiobromination of monoclonal antibody using potassium [^{76}Br] (4 isothiocyanatobenzyl-ammonio)-bromo-decahydro-closo-dodecaborate (Bromo-DABI). *Nucl Med Biol* 2004; 31(2); 205-211.

67. Jennewein, M., Lewis, M. A., Zhao, D., Tsyganov, E., Slavine, N., He, J., Watkins, L., Kodibagkar, V. D., O'Kelly, S., Kulkarni, P., Antich, P. P., Hermanne, A., Rösch, F., Mason, R. P., Thorpe, P. E. Vascular imaging of solid tumors in rats with a radioactive arsenic-labeled antibody that binds exposed phosphatidylserine. *Clin Cancer Res* 2008; 4(5); 1377-1385.

68. Avidin-Biotin Technical Handbook. Overview of protein labeling. Thermo Scientific. Avaliable online: *http://www.piercenet.com/browse.cfm?fldID=4DDCADD2-5056-8A76-4E7E-2E00843BE346.*

69. Reilly, R. M. The Radiochemistry of Monoclonal Antibodies and Peptides. Chapter 2: Monoclonal Antibody and Peptide-Targeted Radiotherapy of Cancer. Reilly, R. M. (Editor) Hoboken, NJ: John Wiley and Sons, 2010; 39-83.

70. Liu, S. Bifunctional Coupling Agents for Radiolabeling of Biomolecules and Target-Specific Delivery of Metallic Radionuclides. *Adv Drug Deliv Rev* 2008; 60(12); 1347–1370.

71. Wadas, T. J., Wong, E. H., Weisman, G. R., Anderson, C. J. Coordinating radiometals of copper, gallium, indium, yttrium, and zirconium for PET and SPECT imaging of disease. *Chem Rev* 2010; 110(5); 2858-2902.

72. Rice, S. L., Roney, C. A., Daumar, P., Lewis, J. S. The next generation of positron emission tomography radiopharmaceuticals in oncology. *Semin Nucl Med* 2011; 41(4); 265-282.

73. Brechbiel, M. W. Bifunctional chelates for metal nuclides. *Q J Nucl Med Mol Imaging* 2008 ; 52(2); 166-173.

74. Fani, M., Good, S., Maecke, H. R. Radiometals (non-Tc, non-Re) and Bifunctional Labeling Chemistry. Handbook of Nuclear Chemistry Vértes A, Nagy S, Klencár Z, Lovas R, Rösch F, Eds.; Springer Heidelberg, 2011; Vol. 4; 2143-2179.

2. Objectives and outline

An increasing numbers of tasks involving molecular imaging based on PET technique necessities of various positron emission radionuclides with different characteristic.

Currently, with rising interest to using biomolecules, such as antibodies and antibody fragments for tumor imaging and therapy radionuclides, radionuclides with long and intermediate half-lives are under great importance.

Several characteristic sre important for selection of appropriate radionuclide for PET imaging:

- Decay characteristics appropriate for PET imaging
- Cost effective production strategy by small or intermediate cyclotrons preferably from not enriched target materials or possibility of radionuclide generator system
- Cost effective, fast separation strategy which allow remote and automated separation process
- Not complicated, fast labeling procedure

The present work was dedicated to develop ^{90}Nb as potential radionuclides for application in *immuno*-PET. Its half-life of 14.6 hours makes it universally applicable with intact antibody as well as with enginereed antibody fragments. It has high positron branching (53%) and suitable mean and end point of positron energy (0.34 MeV and 1.5 MeV, respectively) that allow high spatial imaging resolution with low amount of radioactivity.

All these characteristics make ^{90}Nb a promising radionuclide for application in *immuno*-PET. Therefore, an appropriate production and separation strategy was developed. Further, a conjugation strategy was established to attach ^{90}Nb to biomolecules. Finally, the biodistribution of ^{90}Nb-labeled monoclonal antibody was studied and PET image was obtained first time.

The first task was to prove that ^{90}Nb can be potentially suitable for using in radiopharmaceutical science. Sufficient amount of ^{90}Nb was produced by proton bombardment of natural zirconium metal target with proton energy of 17.5 MeV, which is reachable by “clinical” cyclotrons (up to 18 MeV). Then ^{90}Nb was isolated from irradiated Zr target by multistep separation procedure including liquid-liquid extraction and ion exchange chromatography. Further, the monoclonal antibody (Rituximab) was modified via two strategies with desferrioxamine and labeled with ^{90}Nb at room temperature and pH 7 for 60 minutes. The product was purified by size exclusion chromatography and *in vitro* stability studies in fetal calf serum (FCS) were conducted.

Another study was focused on development of novel rapid separation strategy to provide source of high pure ^{90}Nb for subsequent labeling. Altough a previous separation strategy included multistep separation by liquid-liquid extraction and ion exchange chromatography well suitable to prove that ^{90}Nb is a suitable radionuclide for radiopharmacy, however, for routine daily application this separation strategy is very time consuming (more than 4 hours) and complicated for future automation. Therefore, an alternative separation strategy was evaluated. Ion exchange chromatography was chosen, due high selectivity and easily automation. Due Nb^{V} is element of fifth group with complicated complexation chemistry, and therefore attention was paid to well-studied complexes of Nb^{V} in hydrofluoric media. From previous experimental data (Novgorodov A. F. et al. unpublished data) is known that Nb^{V} forms strong peroxo-complexes and can be easily eluted from anion exchangers with mixtures of HCl and hydrogen preroxide. Distribution coefficients (K_d) for systems anion exchanger (AG 1x8, 200-400 mesh F- form) - HF, HCl/H_2O_2 media and for UTEVA in HCl for Nb^{V} and Zr^{IV} were determinated. Later, some preliminary separation profiles on anion exchange column in concentrated hydrofluoric acid media and in mixture HCl/H_2O_2 were measured. For UTEVA the elution profile of Nb^{V} and Zr^{IV} was studied in various HCl concentrations. On the base of K_d values and preliminary separation results, a final separation strategy was established. After dissolution, the zirconium target was passed through the small cation exchanger to filtrate undissolved particles and 2+ and 3+ charged cations. Next, solution was loaded on the anion exchange column for crude separation from bulk amount of zirconium target in hydrofluoric media. After crude separation of Zr, the niobium fraction was eluted and after heating and dilution loaded on a column filled with UTEVA resin for gentle separation and preconditioning for labeling. To prove that ^{90}Nb obtained by this strategy has appropriate purity and condition for subsequent labeling, a labeling test with monoclonal antibody Rituximab modified with Df was performed. The i*n vitro* stability of ^{90}Nb-Df-mAb was studied in fresh HSA.

To improve the previously developed separation strategy and to simplify automation a direct flow mode to transfer ^{90}Nb fraction from anion exchange column to UTEVA was developed. For Zr^{IV} and Nb^{V} K_d values were determinated for anion exchangers and UTEVA in mixtures HCl/H_2O_2 and HCl/ oxalic aicd. Finally, a direct flow transfer was realized.

Another research was concentrated on an alternative production strategy of ^{90}Nb via the decay of ^{90}Mo, that provide of ^{90}Nb with exceptional radionuclidic purity. Different target materials (Zr, Nb, Mo, Rh, Ag and Pd) were irradiated at high proton beam at the Phasotron facilities of Joint Institute for Nuclear Research, Dubna (Russian Federation) to identify the production yield of ^{90}Mo. A separation strategy to

isolate ^{90}Mo and ^{90}Nb from the irradiated target material was examined. The previously developed separation strategy for a zirconium target was also adopted for the Mo target.

Next, an appropriate bifunctional chelator (BFC) for ^{90}Nb was studied. Eight most common bifunctional chelators including macrocyclic and acyclic chelators were tested on concerning their capacity of complex formation with ^{95}Nb adsorbed on CHELEX resin at room temperature. For the three most efficient BFC, the dependence of pH on the complex formation was studied. Dessferioxamine (Df) showed the best capability for Nb complexation, therefore its complex stoichiometry and kinetics of complex formation were evaluated. Later, Df-Octreotide was labeled with ^{95}Nb at various pH values and optimal labeling conditions were determinated. *In vitro* stability studies with human serum albumin (HSA) for ^{95}Nb-Df and ^{95}Nb-Df-Octreotide complexes were conducted.

A competition study on transchelation of *Nb from Df-Octreotide in presence of other metals was performed. Known concentrations of Fe^{III}, Ga^{III} and Zr^{IV} were employed. These metals can be present in the final Nb fraction from reagents and from the target material. Competition study was done in two setups: at first aliquots of each above mentioned metals were separately added to ^{95}Nb-Df-Octreotide solution and content of retained in complex *Nb was measured. At another setup, aliquots of Fe, Ga and Zr were separatly mixed with Df-Octreotide and after one hour incubation aliquots of *Nb were added to each sample and transchelation kinetics was measured.

Finally, a first *in vivo* evaluation of ^{90}Nb labeled biomolecules was performed and first PET image was obtained. Monoclonal antibody bevacizumab (Avastin®) were labeled with ^{95}Nb and ^{90}Nb and biodistribution study and PET imaging in mice were conducted respectively. Mice were injected via the tail vein with. Groups of three animals were sacrificed at 4, 24, 48 and 72 hours after injection of radiolabeled antibody. Tumors and organs were excised, blotted dry and weighed. For PET imaging, tumor-bearing SCID mice were injected with ^{90}Nb-bevacizumab and were anaesthetized cocktail solution of ketamine/xylazine.

3. Manuscripts and supplementary results

This work is based on the following manuscripts:

1. ^{90}Nb – a Potential PET Nuclide: Production and Labeling of Monoclonal Antibodies. *Radiochim Acta* 2012; 100(11); 857-65.

2. Separation of ^{90}Nb from zirconium target for application in *immuno*-PET. submitted to *Radiochim Acta* (2013).

3. Direct flow separation strategy, to isolate no-carrier-added ^{90}Nb from irradiated Mo or Zr target. in preparation (2013).

4. Desferrioxamine as an appropriate chelator for ^{90}Nb: Comparison of its complexation proprieties for M-Df-Octreotide (M = Nb, Fe, Ga, Zr). submitted *J Nuclear Medicine and Biology* (2013).

5. Conjugation, labeling and initial *in vivo* assessment of an anti-VEGF monoclonal antibody labeled with Niobium isotopes, in preparation (2013).

3.1 ^{90}Nb – a potential PET nuclide: production and labeling of monoclonal antibodies

^{90}Nb – a potential PET nuclide: production and labeling of monoclonal antibodies

V. Radchenko [1], H. Hauser [2], M. Eisenhut [2], D. J. Vugts [3,4], G. A. M. S. van Dongen [3,4], F. Roesch [1,*]

[1] Institute of Nuclear Chemistry, Johannes Gutenberg-University Mainz, Fritz-Strassmann-Weg 2, D-55128 Mainz, Germany

[2] Radiopharmaceutical Chemistry, German Cancer Research Center, Im Neuenheimer Feld 280, D-69120 Heidelberg, Germany

[3] VU University Medical Center, Dept. of Nuclear Medicine and PET Research, De Boelelaan 1085 c, Amsterdam, The Netherlands

[4] VU University Medical Center, Dept. of Otolaryngology/Head and Neck Surgery, De Boelelaan 1117, Amsterdam, The Netherlands.

Abstract

Fast progressing *immuno*-PET gives reasons to develop new potential medium-long and long-lived radioisotopes. One of the promising candidates is ^{90}Nb. It has a half-life of 14.6 hours, that allows visualizing and quantifying processes with medium and slow kinetics, such as tumor accumulation of antibodies and antibodies fragments or polymers and other nanoparticles. ^{90}Nb exhibits a high positron branching of 53% and an optimal energy of β^+ emission of E_{mean} = 0.35 MeV only. Consequently, efficient radionuclide production routes and Nb^V labeling techniques are required.

^{90}Nb was produced by the ^{90}Zr(p,n)^{90}Nb nuclear reaction on natural zirconium targets. No-carrier-added (n.c.a.) ^{90}Nb was separated from the zirconium target via a multi-step separation procedure including extraction steps and ion-exchange chromatography. Protein labeling was exemplified using the bifunctional chelator desferrioxamine attached to the monoclonal antibody rituximab. Desferrioxamine was coupled to rituximab via two different routes, by the use of N-succinyl-desferrioxamine (N-suc-Df) and by means of the bifunctional derivative *p*-isothiocyanatobenzyl-desferrioxamine B (Df-Bz-NCS), respectively. Following antibody modification, labeling with ^{90}Nb was performed in HEPES buffer at pH 7 at room temperature. *In vitro* stability of the radiolabeled conjugates was tested in saline buffer at room temperature and in fetal calf serum (FCS) at 37 °C.

The selected production route led to a high yield of 145± 10 MBq/μAh of ^{90}Nb with high radioisotopic purity of >97%. This yield may allow for large scale production of about 10 GBq ^{90}Nb. The separation procedure resulted in 76-81% yield. The Zr/^{90}Nb decontamination factor reaches 10^7. Subsequent radiolabeling of the two different conjugates with ^{90}Nb gave high yields; after one hour incubation at room temperature, more than 90% of ^{90}Nb-Df-mAb was formed in both cases. At room temperature in aqueous solution, both ^{90}Nb-Df-mAb constructs were more than 99% stable over a period of 18 days.

The developed production and separation strategy provided ^{90}Nb with purity appropriate for radiolabeling applications. Labeling and stability studies proved the applicability of ^{90}Nb as a potential positron emitter for *immuno*-PET.

Keywords: *immuno*-PET/ Niobium-90/ Radiolabeling/ Desferrioxamine/ Monoclonal antibodies / *p*-isothiocyanatobenzyl-desferrioxamine/ TFP-N-succinyl-desferrioxamine

Introduction

A variety of antibodies and antibody fragments for different targets of interest is currently under preclinical investigation [1]. Although a rather low number of all developed antibodies make it to a worldwide use in clinics, 28 different antibodies are approved by the US Food and Drug Administration today [2]. One such approved antibody is rituximab (the first monoclonal antibody approved for the treatment of lymphoma), a genetically engineered monoclonal chimeric antibody, targeting the CD20 antigen expressed on B cells [3]. To improve the evaluation of potential new antibodies and to facilitate the transfer of candidates into the clinic, *immuno*-PET may be applied [4]. Since the 1990s, several positron emitting radionuclides with long and medium half-lives have been tested for their applicability in *immuno*-PET, for recent reviews cf. [5-7]. Antibodies with blood-clearance half-lives of days to weeks call for radionuclides with corresponding half-lives to enable *immuno*-PET scans at, for example, 7-9 days p.i.. Consequently, commercially available and established positron emitters for the imaging peptides and proteins with slow pharmacokinetics are ^{86}Y ($T_{1/2}$ = 14.7 h), ^{89}Zr ($T_{1/2}$ = 78.4 h) and ^{124}I ($T_{1/2}$ = 100.2 h). Nuclear data are summarized in Table 1. One example of application of ^{89}Zr is the use of ibritumomab tiuxetan (Zevalin©) [8] labeled with ^{89}Zr and the development of ^{89}Zr-labeled U36, a chimeric antibody specific for CD44v6 [9]. These results already demonstrate the potential of ^{89}Zr in *immuno*-PET with intact antibodies. *Immuno*-PET maging with ^{124}I-cG250 (anticarbonic anhydrase-IX) resulted in successful detection of 15 of 16 clear-cell carcinomas [10]. However, those antibodies do not provide optimal imaging properties. The long lasting circulation and the very slow kinetics necessitate long delays between administration of the radiotracer and the acquisition of the final PET imaging.

For faster pharmacokinetics, antibodies fragments have been developed [11, 12]. As a result, their enhanced clearance dramatically reduces the interval between radiotracer injection and the actual imaging to hours instead of days. For imaging with engineered antibody fragments radionuclides with medium half-lives are required, for example ^{64}Cu ($T_{1/2}$ = 12.7 h) [13], ^{86}Y ($T_{1/2}$ = 14.7 h.) [14], ^{76}Br ($T_{1/2}$ = 16.2 h) [15]. Their decay data are given in Table 1 [16, 17].

Several crucial factors and characteristics apply to radionuclides for *immuno*-PET. The most important factors are: i) a physical half-life paralleling the biological half-life of the antibody or antibody fragment; ii) a preferably low β^+-energy to allow high-resolution PET imaging; iii) a high positron branching with no or

weak accompanying irradiation (β^-, γ) to offer high-sensitive PET imaging while reducing the radiation burden of the patient and iv) the availability of the radionuclide, i. e. an efficient production route.

In this study, ^{90}Nb is proposed for *immuno*-PET. Its intermediate half-life of 14.6 hours appears appropriate for antibody fragments as well as for antibodies. Another advantage of ^{90}Nb is its decay parameters. Its positron branching is as high as 53% at rather low β^+-energy of E_{mean}= 350 keV (E_{max}= 1.5 MeV) (Table 1), which should allow high resolution images.

Table 1: Decay characteristics of several PET radionuclides relevant to immuno-PET imaging (with increasing $T_{1/2}$), taken from [16] unless otherwise stated.

Radionuclide	Half-life h	Main production route	$E_{\beta+mean}$ in MeV (β^+yields)	Most intensive γ-emissions in MeV (abundance)
^{64}Cu	12.7	^{64}Ni(p,n)^{64}Cu ^{64}Ni(d,2n)^{64}Cu	0.05 (17.8%) [17] (accompnied β^-, $E_{\beta\text{-mean}}$ 0.075 MeV (38.4%)	1.345 (0.54%) [17]
^{90}Nb	14.6	^{90}Zr(p,n)^{90}Nb	0.35 (53.0%)	0.14 (66.7%) 1.13 (92.0%) 2.32 (82.0%)
^{86}Y	14.7	^{86}Sr(p,n)^{86}Y	0.22 (33.0%)	0.63 (32.6%) 1.08 (83.0%) 1.15 (30.5%)
^{76}Br	16.2	^{76}Se(p,n)^{76}Br ^{75}As(^{3}He,2n)^{76}Br	0.64 (58.2%) [17]	0.55 (74.0%) 0.66 (15.9%) 1.85 (14.7%)
^{89}Zr	78.4	^{89}Y(p,n)^{89}Zr ^{89}Y(d,2n)^{89}Zr	0.09 (23.0%)	0.91 (100.0%) 1.71 (0.76%) 1.74 (0.13%)

Continuing our initial work on the production and radiochemical separation of ^{90}Nb [18, 19], and systematic studies on using desferrioxamine for ^{90}Nb labeling [20], this work aims to explore parameters of ^{90}Nb-Df-mAb labeling and stability. Recently, new synthetic approaches towards conjugation of desferrioxamine (Df) derivates to monoclonal antibodies have been described in the context of $^{89}Zr^{IV}$-*immuno*-PET [21, 22]. This chemistry appears promising also for $^{90}Nb^{V}$. Consequently, a monoclonal antibody was selected for ^{90}Nb-labeling utilizing two different strategies of covalently binding Df to the protein.

Materials and Methods

Materials

Reagents were purchased from Sigma-Aldrich (Germany) and used without further purification, unless otherwise stated. Deionized water (18 MΩ cm^{-1}) and ultra-pure HCl solution were used. No further special measures were taken regarding working under strict metal-free conditions. The mAb rituximab (MabThera®, 10 mg/mL) directed against CD20 was bought from Roche Nederland BV (Woerden, The Netherlands). For purification of conjugated and labeled antibodies, PD-10 columns (GE Healthcare Life Science) were applied, for anion exchange separation Aminex A27, 15 ± 2 µm, anionic exchange resin (BioRad) was used.

The production yield, radionuclidic purity, radiochemical purity and separation yield of $^{90/95}$Nb were determined by *γ*-ray spectroscopy using an Ortec HPGe detector system and Canberra Genie 2000 software. The dead time of the detector was always kept below 10%. The detector was calibrated for efficiency at all positions with the certified standard solution QCY48, R6/50/38 (Amersham, UK).

Production of ^{90}Nb and ^{95}Nb

^{90}Nb was produced via the ^{90}Zr(p,n)^{90}Nb reaction at the cyclotron MC32NI of the German Cancer Research Center, Heidelberg. For irradiation, a stack of three discs of natural zirconium (natural abundance: 51.45% ^{90}Zr) foils of 10 mm diameter and a thickness of 0.25 mm each was used (Fig. 1). Irradiation was performed at 20 MeV proton energy and a current of 5 µA for 1 hour. This initial proton energy

decreased, by using an aluminum holder cover of 0.5 mm thickness, to 17.5 MeV while entering the first foil of Zr. 24 hours after end of irradiation (EOB), production yield and impurities were measured by gamma ray spectroscopy. The absolute activity of ^{90}Nb was calculated as average of its two gamma-lines at 141.2 keV (66.8% abundance) and 1129.2 keV (92.7%). The irradiation yield of ^{90}Nb was calculated as the mean of three irradiations.

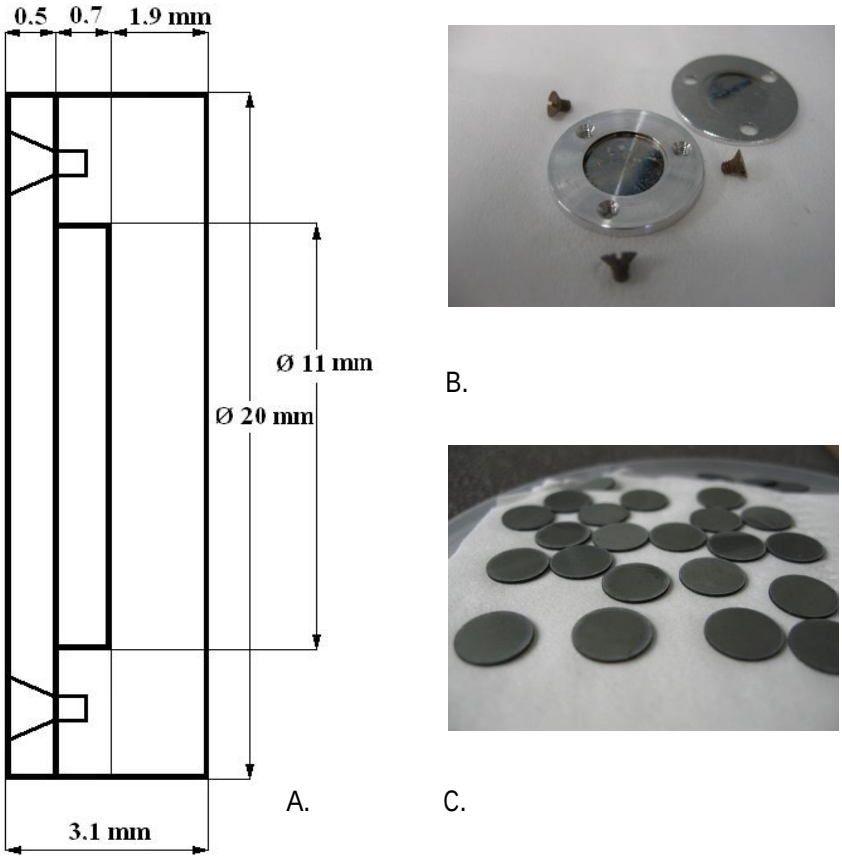

Figure 1: Irradiation setup A: Schematic view of the target holder (profile). B: Open target holder (full face) with aluminium cover. C: Natural zirconium discs for irradiation (Ø 10 mm, 0.25 mm thickness).

^{97}Nb ($T_{1/2}$ = 74 min) and ^{95}Nb ($T_{1/2}$ = 35 d) were employed for the development of the separation chemistry (as well as determination of the decontamination factor and testing purposes). ^{97}Nb was produced via the ^{96}Zr(n, γ)→^{97}Zr(β$^-$, $T_{1/2}$ = 16.9 h)→^{97}Nb reaction and ^{95}Nb was produced via the ^{94}Zr(n, γ)→^{95}Zr(β$^-$, $T_{1/2}$ = 64 d)→^{95}Nb reaction from natural zirconium granules (1-3 mm, 99.8% ChemPur, Germany). Neutron irradiations were performed at the TRIGA reactor at the University of Mainz, Germany, and at the

research reactor BERII at the Helmholtz Center Berlin, Germany. In the latter case 300 mg were irradiated at a neutron flux of $2 \cdot 10^{14}$ $s^{-1} \cdot cm^{-2}$ (BER II) for 50 days and more than 1.5 GBq of ^{95}Zr was obtained. Production of both isotopes, ^{95}Zr and ^{95}Nb, was monitored by gamma ray spectroscopy, via emissions at 724.2 keV (44.2%) and 756.7 keV (54.0%) for ^{95}Zr and via the 765.8 keV (100%) for ^{95}Nb. ^{97}Zr was monitored by gamma emission at 743.4 keV (93%) and ^{97}Nb at 658.1 keV (98%). The maximum daughter activity of ^{95}Nb generated from ^{95}Zr was obtained at ~67 d, EOB.

Separation and purification of n.c.a. $^{90/95}$Nb

The separation procedure was modified following the procedure described by Busse *et al.* [19]. In short, the zirconium metal target (260±3 mg) was transferred into a 50 mL vial and 2 mL of water were added. Under ice-cooling, 48% HF (0.63 mL) was added in small portions. After complete dissolution, 10 M HCl (6 mL) and saturated boric acid (3.4 mL) were added. The $^{90/95}$Nb fraction was extracted with 0.02 M *N*-benzoyl-*N*-phenylhydroxylamine (BPHA) in $CHCl_3$ (5 mL) by vigorous stirring of the two phases in a 50 mL vial for 20 min. The aqueous phase was additionally washed with $CHCl_3$ (3 mL). The organic phases were combined and washed with a mixture of 9 M HCl/0.001 M HF (2 mL) and with 9 M HCl (2 mL) and finally extracted with aqua regia (5 mL).

For a final purification of $^{90/95}$Nb from remaining trace amounts of zirconium, an anionic exchange method was employed. After aforementioned back extraction, the aqueous phase was evaporated to dryness. The residue was dissolved in a mixture of 0.25 M HCl/0.1 M oxalic acid (0.5 mL) and adsorbed on a small Aminex A27, 15 ± 2 µm, anionic exchange column (20 x 1.5 mm). Elution was performed under slight overpressure of 0.3 bars. After loading, the column was washed with 10 M HCl (100 µL). Residues of Zr were removed by washing with a mixture of 9 M HCl/0.001 M HF (200 µL). $^{90/95}$Nb was eluted by a mixture of 6 M HCl/0.01 M oxalic acid (200 µL).

Preparation of TFP-N-suc-Df-mAb

Conjugation of TFP-N-suc-Df to rituximab (MabThera®) was performed at VU University Medical Center, Amsterdam. Conjugation follows the multi-step procedure as previously described [21] (Fig. 2). In short, the chelate Df was succinylated (N-suc-Df), temporarily filled with stable iron Fe(III), and coupled to the

lysine residues of rituximab (5 mg/ml) by means of a tetrafluorophenol-N-suc-Df ester. After removal of Fe(III) by transchelation to EDTA at 35 °C, the modified mAb was purified on a PD-10 column using normal saline as eluent.

Preparation of Df-Bz-NCS-mAb

Df-Bz-NCS was purchased from Macrocyclics. Rituximab was modified with Df-Bz-NCS as illustrated in Fig. 3 [22]. In short, while gently shaking, a threefold molar excess of Df-Bz-NCS (in 20 µL DMSO) was added to the mAb (3 mg/mL in 1 ml 0.1 M $NaHCO_3$ buffer, pH 9.0), and incubated for 30 min at 37 °C. Non-conjugated chelator was removed by size exclusion chromatography (SEC) using a PD-10 column and 0.9% sodium chloride solution as eluent.

Determination of chelate-to-mAb ratio

In the coupling of desferrioxamine to the mAb through the N-suc-Df-mAb method, the chelate-to-mAb ratio was monitored via UV absorbance of Fe^{3+} at 430 nm [21]. Iron was removed by complexation with EDTA before the actual radiolabeling procedure.
In case of the coupling of desferrioxamine to mAb through the Df-Bz-NCS, the chelate-to-mAb molar ratio for rituximab was determined in previous studies [22] following the method described by Meares *et al.* [23]. In short, conjugates were labeled according to the aforementioned procedure with a known nanomolar excess of zirconium oxalate solution spiked with ^{89}Zr.

Preparation of ^{90}Nb-labeled N-suc-Df-mAb

N-suc-Df-mAb was labeled with ^{90}Nb in HEPES buffer at pH 7.0. To ^{90}Nb (37–50 MBq) in 6 M HCl/0.01 M oxalic acid solution (200 µL) 6 M NaOH (180 µL) and afterwards 1 M NaOH (230 µL) were added to neutralize the acidic solution. 0.5 M HEPES buffer (pH 7.0) (300 µL), N-suc-Df-mAb (5 mg/mL) (250 µL) and 0.5 M HEPES (pH 7.0) (860 µL) were added and incubated for 1 hour at room temperature. The overall volume of the reaction mixture was 2 mL. Finally, ^{90}Nb-N-suc-Df-mAb was purified on a PD-10 column using 0.9% sodium chloride solution as mobile phase.

Preparation of ^{90}Nb-labeled Df-Bz-NCS-mAb

Df-Bz-NCS-mAb was labeled with ^{90}Nb at room temperature in a volume of 2 mL under gently stirring for 60 min. To ^{90}Nb (37–50 MBq) 6 M HCl/0.01 M oxalic acid solution (200 µL) 6 M NaOH (180 µL) and 1 M NaOH (230 µL) were added. 0.5 M HEPES buffer (pH 7.0) (390 µL) and Df-Bz-NCS-mAb (1.5 mg/mL) (1.0 mL) were added. Finally, ^{90}Nb-Df-Bz-NCS-mAb was purified by PD-10 column using a 0.9% sodium chloride solution as mobile phase.

Analytical check of ^{90}Nb labeling procedures

After each preparation of ^{90}Nb-labeled Df-Bz-NCS-mAb or N-suc-Df-mAb, the conjugates were analyzed by instant thin-layer chromatography (ITLC), and by high-performance liquid chromatography (HPLC) for radiolabeling efficiency and radiochemical purity. ITLC analyses of ^{90}Nb-labeled N-suc-Df-mAb or Df-Bz-NCS-mAb was performed on chromatography strips (Biodex, NY). As mobile phase, 0.02 M citrate buffer (pH 5.0) was used. HPLC monitoring of the final products was performed on a Waters HPLC system using a BioSep-SEC-S 2000 size exclusion column (Phenomenex). As eluent, a mixture of 0.05 M sodium phosphate and 0.15 M sodium chloride (pH 6.8) solution was used at a flow rate of 0.5 mL/min.

In vitro stability

Fetal calf serum for stabilities studies was provided by the University Medical Center of the Johannes Gutenberg University Mainz, Germany.

The final activity was adjusted between 15–25 MBq/mL, mAb concentrations varied between 1.25 and 1.5 mg/mL.

For assessing the *in vitro* stability of ^{90}Nb-Df-Bz-NCS-mAb and ^{90}Nb-N-suc-Df-mAb, two sets of experiments were performed. In the first set, the labeled mAbs were stored at 4 °C (storage and transportation conditions) in 0.9% sodium chloride solution. At various time points, aliquots were taken and analyzed by ITLC and HPLC.

In a second set, purified radiolabeled mAbs were added to fetal calf serum (FCS) (1:4 v/v dilution; sodium azide added to 0.02%). The samples were incubated at 37 °C. At various time points, aliquots were taken and analyzed by ITLC and HPLC.

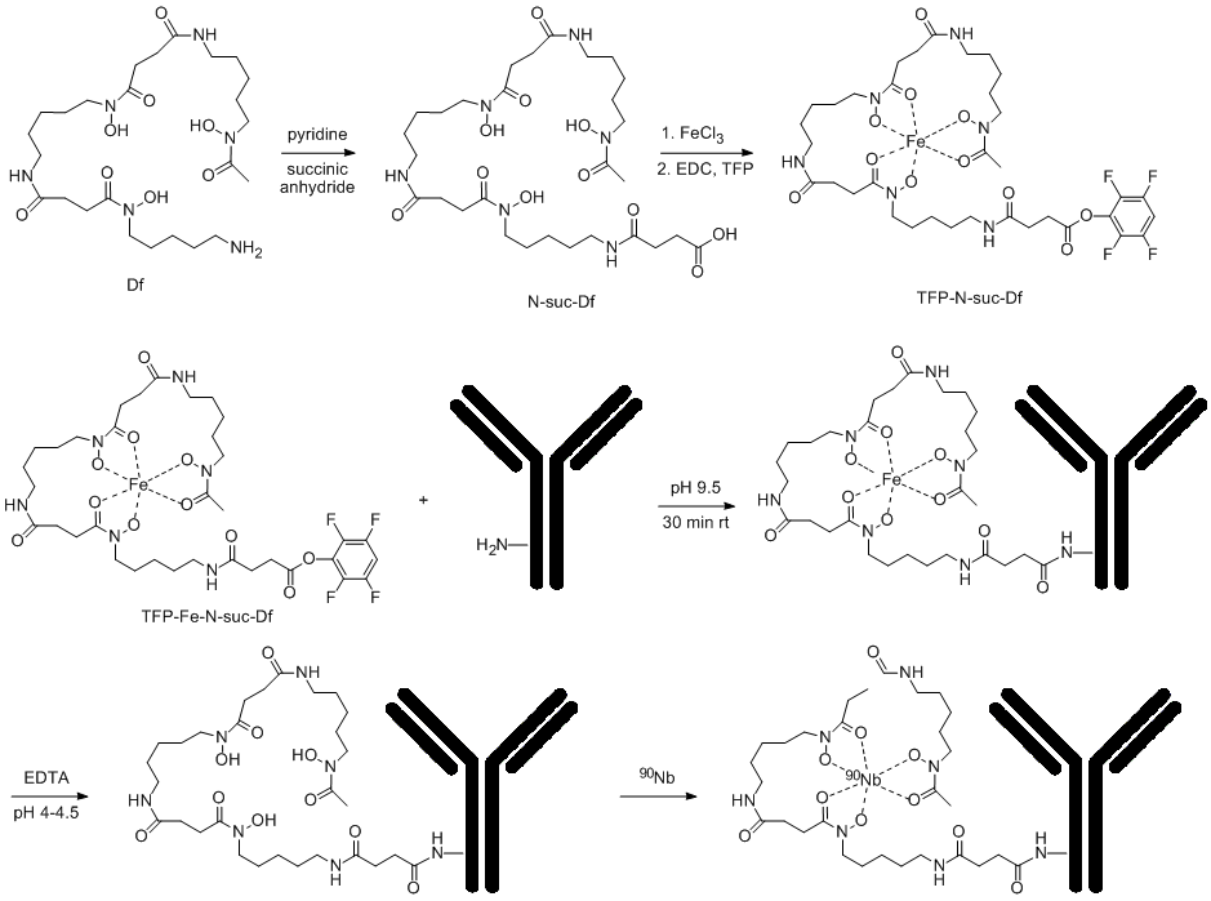

Figure 2: Df-conjugation via TFP-N-suc-Df-Fe and labeling with ^{90}Nb.

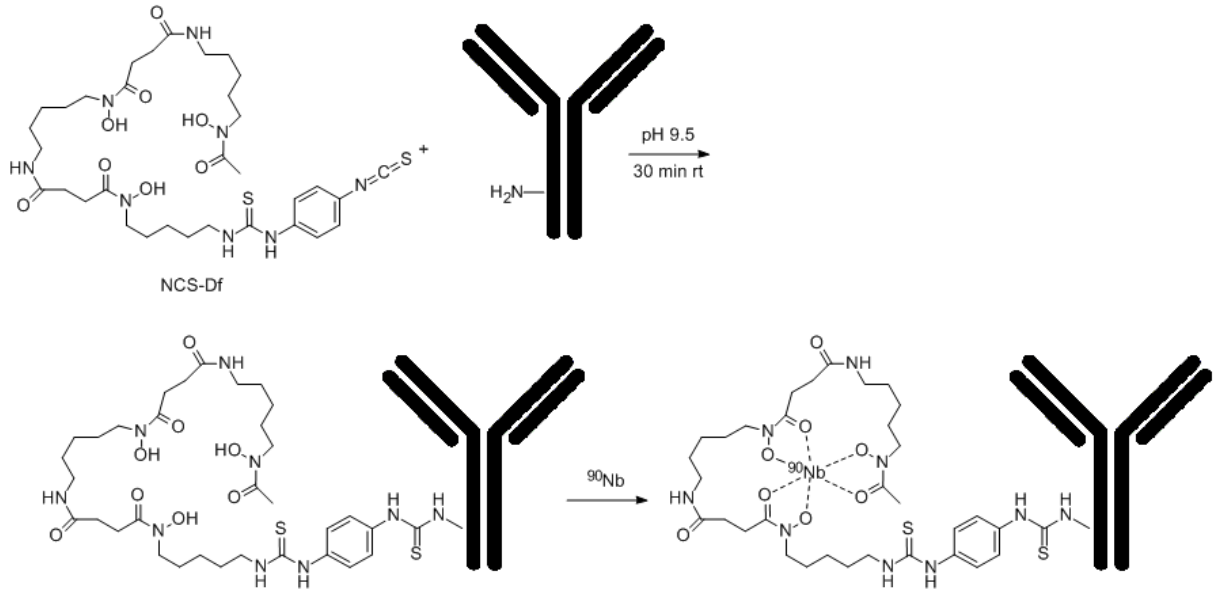

Figure 3: Df-conjugation via the bifunctional chelator Df-Bz-NCS and labeling with ^{90}Nb.

Results and Discussion

Production of ^{90}Nb

The overall irradiation yield of ^{90}Nb for three 1 h and 5 μA irradiations was 720± 50 MBq, i. e. 145±10 MBq/μAh under given irradiation parameters. The distribution of ^{90}Nb activity in the 3 foils was: 49%, 40% and 10% for the 1st, 2nd and 3rd foil, respectively. As the third foil got only 10% of the total activity while carrying 1/3 of the mass of the whole target, it may then be eliminated in routine production procedure, in particular to facilitate radiochemical processing. The radionuclidic purity of ^{90}Nb after EOB was more than 97%. Minor isotopic impurities found were: ^{92m}Nb ($T_{1/2}$ = 10.2 d) = 1.64%, ^{95}Nb ($T_{1/2}$ = 35.0 d) = 0.08%, ^{95m}Nb ($T_{1/2}$ = 3.6 d) = 0.29% and ^{96}Nb ($T_{1/2}$ = 23.35 h) = 0.88%.

Separation and purification of no-carrier added ^{90}Nb

The extraction steps provided crude separation of ^{90}Nb from the target material with the organic phase collecting more than 99% of ^{90}Nb. After the back extraction procedure, the 5 mL aqueous phase contained

90-95% of the ^{90}Nb activity. After both extractions this corresponds to a high reduction of Zr mass by a factor of 10^4. Subsequent anionic exchange separation further removed traces of Zr. The final separation yield of ^{90}Nb was 76-81% and the decontamination factor for Zr/Nb was $\geq 10^7$, representing ≤ 26 ng of Zr present in the final ^{90}Nb fraction.

Preparation of ^{90}Nb-labeled N-suc-Df-mAb and ^{90}Nb-labeled Df-Bz-NCS-mAb

Analysis via HPLC showed that TFP-N-suc-Df modification strategies yield about 1.5 molecules of Df per molecule of rituximab. Similar results were obtained also for the NCS-Df modification [22]. For each modification, the ^{90}Nb labeling yield was >90% (91% ITLC, 94% HPLC) after 1 hour. Labeling kinetics indicate that the labeling yields reached 77% already at 15 min and increased to more than 90% after 50 min. After SEC separation on a PD-10 column, the two ^{90}Nb-Df-mAb derivatives had 99.0% purity. Specific activity of radiolabeled retuxiamb varied between 24.7 and 40 MBq/mg.

In vitro stability

For both ^{90}Nb-labeled mAb derivatives less than 1% of degradation was observed at room temperature in aqueous solution after 18 days. In the presence of fetal calf serum, the ^{90}Nb-labeled mAbs were more than 95% intact after 5 days and about 90% intact after 9 days.
Differences between the two modification methods were insignificant.

Discussion

The development of new long-lived *immuno*-PET isotopes is a complex task and requires many factors to be considered: nuclear decay parameters (half-life, β^+ energy and branching), production yield, specific activity, labeling strategies, *in vitro* and *in vivo* stabilities. The medium-long half-life of ^{90}Nb of 14.6 hours makes this isotope particularly suitable for application with antibodies and antibody fragments. Another advantage of ^{90}Nb is its decay characteristics: relatively high positron branching of 51% and a rather low β^+-energy of E_{mean} = 350 keV (E_{max} = 1.5 MeV), which allows high quality PET imaging.

Following our earlier investigations [18-20] on production, separation and labeling chemistry of the new potential *immuno*-PET isotope ^{90}Nb, the conjugation of ^{90}Nb to rituximab as a proof of principle monoclonal antibody was investigated.

The excellent production yield of ^{90}Nb obtained in this study (145±10 MBq/μAh) is high in comparison with other *immuno*-PET isotopes (^{124}I, ^{89}Zr, ^{72}As) presented in Table 2, mainly due to its shorter half-life. Furthermore, according to previous studies [18] it may even be enhanced by a factor of two. Some variation in production yields results from different setups at cyclotron facilities, such as beam parameters, target design and cooling arrangement.

As radiolabeling chemistry of $^{90}Nb^{V}$ appears to be quite similar to that of $^{89}Zr^{IV}$ [21, 22], an almost complete removal of Zr^{IV} from the cyclotron target is essential. A high decontamination factor is crucial, because zirconium also creates very stable complexes with desferrioxamine and competes with niobium, affecting labeling efficiency and causing purity and purification problems. After a multi-step separation procedure, the decontamination factor for Zr/Nb of 10^7 was achieved. With 260 mg of Zr applied for irradiation this reflects ~26 ng of Zr remaining after separation.

The separation yield of ^{90}Nb from metallic Zr target varied between 76% and 81%. The whole separation procedure took around 5 hours. For routine applications of ^{90}Nb-labeled compounds, this separation procedure would need to be further optimized to a simpler and faster method.

Labeling of rituximab with ^{90}Nb was performed via the bifunctional chelator desferrioxamine. The monoclonal antibody was successfully modified through two difference methods. The molar ratio for the N-suc-Df method as well as for the Df-Bz-NCS method was 1.5 molecules of desferrioxamine per antibody molecule. Subsequent labeling with ^{90}Nb showed for both modification strategies the same high yield of more than 90%. *In vitro* stability studies in aqueous solution as well as in the presence of fetal calf serum proved that the ^{90}Nb-desferrioxamine-antibodies are highly stable over several periods of half-life of ^{90}Nb, which allows their use in *immuno*-PET.

For future labeling, a modification through the Df-Bz-NCS is preferable for reasons of simpler and faster preparation.

Table 2: Production yields of a few PET radionuclides [6, 7].

Radionuclide	Commonly used production route	Proton energy range (MeV)	Calculated yield (MBq/μAh)
^{124}I	^{124}Te(p, n)^{124}I	12→8	16
^{89}Zr	^{89}Y(p, n)^{89}Zr	12 →6	43
^{72}As	^{nat}Ge(p, xn)^{72}As	18 →8	93
^{55}Co	^{58}Ni(p, α)^{55}Co	15 →7	14

Conclusion

High production yields and separation efficacies of ^{90}Nb, high labeling yield procedures for the synthesis of ^{90}Nb-labeled monoclonal antibodies as well as excellent stability of the ^{90}Nb-labeled antibody rituximab prove the high potential of ^{90}Nb as isotope for *immuno*-PET. The high stability of the ^{90}Nb-Df complexes appears promising for further applications of ^{90}Nb in combination with biomolecules of intermediate and slow kinetic processes.

Acknowledgement

This project was financially supported by the COST action BM0607.

The authors thank the teams of TRIGA reactor Mainz for the production of ^{97}Zr the research reactor BERII at the Helmholtz Center in Berlin for production of ^{95}Zr,

Special thanks to Pr. H. Lueddens, the University Medical Center of the Johannes Gutenberg University Mainz, Germany for providing materials for *in vitro* evaluations.

References

1. Wu, A. M., Olafsen, T. Antibodies for molecular imaging of cancer. *Cancer J* 2008*;* 14; 191-7.
2. U. S. Food and Drug Administration, U. S. Department of Health and Human Services. [Website] 2010, *Available, from http://www.fda.gov*
3. Grillo-Lopez, A. J., White, C. A., Dallaire, B. K., Varns, C. L., Shen, C. G., Wei, A., Leonard, J. E., McClure, A., Weaver, L., Cairelli, S., Rosenberg J. Rituximab: the first monoclonal antibody approved for the treatment of lymphoma. *Curr. Pharm. Biotechnol 2000;* 1; 1-9.
4. van Dongen, G. A. M. S., Visser, G. W. M., Lub-de Hooge, M. N., de Vries, E. G., Perk, L. R. *Immuno-PET*: A navigator in monoclonal antibody development and applications. *Oncologist2007;* 12; 1379-89.
5. Nayak, T. K., Brechbiel, M. W. Radioimmunoimaging with longer-lived positron-emitting radionuclides: potentials and challenges. *Bioconjug. Chem.* 2009; 20, 825- 41.
6. Qaim, S. M. Decay data and production yields of some non-standard positron emitters used in PET. *Q J Nucl Med Mol Imaging* 2008; 52; 111-20.
7. Qaim, S. M. Development of novel positron emitters for medical applications: nuclear and radiochemical aspects. *Radiochim Acta* 2011; 99; 611-625.
8. Perk, L. R., Visser, O. J., Stigter-van Walsum, M., Vosjan, M. J. V. D., Visser, G. V. M. Zijlstra, J. M., Huijgens, P. C., van Dongen, G. A. M. S. Preparation and evaluation of ^{89}Zr-Zevalin for monitoring of ^{90}Y-Zevalin biodistribution with positron emission tomography. *Eur J Nuc. Med Mol Imaging* 2006; 33; 1337-45.
9. Börjesson, P. K., Jauw, Y. W., Boellaard, R., Bree, de R., Comans, E. F. I., Roos, J. C., Castelijns, J. A., Vosjan, M. J. V. D., Kummer, J. A., Leemans, C. R., Lammerstma, A. A., van Dongen, G. A. M. S. Performance of immuno-positron emission tomography with zirconium-89-labeled chimeric monoclonal antibody U36 in the detection of lymph node metastases in head and neck cancer patients. *Clin Canc Res* 2006; 12; 2133-40.
10. Divgi, C. R., Pandit-Taskar, N., Jungbluth, A. A., Reuter, V. E., Goenen, M., Ruan, S., Pierre, C., Nagel, A., Pryma, D. A., Humm, J., Larson, S.M., Old, L. J., Russo, P. Preoperative characterisation of clear-cell

renal carcinoma using iodine-124-labelled antibody chimeric G250 (^{124}I-cG250) and PET in patients with renal masses: a phase I trial. *Lancet Oncol* 2007; 8; 304-10.

11. Deffar, K., Hengliang, S., Liang, L., Wang, X., Zhu, X. Nanobodies—the new concept in antibody engineering. *African J Biotechnology* 2009; 8; 2645-52.

12. Eder, M., Knackmuss, S., Le Gall, F., Reusch, U., Rybin, V., Little, M., Haberkorn, U., Mier, W., Eisenhut, M. ^{68}Ga-labelled recombinant antibody variants for immuno-PET imaging of solid tumours. *Eur J Nucl Med Mol Imaging* 2010; 37; 1397-407.

13. Paudyal, B., Paudyal, P., Oriuchi, N., Hanaoka, H., Tominaga, H., Endo, K. Positron emission tomography imaging and biodistribution of vascular endothelial growth factor with ^{64}Cu-labeled bevacizumab in colorectal cancer xenografts. *Cancer Science* 2011; 102; 117-21.

14. Herzog, H., Rösch, F., Stöcklin, G., Lueders, C., Qaim, S. M., Feinendegen, L. E. Measurement of pharmacokinetics of yttrium-86 radiopharmaceuticals with PET and radiation dose calculation of analogous yttrium-90 radiotherapeutics. *J Nucl Med* 1993; 34; 2222-6.

15. Rossin, R., Berndorff, D., Friebe, M., Dinkelborg, L. M., Welch, M. J. Small-animal PET of tumor angiogenesis using a ^{76}Br-labeled human recombinant antibody fragment to the ED-B domain of fibronectin. *J Nucl Med* 2007; 48; 1172-9.

16. Browne, E., Firestone, R. B.: Table of Radioactive Isotopes, Lawrence Berkeley Laboratory University of California 1986.

17. Qaim, S. M., Bisinger, T., Hilgers, K., Nayak, D., Coenen, H. H. Positron emission intensities in the decay of ^{64}Cu, ^{76}Br and ^{124}I. *Radiochim Acta* 2007; 95; 67-73.

18. Busse, S., Brockmann, J., Roesch, F. Radiochemical separation of no-carrier-added radioniobium from zirconium targets for application of ^{90}Nb-labelled compounds. *Radiochim Acta* 2002; 90; 411-415.

19. Busse, S., Roesch, F., Qaim, S. M. Cross section data for the production of the positron emitting niobium isotope ^{90}Nb *via* the ^{90}Zr(*p, n*)-reaction. *Radiochim Acta* 2002; 90; 1-5.

20. Busse, S. Produktion, radiochemische Abtrennung und koordinative Kopplung von ^{90}Nb zur Synthese potentieller Radiopharmaka für die Positronenemissionstomographie. PhD. thesis, *Univeristy of Mainz;* 2000

21. Verel, I., Visser, G. W. M., Boellaard, R., van Walsum, S. M., Snow, G. B., van Dongen, G. A. M. S. ^{89}Zr *immuno*-PET: comprehensive procedures for the production of ^{89}Zr-labeled monoclonal antibodies. J Nucl Med 2003; 44; 1271-81.

22. Perk, L. R., Vosjan, M. J., Visser, G. W., Budde, M., Jurek, P., Kiefer, G. E., van Dongen G. A. M. S. p-Isothiocyanatobenzyl-desferrioxamine: a new bifunctional chelate for facile radiolabeling of monoclonal antibodies with zirconium-89 for immuno-PET imaging. *Eur J Nucl Med Mol Imaging* 2009; 37; 250-259.

23. Meares, C. F., McCall, M. J., Reardan, D. T., Goodwin, D. A., Diamanti, C. I., McTique, M. Conjugation of antibodies with bifunctional chelating agents: isothiocyanate and bromoacetamide reagents, methods of analysis, and subsequent addition of metal ions. *Anal Biochem* 1984; 142; 68-78.

3.2 Separation of ^{90}Nb from zirconium target for application in *immuno*-PET

Separation of ^{90}Nb from zirconium target for application in *immuno*-PET

V. Radchenko[1], D. V. Filosofov[2], O. K. Bochko[2], N. A. Lebedev[2], A. V. Rakhimov[2], H. Hauser[3], M. Eisenhut[3], N. V. Aksenov[4], G. A. Bozhikov[4], B. Ponsard[5], F. Roesch[1*]

[1] Institute of Nuclear Chemistry, Johannes Gutenberg-University Mainz, Fritz-Strassmann-Weg 2, D-55128 Mainz, Germany;

[2] Dzhelepov Laboratory of Nuclear Problems, Joint Institute of Nuclear Research, Joliot-Curie 6, 141980, Dubna, Moscow region, Russian Federation;

[3] Radiopharmaceutical Chemistry, German Cancer Research Center, Im Neuenheimer Feld 280, D-69120 Heidelberg, Germany;

[4] Flerov Laboratory of Nuclear Reactions, Joint Institute of Nuclear Research, Joliot-Curie 6, 141980, Dubna, Moscow region, Russian Federation;

[5] Radioisotopes and Silicon Production, Belgian Nuclear Research Centre, Boeretang 200, BE-2400 Mol, Belgium

Abstract

Fast progressing *immuno*-PET asks to explore new radionuclides. One of the promising candidates is ^{90}Nb. It has a half-life of 14.6 hours that allows visualizing and quantifying biological processes with medium and slow kinetics, such as tumor accumulation of antibodies and antibodies fragments or drug delivery systems and nanoparticles. ^{90}Nb exhibits a positron branching of 53% and an average kinetic energy of emitted positrons of E_{mean} = 0.35 MeV. Currently, efficient radionuclide production routes and Nb^{V} labeling techniques are explored to turn this radionuclide into a useful imaging probe. However, efficient separation of ^{90}Nb from irradiated targets remains in challenge.

Ion exchange based separation of 90Nb from zirconium targets was investigated in systems AG 1x8 – HCl/ H_2O_2 and UTEVA - HCl. ^{95}Nb ($t_{1/2}$ =35.0 days), ^{95}Zr ($t_{1/2}$ = 64.0 days) and ^{92m}Nb ($t_{1/2}$ = 10.15 days) were chosen for studies on distribution coefficients. Separation after AG1x8 anion exchange yields 99% of $^{90/95}$Nb. Subsequent use of a solid-phase extraction step on UTEVA resin further decontaminates $^{90/95}$Nb from traces of zirconium with yields 95% of $^{90/95}$Nb.

A semi-automated separation takes one hour to obtain an overall recovery of $^{90/95}$Nb of 90%. The amount of Zr was reduced by factor of 10^8. The selected separation provides rapid preparation (< 1 h) of high purity ^{90}Nb appropriate for the synthesis of ^{90}Nb-radiopharmaceutical, relevant for purposes of *immuno*-PET. Applying the radioniobium obtained, $^{90/95}$Nb-labeling of a monoclonal antibody (rituximab) modified with desferrioxamine achieved labeling yields of > 90% after 1 hour incubation at room temperature.

Keywords: niobium-90, niobium-95 / anion exchange / cation exchange / solid extraction / UTEVA / monoclonal antibody / desferrioxamine / labeling

Introduction

Molecular imaging plays a key role in tumour diagnosis as well as in evaluation of new drugs for tumour treatment [1, 2]. The advantage of molecular imaging techniques over more conventional readouts is that they can be performed *in vivo* with sufficient spatial and temporal resolution and high sensitivity and selectivity. In particular, positron emission tomography (PET) offers sensitivity with unlimited depth

penetration imaging on a picomolar level of concentrations, which is not achievable by other techniques so far [3].

2-[^{18}F]fluoro-desoxy-D-glucose(FDG) is the most widely used tracer for PET imaging in oncology and has been extensively evaluated and established in clinical routine for initial staging, assessment of response to therapy, and diagnosis of recurrent disease in many tumors including lymphoma, non-small-cell lung cancer, head and neck cancer, and colorectal cancer. However, [^{18}F]FDG is not a specific tracer and e. g. not able to discriminate cancer or inflammation and infection. In addition, many tumours do not exhibit high metabolic rates and thus are not properly diagnosed with [^{18}F]FDG. Therefore, there is an urgent need for new PET-radiopharmaceuticals for the specific detection of cancer which address tumor specific targets. In this context antibodies are appropriate candidates [4].

Although a rather low number of all antibodies developed make it to a worldwide use in clinics, more than 20 antibodies are currently approved by the US Food and Drug Administration [5]. A variety of engineered monoclonal antibodies (mAb) and antibody fragments for difference targets of interest is currently under preclinical investigation [6-8]. I*mmuno*-PET, which is tracking and quantifying of mAbs with PET, can be of great value in several stages of mAb development and application [9]. For faster pharmacokinetics, antibodies fragments with lower size have been developed [10]. Their enhanced clearance dramatically reduces the interval between radiotracer injection and the actual imaging to hours instead of days. Positron-emitting radionuclides with medium-long half-lives of interest for the PET-imaging with antibody fragments are, for example, ^{64}Cu ($t_{1/2}$ = 12.7 h) [11-13], ^{86}Y ($t_{1/2}$ = 14.7 h) [14, 15], ^{76}Br ($t_{1/2}$ = 16.0 h) [16, 17].

Several crucial factors and characteristics apply to radionuclide candidates for *immuno*-PET. The most important ones are: i) a physical half-life paralleling the biological half-life of the mAb or antibody fragment; ii) a high positron branching with no or weak accompanying other radiation (β^-, γ) to offer high-sensitive PET imaging while reducing the radiation burden of the patient; iii) a preferably low β^+-energy to allow high-resolution PET imaging; and iv) the availability of the radionuclide, i. e. an efficient production and radiochemical separation route.

In previous reports we proposed ^{90}Nb as promising candidate for application in *immuno*-PET [18-20]. Its intermediate half-life of 14.6 hours and a high positron branching of 53% may make ^{90}Nb an ideal candidate for application with antibody fragments, monoclonal antibodies, drug delivery systems and nanoparticles. A recent work described efficient labeling of a proof-of-principle monoclonal antibody (rituximab) with ^{90}Nb. The *in vitro* stability of the ^{90}Nb-Df-mAb was high. These promising results urge us

to continue investigation on ^{90}Nb. In the present study an improved rapid separation strategy of ^{90}Nb from zirconium targets was developed. A reliable, fast and efficient separation process is mandatory to continue to investigate the preparation of ^{90}Nb-labeled monoclonal antibody on a more routine scale.

Materials and Methods

Materials

Reagents where purchased from Sigma-Aldrich (Germany) and used without further purification unless otherwise stated. Deionized water (18 MΩ cm^{-1}) and ultra pure HCl solution were used. No further special measures were taken regarding working under strict metal-free conditions. The mAb rituximab (MabThera®, 10 mg/ml) directed against CD20 was purchased from Roche Nederland BV (Woerden, The Netherlands). For purification of conjugated and labeled antibodies, PD-10 columns (GE Healthcare Life Science) were applied, for ion exchange chromatography resins AG 1x8 (200-400 mesh) (BioRad, USA,) and DOWEX 50x8 (200-400 mesh) (BioRad, USA) were used and for solid extraction UTEVA (diamyl, amylphosphonate) resin (100-150 μm) (Triskem, France) was applied.

Distribution coefficients as well as the production yield, radionuclidic purity, radiochemical purity and separation yield of $^{90/95}$Nb were determined by γ-ray spectroscopy. The γ-ray spectroscopy was performed using an Ortec HPGe detector system and Canberra Genie 2000 software. The dead time of the detector was always kept below 10%. The detector was calibrated for efficiency at all positions with the certified standard solution QCY48, R6/50/38 (Amersham, UK).

Production of $^{90/92m/95}$Nb and ^{95}Zr isotopes

Radionuclides for measurement of distribution coefficients

For determination of distribution coefficients ^{92m}Nb ($t_{1/2}$ = 10.12 days) and ^{95}Zr ($t_{1/2}$ = 64.0 days) were applied.

For production of ^{92m}Nb natural zirconium target foils (1.9 mg, 18x26 mm, 0.1 mm thickness) were irradiated for 1 hour at the Phasotron facility at the Joint Institute of Nuclear Research (JINR), Dubna, Russian Federation, at 100 MeV proton energy and 3 μA current.

^{95}Zr was extracted from thorium metal target (1.2 g) irradiated at Phasotron facilities in JINR with protons energy 300 MeV and current 5 μA for 5 hour.

Radionuclides for development of separation strategies

To optimize a radioniobium/ zirconium separation protocol, ^{90}Nb and ^{95}Nb were employed. ^{95}Nb was produced via the ^{94}Zr(n, γ)→^{95}Zr(β^-, $t_{1/2}$ = 64 d)→^{95}Nb reactions from natural zirconium granules (1-3 mm, 99.8% ChemPur, Germany). Neutron irradiations were performed at the TRIGA reactor at the University of Mainz, Germany, and at the research reactor BR2 at the Belgian Nuclear Research Centre, Belgium. In the latter case 400 mg of zirconium granules were irradiated at a neutron flux of $3.5 \cdot 10^{14}$ $s^{-1} \cdot cm^{-2}$ (BR2) for 14 days.

^{90}Nb was produced via the ^{90}Zr(p,n)^{90}Nb reaction at the cyclotron MC32NI of the German Cancer Research Center Heidelberg. For irradiation, a stack of three discs of natural zirconium (natural abundance 51.45% ^{90}Zr) foils of 10 mm diameter and a thickness of 0.25 mm each were used. Irradiation was performed at 20 MeV proton energy and a current of 5 μA for 1 hour. This initial proton energy was decreased by using an aluminum holder cover of 0.5 mm thickness to 17.5 MeV entering the 1st foil of Zr. At 24 hours after end of irradiation (EOB), activities of $^{90/92m/95}$Nb and ^{95}Zr were measured by γ-ray spectroscopy and production yields and impurities were determined.

Main gamma lines of the radionuclides are listed in Table 1.

Table 1: Main gamma emission energies of radionuclides used in this work [21].

Radionuclide	$T_{1/2}$ days	Main γ emission energies (KeV)	Abundance (%)
^{92m}Nb	10.2	934.5	99.0
^{90}Nb	0.61	1129.0	82.0
^{95}Zr	64.0	724.2	44.2
		756.7	54.0
^{95}Nb	35.0	765.8	100.0

Determination of distribution coefficients and preliminary separation experiments

Preparation of stock solutions

^{92m}Nb was extracted from the irradiated zirconium target by anion exchange chromatography. In short, the zirconium target was placed into a plastic vial, and water (3 mL) and 28 M HF (1.5 mL) were added. For complete target dissolution an excess of conc. hydrofluoric acid (4 mL) was added. The mixture was loaded on a column filled with 500 mg of AG 1x8 resin, 200-400 mesh in F^- form. The column was washed with conc. HF (20 mL) and ^{92m}Nb was eluted with a mixture of 6 M HCl / 1% H_2O_2 (2 mL).

The procedure for extraction of ^{95}Zr from irradiated thorium target was described in [22].

Finally, fractions contained ^{92m}Nb and ^{95}Zr were evaporated to dryness and dissolved in 6 M HCl (2 mL).

Preparation and conditioning of resins

For determination of distributions coefficients, the anion exchange resin AG 1x8, 200-400 mesh (4 g) was applied. The resin was first washed with water (10 mL), and then transferred to the Cl^- form via washing with 12 M HCl (20 mL). Finally, the resin was additionally washed with water (10 mL) to remove excess of Cl^-, and kept until drying for 48 hours at room temperature.

The UTEVA resin was applied without further preconditioning.

Procedure for distribution coefficients determination

Distribution coefficients were determined by batch mode according to the following procedures:

50 mg of resin were placed in a 2 mL tube, then 1 mL of solution of appropriate concentrations of HF or HCl/H_2O_2 and 5 µL of the radionuclides stock solution were added. The mixture was vigorously stirred and allowed to stay for 24 hours (4 hours for mixtures contained hydrogen peroxide) at room temperature. Next, the mixtures were centrifuged and 900 µL of the solution was taken and measured by γ-ray spectroscopy. Distribution coefficient were calculated from equations (1), were $A_{50mg(res.)}$ is the activity in 50 mg of the resin and $A_{50\mu L(sol.)}$ is the activity in 50 µL of solution.

$$K_d = \frac{C^{eq.}_{phase1}}{C^{eq.}_{phase2}} = \frac{A_{1g(res.)}}{A_{1mL(sol.)}} = \frac{A_{50mg(res.)}}{A_{50\mu L(sol.)}} \qquad (1)$$

Preliminary separation experiments

The K_d values determined in the batch mode served for understanding of the principle behavior of Nb^{V} and Zr^{IV} on anion exchange resins and on UTEVA in hydrofluoric and mixed hydrochloric and peroxide media. In addition, dynamic experiments were conducted.

Separation of Zr^{IV} and Nb^{V} on anion exchange column

500 mg of pre-conditioned anion exchange resin in F^- from was placed in plastic column (1.5x7 cm). 260 mg of natural metallic zirconium spiked with ^{95}Zr and ^{92m}Nb was dissolved in 28 M hydrofluoric acid (5 mL) and passed through the column. The column was additionally washed with 28 M hydrofluoric acid (35 mL) to examine the breakthrough of Nb^{V}. Elution of niobium was performed later on by using of mixture 6M HCl/2.44% H_2O_2. Fractions of 1 mL were collected.

Dependence of concentration of hydrogen peroxide on elution of Nb^{V}

The elution profile of Nb^{V} was examined in the presence of various hydrogen peroxide concentrations. A procedure similar to one described in the previous chapter was applied until the step of niobium elution. Then the column was washed with 6 M HCl (11 mL) and later with 6 M HCl/0.5 % H_2O_2 (8 mL). Fractions of 1 mL were collected.

Separation of Zr^{IV} and Nb^{V} on UTEVA resin

The behavior of Zr^{IV} and Nb^{V} on UTEVA resin was evaluated in HCl media. Separation profiles for no-carrier-added $^{95}Zr^{IV}$ and $^{92m}Nb^{V}$ were measured for UTEVA (100-150 μm) in 4x75 mm columns in HCl. Aliquots from the stock solution were loaded on the column in 9 M HCl (1 mL) and next the column was consistently washed with 5.5 M HCl (3 mL), 4.5 M HCl (3 mL) and 2 M HCl (6 mL).

Separation strategy

Target dissolution

The irradiated zirconium target, typically (260±3 mg), was placed into a 15 mL plastic vial and water (500 μL) was added. For dissolution, 28 M hydrofluoric acid (500 μL) was portionally added and after full dissolution concentrated hydrofluoric acid (1 mL) was added.

Crude separation

Based on the distribution coefficients and preliminary separations, the following separation strategy was established.

2 mL of 21 M hydrofluoric acid containing the irradiated zirconium target were passed trough the cation exchange column (DOWEX 50x8 resin, 200-400 mesh, 10x5 mm, 100 mg) resin in F^- form for removal of colloids, unsolved target particles and possible trace contamination of 2+ and 3+ charged metal cations, which may originate from target impurities. The column was additionally washed with concentrated hydrofluoric acid (1 mL). The solution (3 mL) which passed the cation exchange resin was transferred to an anion exchange column (300 mg, 25x5 mm) filled with AG 1x8 resin (200-400 mesh) resin in F^- form. Nb^V remained on this resin and the bulk amount of Zr^{IV} passed through. The column was washed with concentrated HF (4.5 mL) to elute traces of Zr^{IV}, while $^{90/95}$Nb stays on the column. To completely remove traces of hydrofluoric acid prior to elution of Nb^V, the column was washed with 1 M HCl (1 mL). Next 6 M HCl/1% H_2O_2 (500 μL) were passed through the column and collected. Finally, $^{90/95}$Nb was eluted with another 500 μL of the same mixture. To remove the hydrogen peroxide, this $^{90/95}$Nb fraction was heated for 5 minutes at 120°C.

Final purification of $^{90/95}$Nb on UTEVA resin

A small column (100 mg, 10x5 mm) was filled with UTEVA resin. To 6 M HCl (700 μL) fraction containing $^{90/95}$Nb, 12 M HCl (700 μL) were added. This 1.4 mL of solution was passed through the UTEVA which was next washed with 5 M HCl (5 mL). Traces of zirconium(IV), and Nb^V remains absorbed on the column. For elution of $^{90/95}$Nb 1 M oxalic acid was applied. The column was washed with 200 μL and Nb eluted with another 400 μL of 1 M oxalic acid. The decontamination factor Zr/Nb was measured by inductively coupled plasma mass spectrometry (ICP-MS) and γ-ray.

Development of a semi-automated module

The manually performed process takes about 1.5 - 2 hours. To shorten the separation time, a semi-automated module was developed, cf. Fig. 1.

The transfer of solutions is carried out under pressure of argon (99.996 Vol. %, Westfalen AG, Germany). All parts of the module were made from resistant to hydrofluoric acid materials (polyethylene, polyether ether ketone (PEEK), teflon).

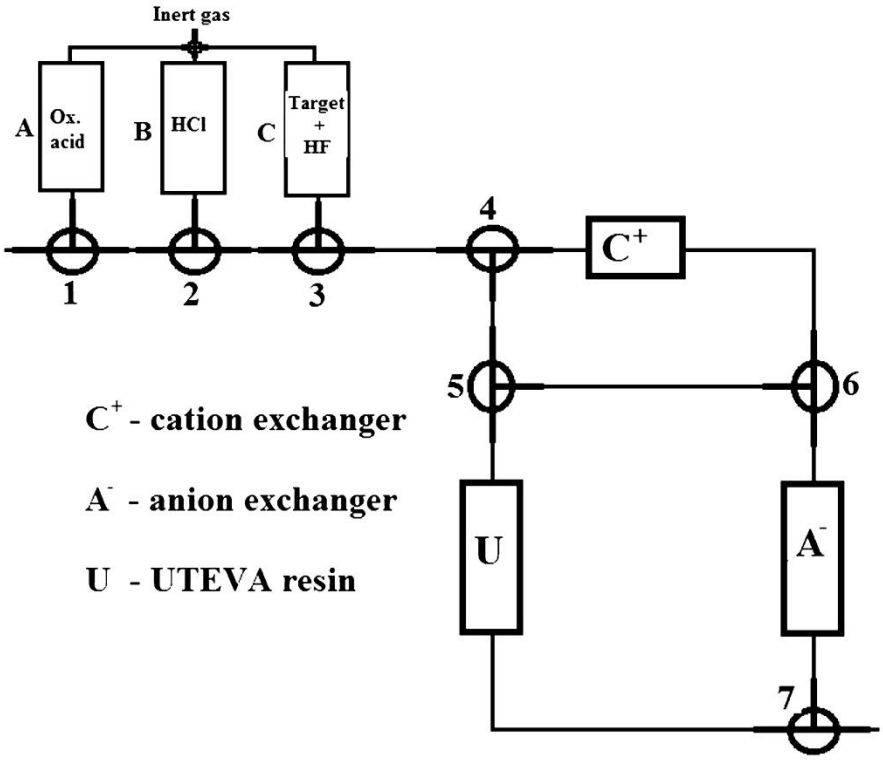

Figure 1: Schematic view of semi-automated separation module.

The irradiated zirconium target was placed into vial C with addition of water (500 µL). Hydrofluoric acid (500 µL) was added portionally through the tube, and after full target dissolution 1 mL HF was added. The two milliliters were passed through the cation and anion exchange columns (valves 3, 4 and 6). To vial C another 1 mL of hydrofluoric acid was added to pass by the same way. Subsequently, 4.5 mL of 28 M HF was passed through the anion exchange column (valves 4, 5 and 6). The anion exchange column was washed with 1 M HCl (1 mL) from vial B (valves 2 and 3). ^{95}Nb was eluted from anion exchanger with a mixture of 6 M HCl/ 1% H_2O_2. The first 500 µL were passed through and another 700 µL contained $^{90/95}$Nb.

After 5 minutes heating at 120 °C another 700 µL of 12 M HCl were added. The mixture was loaded in vial B and passed through the UTEVA resin (valves 5 and 7). In vial B 5 M HCl (5 mL) was loaded and passed through the UTEVA resin. Finally, 1 M oxalic acid from vial A, was applied to elute $^{90/95}$Nb. The first 200 µL of oxalic acid were passed through UTEVA resin (valves 1 and 2) and $^{90/95}$Nb was eluted with the following 400 µL into an extern product vial.

Preparation of ^{90}Nb-labeled N-suc-Df-rituximab

To demonstrate the potential of $^{90/95}$Nb separated as described, the Df-conjugated monoclonal antibody N-suc-Df-rituximab [23], Fig. 2, was labeled with ^{90}Nb in HEPES buffer at pH 7.0. The labeling procedure was similar to a protocol developed for ^{89}Zr [24]. In short, to 200 µL $^{90/95}$Nb (37 MBq for ^{90}Nb) in 1 M oxalic acid a solution of 2 M Na_2CO_3 (90 µL) was added and the mixture was allowed to stay for 3 minutes. Next, 0.5 M HEPES buffer (300 µL) pH 7.2 and N-suc-Df-mAb (250 µg) were added. Finally, 0.5 M HEPES buffer (700 µL) were added. The overall volume of the reaction mixture was 2 mL. The mixture was incubated for 1 hour at room temperature. $^{90/95}$Nb-N-suc-Df-mAb was purified on a PD-10 column using 0.9% sodium chloride solution as mobile phase.

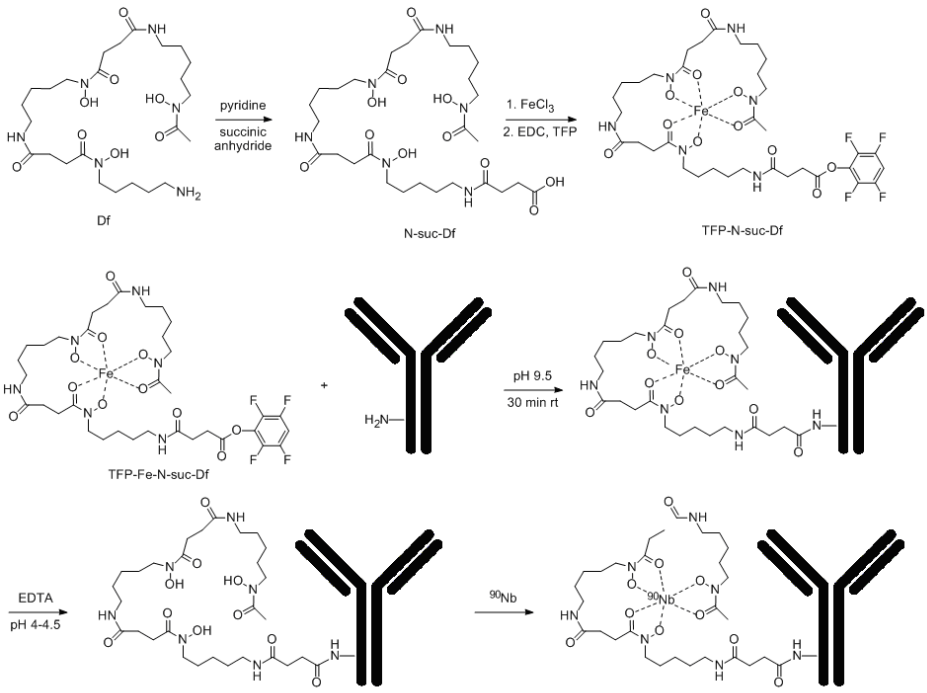

Figure 2: Df-conjugation via TFP-N-suc-Df-Fe and labeling with ^{90}Nb.

Results

Production of niobium and zirconium isotopes

^{92}Nb: Two weeks after irradiation, the isotopic content of the irradiated zirconium target was evaluated by γ-ray spectroscopy. At this time point, the activity of ^{92m}Nb ($t_{1/2}$ = 10.15 days) was 2.5 MBq, Radiochemical separation recovered more than 90% of ^{92m}Nb.

^{95}Zr/^{95}Nb: More than 500 MBq of ^{95}Zr was produced at the BR2 reactor after 14 days of irradiation at a flux of thermal neutrons of $3.5 \cdot 10^{14}$ $s^{-1} \cdot cm^{-2}$. The maximum daughter activity of ^{95}Nb as generated from ^{95}Zr was obtained at ~67 d after EOB.

^{90}Nb: The overall ^{90}Zr(p, n) irradiation yield of ^{90}Nb for 1 h and 5 μA irradiations was 720 ± 50 MBq, i. e. 145±10 MBq/μAh under the given irradiation parameters. The isotopic purity of ^{90}Nb after EOB was more than 97%. Minor isotopic impurities found were: ^{92m}Nb ($t_{1/2}$ 10.2 d) = 1.64%, ^{95}Nb ($t_{1/2}$ 35.0 d) = 0.08%, ^{95m}Nb ($t_{1/2}$ 3.6 d) = 0.29% and ^{96}Nb ($t_{1/2}$ 23.35 h) = 0.88%.

Determination of distribution coefficients

Distribution coefficients to understanding the behaviour of Zr^{IV} and Nb^{V} on anion exchange resin and UTEVA in HCl/ H_2O_2 media in static system are shown in Figures 3,4 and 5 respectively.

However, determination of K_d values in HCl/H_2O_2 were accompanied with some complicity. Incubation time is needed to setup equilibrium between tracers, resin and media, but this equilibrium is disturbed because hydrochloric acid reacts with hydrogen peroxide and with time changes its concentration. Therefore 4 hours was founded to be optimum incubation time for radionuclides equilibrium from one hand and for the other hand not sufficient concentration change. Errors in samples without peroxide were below 10% and in presence of peroxide up to 30%.

Zr^{IV} and Nb^{V} distribution coefficients in the system AG 1x8 - HCl/H_2O_2

Distribution coefficients in various hydrochloric acid concentrations and mixtures of HCl and hydrogen peroxide are illustrated in Fig. 3 for the anion exchange process.

Any significant difference in presence of hydrogen peroxide was not observed. However, K_d values are slightly high with H_2O_2. With increasing of concentration of hydrochloric acid, distribution coefficients, decrease especially in low HCl concentrations (0-4 M). From 6 M HCl while on effects insignificant. Such relation is in good agreement with previous work [25].

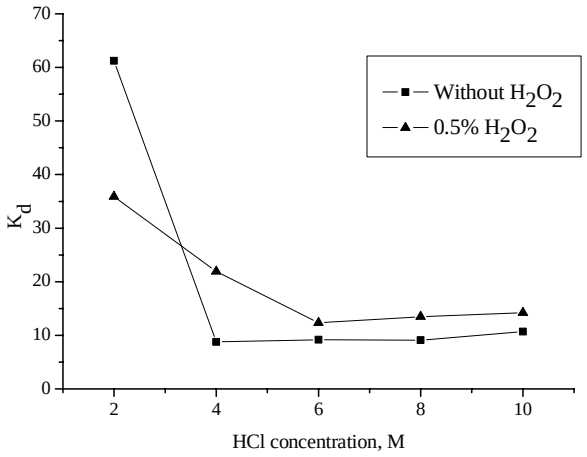

Figure 3: K_d values for Nb^{V} in the system AG 1x8 (200-400 mesh) – HCl.

Slightly different behaviour of Zr^{IV} and Nb^{V} in presence of 0.5 % peroxide was observed. K_d values for Zr^{IV} are lower than for Nb^{V}, and maximal differences can be seen at low HCl concentrations (0-4 M) (Fig. 4). This represents an advantageous option for additional decontamination of niobium from zirconium.

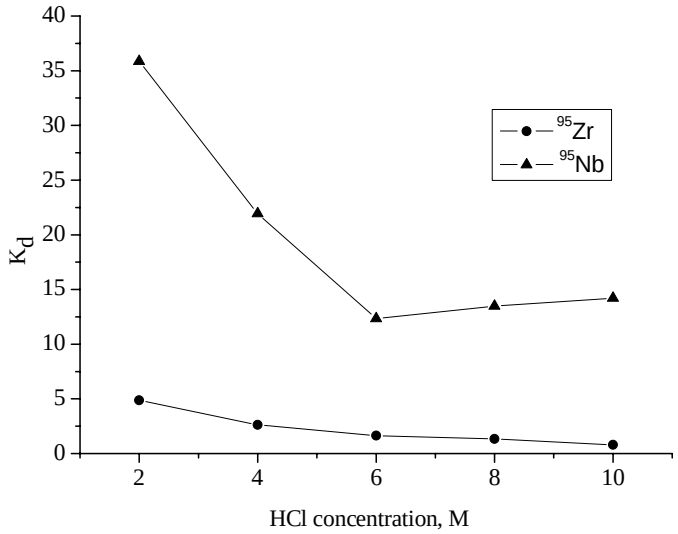

Figure 4: K_d values for Zr^{IV} and Nb^{V} in system AG 1x8 (200-400 mesh) – HCl – 0.5 % H_2O_2.

Zr^{IV} and Nb^{V} distribution coefficients in the system UTEVA-HCl.

Studies on sorption of zirconium and niobium on UTEVA resin in hydrochloric acid are shown in Figure 5. At low HCl concentration, Zr^{IV} and Nb^{V} show a similar distribution. However, with increasing concentration of hydrochloric acid significant differences in K_d appear. Between 6 and 8 M HCl, K_d values are much higher for Nb^{V}

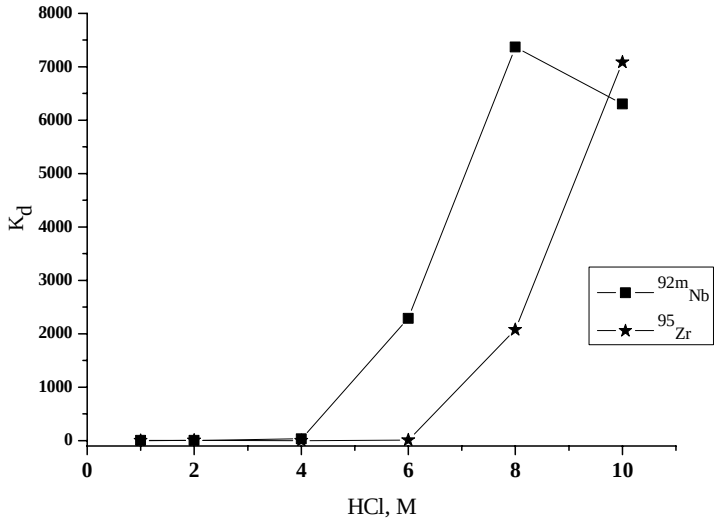

Figure 5: K_d values for Zr^{IV} and Nb^{V} in the system UTEVA – HCl.

Preliminary separation experiments

To transfer data on distribution coefficients from static condition to "real" situations, several preliminary separation experiments were conducted to determine optimal parameters for final separation procedure.

Separation of Zr^{IV} and Nb^{V} on anion exchange column

The separation profile of Zr^{IV} and Nb^{V} (Fig. 7) allow a crude separation of radioniobium from bulk amounts of zirconium.

The first fraction (40 mL) contained >99% of the ^{95}Zr while no breakthrough of Nb^{V} was measured. Subsequent washing the column with a mixture of 6 M HCl/2.44% H_2O_2 elutes ^{92m}Nb . Most of its activity (≥ 99%) was found in fractions 5-7 (3 mL), with no activity of ^{95}Zr detected.

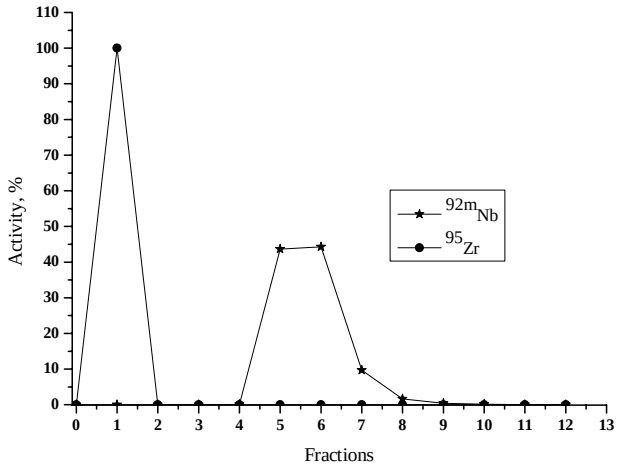

Figure 6: Separation profile of Zr^{IV} and Nb^{V} on anion exchange column in hydrofluoric media.

Effect of H_2O_2 on the elution of Nb^{V}

Despite the K_d values which did not show sufficient differences in presence of hydrogen peroxide and without, there is a significant effect when eluting ^{92m}Nb from the anion exchange column. 6 M HCl elutes radioniobium as broad peak f10-f20 (10 mL) and allows eluting ≤ 50% of the ^{92m}Nb activity. However, after applying a mixture of 6 M HCl/ 0.5% H_2O_2 from fraction 21, the remaining ^{92m}Nb was eluted in 1.5 mL of that mixture (Figure 8). Such disagreement between column separation and distribution coefficients can be explained by the phase contact time.

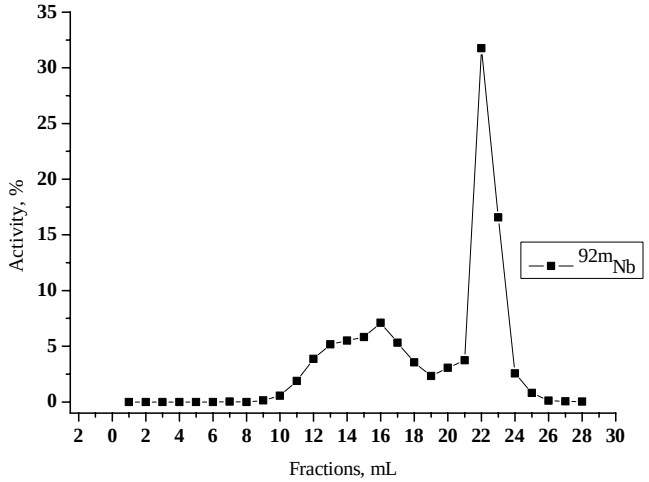

Figure 7: Elution profile of Nb^{V} from anion exchange column in HCl/H_2O_2.

Separation of Zr^{IV} and Nb^{V} on UTEVA resin

Based on distribution coefficients, a preliminary separation was tested with no-carrier-added Zr^{IV} and Nb^{V} on UTEVA resin in various concentrations of HCl. The most effective separation was achieved with HCl (Fig. 9). Elution of Zr^{IV} at 5.5 M HCl was almost quantitative (≥ 99%), Nb^{V} was eluted completely with of 2 M HCl (4 mL).

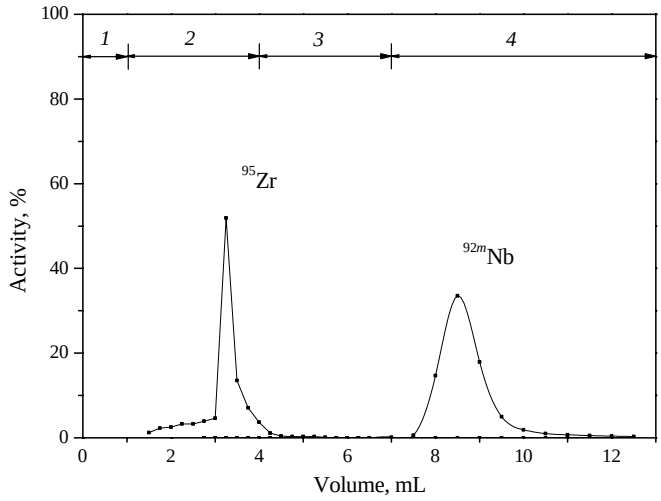

Figure 8: Elution profile of Zr^{IV} and Nb^{V} from UTEVA column (4x75 mm) with various HCl concentrations: 1- 9 M HCl, 2- 5.5 M HCl, 3- 4.5 M HCl, 4- 2 M HCl.

Separation strategy

The overall separation proceeds with a separation yield of more than 99% of $^{90/95}$Nb after anion exchange. The final fraction of 1 M oxalic acid (400 µL) contains more than 95% of $^{90/95}$Nb. The whole separation procedure takes around 1.5 hours, which is almost 4 times faster than the previous separation method [19]. The decontamination factor for Zr after anion exchange was $1 \cdot 10^{5}$ and after UTEVA purification $3 \cdot 10^{8}$. This decontamination factor equals 0.77 ng of zirconium presented in final fraction for a 260 mg zirconium target.

This procedure was adapted to a semi-automated separation module. The separation yield of $^{95/90}$Nb in the final fraction was somewhat lower (90%) what can be explained by losses on valves and tubes during

the separation procedure. However, this takes even shorter time (1 hour) and allows remote operation that is very important factor in case of high activity irradiations.

Proof-of-principle labeling of N-suc-Df-rituximab

The N-suc-Df-rituximab modification yielded about 1.5 molecules of N-suc-Df per antibody. The $^{90/95}$Nb labeling kinetics indicate that radiochemical yield reached 60% already after 15 min and increased to more than 90% after 50 min (95% analyzed by instant thin layer chromatography (ITLC) and 93% by size exclusion chromatography (SEC)). After SEC separation on a PD-10 column, the $^{90/95}$Nb-Df-mAb was of 99.0% purity.

Discussions

Our aim was to develop an improved separation protocol. Isolation of ^{90}Nb should be fast, effective and less complicated compared to known protocols. It should provide a reliable source of ^{90}Nb with appropriate properties for following labelling reactions.

From many complexes which Nb^{V} forms with different compounds, flouro complexes of niobium are mainly studied and predictable. Therefore we initially designed our new separation strategy on the very different behaviour of Zr^{IV} and Nb^{V} in hydrofluoric media. Due to future application of ^{90}Nb for medical purposes, however, the absence of traces of hydrofluoric acid in the final product are obligatory. Therefore we decided applying a two-step separation procedure, were the first step allows crude removal of the target material, followed by a second step for additional purification and conditioning for following medical application.

Compared to previous separation methods [19], including multistep separations by liquid-liquid extraction and anion exchange, the alternative separation strategy developed is: i) decreased separation time by factor of four (from 4 to 1 hour); ii) increased separation yield to 90-95% (instead of 76-81% for previous strategy); iii) 10 fold improved decontamination factor for Zr/Nb (> 10^{8}), that will allow preparation of radiopharmaceuticals with higher specific activity (in case of a standard target setup, just 0.77 ng of Zr will be presented in final fraction); and iv) designed and tested in a semi-automated separation module for remote separation.

The final elution of Nb^{V} in 1 M oxalic acid allows keeping radio-Nb in an appropriate species for subsequent labeling and prevents possible hydrolyzation. The $^{90/95}$Nb fraction obtained is adequate to subsequent radiolabeling

The purified $^{90/95}$Nb proved excellent labelling of a N-suc-Df conjugated for purposes of *immuno*-PET. Thus developed separation strategy provides a reliable source of ^{90}Nb for application in *immuno*-PET.

Acknowledgment

The authors thank the teams of TRIGA reactor Mainz for the production of ^{97}Zr the research reactor BR2 at Belgian Nuclear Science Centre in Mol, Belgium for production of ^{95}Zr, and the team of Phasotron operators at JINR for production of Nb and Zr isotopes.

Specially thanks to Dr. Happel for providing of UTEVA resin.

Thanks to Danielle Vugts VU University Medical Centre in Amsterdam for providing of premodified antibody for testing labeling.

References

1. Willmann, J. K., van Bruggen, N., Dinkelborg, L. M., Gambhir, S. S. Molecular imaging in drug development. *Nature Rev Drug Disc* 2008; 7; 591-607.
2. Ottobrini, L., Ciana, P., Biserni, A., Lucignani, G., Maggi, A. Molecular imaging: a new way to study molecular processes *in vivo*. *Mol Cell Endocrinol* 2006; 246(1-2); 69-75.
3. Czernin, J., Weber, W. A., Herschman, H. R. Molecular imaging in the development of cancer therapeutics. *Annu Rev Med* 2006; 57; 99-118.
4. Wu, A. M., Olafsen, T. Antibodies for molecular imaging of cancer. *Cancer J* 2008; 14; 191-7.
5. U. S. Food and Drug Administration, U. S. Department of Health and Human Services. [Website] 2010, Available, from http://www.fda.gov.
6. Carter, P. J. Potent antibody therapeutics by design. *Nature Rev Immunol* 2006; 6; 343-57.
7. Reichert, M. J., Rosensweig, C. J., Faden, L. B., Dewitz, M. C. Monoclonal antibody successes in the clinic. *Nature Biotechnology* 2005; 23; 1073-78.

8. Mould, D. R., Sweeney, K. R. D. The pharmacokinetics and pharmacodynamics of monoclonal antibodies –mechanistic modeling applied to drug development. *Cur Opinion in Drug Disc Dev* 2007; 10(1); 84-96.

9. van Dongen, G. A. M. S., Vosjan M. J. W. D. Immuno-Positron Emission Tomography: Shedding Light on Clinical Antibody Therapy. *Canc Biother & Radiopharm* 2010; 25(4); 375-85.

10. Boder, E. T., Jiang W. Engineering Antibodies for Cancer Therapy. *Ann Rev Chem and Biomol Engin* 2011; 2(1); 53-75.

11. Paudyal, B., Paudyal, P., Oriuchi, N., Hanaoka, H., Tominaga, H., Endo, K. Positron emission tomography imaging and biodistribution of vascular endothelial growth factor with ^{64}Cu-labeled bevacizumab in colorectal cancer xenografts. *Cancer Science* 2011; 102(1); 117-21.

12. Zhou, Y., Liu, S. ^{64}Cu-labeled phosphonium cations as PET radiotracers for tumor imaging. *Bioconjug Chem* 2011; 22(8); 1459-72.

13. Di Bartolo, N., Sargeson, A. M., Smith, S. V. New ^{64}Cu PET imaging agents for personalised medicine and drug development using the hexa-aza cage, SarAr. *Org Biomol Chem* 2006; 4(17); 3350-7.

14. Herzog, H., Rösch, F., Stöcklin, G., Lueders, C., Qaim, S. M., Feinendegen, L. E. Measurement of pharmacokinetics of yttrium-86 radiopharmaceuticals with PET and radiation dose calculation of analogous yttrium-90 radiotherapeutics. *J Nucl Med* 1993; 34; 2222-2226.

15. Nayak, T. K., Garmestani, K., Baidoo, K. E., Milenic, D. E., Brechbiel, M. W. PET imaging of tumor angiogenesis in mice with VEGF-A-targeted (86)Y-CHX-A″-DTPA-bevacizumab. *Int J Cancer* 2011; 128(4); 920-6.

16. Rossin, R., Berndorff, D., Friebe, M., Dinkelborg, L. M., Welch, M. J. Small-animal PET of tumor angiogenesis using a ^{76}Br-labeled human recombinant antibody fragment to the ED-B domain of fibronectin. *J Nucl Med* 2007; 48; 1172-9.

17. Watanabe, S., Hanaoka, H., Liang, J. X., Iida, Y., Endo, K., Ishioka, N. S.: PET imaging of norepinephrine transporter-expressing tumors using ^{76}Br-meta-bromobenzylguanidine. *J Nucl Med* 2010; 51(9); 1472-9.

18. Busse, S., Rösch, F., Qaim, S. M. Cross section data for the production of the positron emitting niobium isotope ^{90}Nb *via* the ^{90}Zr(*p, n*)-reaction. *Radiochim Acta* 2002; 90; 1-5.

19. Busse, S., Brockmann, J., Roesch, F. Radiochemical separation of no-carrier-added radioniobium from zirconium targets for application of ^{90}Nb-labelled compounds. *Radiochim Acta* 2002; 90; 411-15.

20. Radchenko, V., Hauser, H., Eisenhut, M., Vugts, J. D., van Dongen, G. A. M. S., Roesch, F. ^{90}Nb – a Potential PET Nuclide: Production and Labeling of Monoclonal Antibodies *Radiohim Acta* 2012; 100(11); 857-865.

21. Browne, E., Firestone, R. B. Table of Radioactive Isotopes, Lawrence Berkeley Laboratory *University of California*; 1986.

22. Filosovof, D. V., Bojikov, G. A., Sadiikov, I. I., Karaivanov, D. V., Lebedev, N. A., Norseev, Yu. V., Rakhimov A. V. Extraction of various radionuclides from Th target irradiated by 300 MeV protons. submitted to *Radiochimya*; 2013.

23. Verel, I., Visser, G. W. M., Boellaard, R., van Walsum, S. M., Snow, G. B., van Dongen, G. A. M. S. ^{89}Zr *immuno*-PET: comprehensive procedures for the production of ^{89}Zr-labeled monoclonal antibodies. *J Nucl Med* 2003; 44; 1271-81.

24. Vosjan, M. J. W. D., Perk, L. R., Visser, G. V. M., Budde M., Jurek, P., Kiefer, G. E., van Dongen, G. A. M. S. Conjugation and radiolabeling of monoclonal antibodies with zirconium-89 for PET imaging using the bifunctional chelate *p*-isothiocyanatobenzyl-desferrioxamine. *Nature Protocols* 2010; 5(4); 739-43.

25. Marchol, M. Ion Exchangers in Analytical chemistry: Their Properties and Use in Inorganic Chemistry. Volume 2, Prague, Czech Republic: *Academia*; 1982.

3.3 Direct flow separation strategy, to isolate no-carrier-added ^{90}Nb from irradiated Mo or Zr targets.

Direct flow separation strategy, to isolate no-carrier-added ^{90}Nb from irradiated Mo or Zr targets.

V. Radchenko[1], D. V. Filosofov[2], J. Dadakhanov[2], F. Roesch[1*]

[1] Institute of Nuclear Chemistry, Johannes Gutenberg-University Mainz, Fritz-Strassmann-Weg 2, D-55128 Mainz, Germany;

[2] Dzhelepov Laboratory of Nuclear Problems, Joint Institute of Nuclear Research, Joliot-Curie 6, 141980, Dubna, Moscow region, Russian Federation;

Abstract

immuno-PET is an emerging tool providing non-invasive, accurate imaging allows tumour visualization and precise therapy planning. Several radionuclides with long and intermediate half-lives are recently under evaluation.

^{90}Nb has an intermediate half-life of 14.6 hours, a high positron branching of 53% and an optimal energy of β^+ emission of E_{mean} 0.35 MeV only. It seems to be a potential candidate for application in *immuno*-PET. Out recent aim was to conduct studies on distribution coefficients for Zr^{IV} and Nb^{V} measurements in mixtures HCl/H_2O_2 and HCl/ oxalic acid for anion exchange resin (AG 1x8) and UTEVA to develop direct flow separation strategy for ^{90}Nb. Finally we also improved that this separation strategy also applicable in case of isolation of ^{90}Nb from irradiated molybdenum target.

Keywords: niobium-90 / zirconium, molybdenum / hydrogen peroxide / oxalic acid / anion exchange / cation exchange / UTEVA

Introduction

Molecular imaging is a powerful diagnostic tool which e. g. allows early tumor detection and precise therapy planning [1-3]. Positron Emission Tomography (PET) is modern diagnostic method based on positron annihilation, which provide non-invasive and quantitative imaging on picomolar level of tracer concentrations [4]. Currently, a “gold standard” for tumor diagnostic is ^{18}F-FDG, a probe of glucose utilization [5, 6]. This probe cannot provide such precise imaging which recent progress is needed. Novel tracers based on biomolecules such as antibodies, antibody fragments and peptides were developed to address specific molecular targets overexpressed in the course of tumor growth [7-10]. Labeling of, those biomolecules with positron emitting radionuclides in the last decade formed a branch called *immuno*-PET [11-14]. Here, radionuclides are needed which correlate with the pharmacology of these targeting vectors, such as the time needed to reach a maximal tumor-to-non-tumor ratio. This time can vary from several hours up to several days. Therefore radionuclides with appropriate half-life should be employed. In this context, several positron emitting radionuclides are under investigation (Tab. 1) [16, 17]. For longer lasting processes of up to one week (intact antibodies), radionuclides such as ^{89}Zr ($t_{1/2}$ = 78.4 h) [18-20] and ^{124}I ($t_{1/2}$ = 100.2 h) [21, 22] already commercially available. For distribution processes lasting a few

days, several radionuclides are currently under investigation for example, ^{64}Cu ($t_{1/2}$ = 12.7 h) [23-25], ^{86}Y ($t_{1/2}$ = 14.7 h) [26, 27], ^{76}Br ($t_{1/2}$ = 16.0 h) [28, 29].

Table 1: Decay characteristic of several PET radionuclides (nuclear data from [15]) relevant to immuno-PET imaging (listed with increasing $t_{1/2}$).

Radionuclide	Half-life (h)	Main production route	$E_{\beta+mean}$ (MeV) [β^+ abundance]	Three most intensive γ-emission (MeV) [abundance]
^{64}Cu	12.7	$^{64}Ni(p,n)^{64}Cu$ $^{64}Ni(d,2n)^{64}Cu$	0.05 [18.0%] (accompnied β^-, $E_{\beta\text{-mean}}$ 0.075 MeV [39.0%]	0.0074 [4.8%] 0.0075 [9.6%] 1.345 [0.48%]
^{90}Nb	14.6	$^{90}Zr(p,n)^{90}Nb$	0.35 [53.0%]	0.14 [66.7%] 1.13 [92.0%] 2.32 [82.0%]
^{86}Y	14.7	$^{86}Sr(p,n)^{86}Y$	0.22 [33.0%]	0.63 [32.6%] 1.08 [83.0%] 1.15 [30.5%]
^{76}Br	16.2	$^{76}Se(p,n)^{76}Br$ $^{75}As(^{3}He,2n)^{76}Br$	0.64 [54.0%]	0.55 [74.0%] 0.66 [15.9%] 1.85 [14.7%]
^{89}Zr	78.4	$^{89}Y(p,n)^{89}Zr$ $^{89}Y(d,2n)^{89}Zr$	0.09 [23.0%]	0.91 [100.0%] 1.71 [0.76%] 1.74 [0.13%]
^{124}I	100.2	$^{124}Te(p, n)^{124}I$ $^{124}Te(d, 2n)^{124}I$	0.19 [24.0%]	0.60 [63.0%] 0.72 [10.4%] 1.69 [10.9%]

Several crucial factors and characteristics apply to radionuclide candidates for *immuno*-PET. The most important ones are: i) a physical half-life paralleling the biological half-life of the mAb or antibody fragment; ii) a high positron branching with no or weak accompanying other radiation (β^-, γ) to offer high-sensitive PET imaging while reducing the radiation burden of the patient; iii) a preferably low β^+-energy to allow high-resolution PET imaging; and iv) the availability of the radionuclide, i. e. an efficient production and radiochemical separation route.

In our previous studies we proposed ^{90}Nb ($t_{1/2}$ =14.6 hours) with its positron branching of 53%, an optimal β^+ energy of E_{mean} 0.35 MeV as potential candidate for labeling of antibody fragments as well some intact antibodies. When searching for the most appropriate bifunctional chelator to attach ^{90}Nb to the biomolecules, desferrioxamine was examinated. In parallel we efficient production and separation strategies to isolate ^{90}Nb from irradiated zirconium targets, to provide adequate radionuclidic and radiochemical purity for subsequent application for *immuno*-PET [30, 31]. We were able to provide proof-of-principle by labeling of ^{90}Nb with monoclonal antibody (Rituximab) and demonstrated high labeling yields as well as stability of the labeled mAb [32]. For the latter, however, the two step protocol, i. e. transfer of Nb^V from ion exchange columns (allowing crude separation) to final purification by solid-phase extraction (SPE) on UTEVA including elution with a mixture of 6 M HCl/1% H_2O_2, though working very well, still asks for further improvement and simplification. Therefore, in this work we describe a “one pot” system for direct transfer of ^{90}Nb from anion exchange column to SPE. Additionally, we adopted this separation strategy to the separation of nca ^{90}Nb from irradiated molybdenum target instead of zirconium. By this separation strategy, Nb^V can be isolated from elements of the I to VII groups of periodic table which, can be present in no-carrier-added condition in the irradiated target materials.

Materials and methods

Materials

Reagents were purchased from Sigma-Aldrich (Germany) and used without further purification unless otherwise stated. Deionized water (18 MΩ cm^{-1}) and ultra-pure HCl solution were used. No further special measures were taken regarding working under strict metal-free conditions. Ion exchange chromatography

resins AG 1x8 (200-400 mesh) (BioRad®) and DOWEX 50x8 (200-400 mesh) (BioRad®) were used. For solid phase extraction UTEVA (diamyl, amylphosphonate) resin (100-150 μm) (Triskem, France) was applied. Distribution coefficients as well as the production yield, radionuclidic purity, radiochemical purity and separation yield of ^{90}Nb were determined by γ-ray spectroscopy. The γ-ray spectroscopy was performed using an Ortec HPGe detector system and Canberra Genie 2000 software. The dead time of the detector was always kept below 10%. The detector was calibrated for efficiency at all positions with the certified standard solution QCY48, R6/50/38 (Amersham, UK).

Production of $^{90/92m/95}$Nb and $^{95/88}$Zr isotopes

Radionuclides for measurement of distribution coefficients

For determination of distribution coefficients ^{92m}Nb ($T_{1/2}$ = 10.12 days), ^{95}Nb ($T_{1/2}$ = 35.0 days) and ^{88}Zr ($T_{1/2}$ = 83.4 days) were applied.

For production of ^{92m}Nb and ^{95}Nb natural molybdenum foil (0.761 g, 18x26 mm, 0.1 mm thickness) were irradiated for 30 minutes at the Phasotron facility at the Joint Institute of Nuclear Research (JINR), Dubna, Russian Federation, at 100 MeV proton energy and 3 μA current.

^{88}Zr was extracted from silver metal target (1.646 g) irradiated at Phasotron facilities in JINR with protons energy 660 MeV and current 2 μA for 3 hours.

Radionuclides for development of separation strategies

To optimize a radioniobium/zirconium separation protocol, ^{90}Nb and ^{95}Nb were employed. ^{95}Nb was produced via the ^{94}Zr(n, γ)→^{95}Zr(β^-, $t_{1/2}$ = 64 d)→^{95}Nb reactions from natural zirconium granules (1-3 mm, 99.8% ChemPur, Germany). Neutron irradiations were performed at the TRIGA reactor at the University of Mainz, Germany, and at the research reactor BERII at the Helmholtz Centre Berlin, Germany. In the latter case 400 mg were irradiated at a neutron flux of 2×10^{14} s^{-1} cm^{-2} (BER II) for 50 d .

^{90}Nb was produced via the ^{90}Zr(p,n)^{90}Nb reaction at the cyclotron MC32NI of the German Cancer Research Center Heidelberg. For irradiation, a stack of three discs of natural zirconium (natural abundance 51.45% ^{90}Zr) foils of 10 mm diameter and a thickness of 0.25 mm each were used. Irradiation was performed at 20 MeV proton energy and a current of 5 μA for 1 hour. This initial proton energy was decreased by using an aluminum holder cover of 0.5 mm thickness to 17.5 MeV entering the 1st foil of Zr. At 24 hours after end of irradiation (EOB), production yields and impurities were measured.

The activities of $^{90/92m/95}$Nb and $^{95/88}$Zr were measured by γ-ray spectroscopy. Main gamma lines, for used radionuclides, are listed in Table 2.

Table 2: Main gamma emission energies of radionuclides used in this work (nuclear data from [15]).

Radionuclide	$t_{1/2}$ (days)	Main γ emission	
		Energies (keV)	Abundances (%)
^{92m}Nb	10.2	934.5	99.0
^{90}Nb	0.61	1129.0	82.0
^{95}Zr	64.0	724.2	44.2
		756.7	54.0
^{95}Nb	35.0	765.8	100.0

Determination of distribution coefficients

Preparation of stock solutions

^{92m}Nb and ^{95}Nb were isolated from irradiated molybdenum targets by anion exchange chromatography. In short, molybdenum targets were placed into a plastic vial and 28 M HF (3 mL) and 16 M HNO_3 (1 mL) were added. After complete dissolution, the mixture was loaded on a column filled with 500 mg of AG 1x8 resin, 200-400 mesh in F^- form. The column was washed with conc. HF (20 mL) and $^{92m/95}$Nb was eluted with a mixture of 6 M HCl / 1% H_2O_2 (2 mL).

^{95}Zr was extracted from irradiated silver target.

Finally, fractions containing ^{92m}Nb and ^{95}Zr were evaporated to dryness and dissolved in 6 M HCl (2 mL).

Preparation and conditioning of resins

For determination of distributions coefficients, the anion exchange resin AG 1x8, 200-400 mesh, (4 g) was applied. The resin was first washed with water (10 mL), and then transferred to the Cl^- form via washing with 12 M HCl (20 mL). Finally, the resin was additionally washed with water (10 mL) to remove excess of Cl^-, and kept until drying for 48 hours at room temperature.

The UTEVA resin was applied without further preconditioning.

Procedure for distribution coefficients determination

Distribution coefficients were determined by batch mode according to the following procedures:

50 mg of resins were placed in a 2 mL tube, then 1 mL of solution of appropriate concentrations of HCl/ oxalic acid and 10 µL of the radionuclides stock solution were added. The mixture was vigorously stirred and allowed to stay for 24 hours (4 hours for mixtures contained hydrogen peroxide) at room temperature. Next, the mixtures were centrifuged and 900 µL of the solution was taken and measured by γ-ray spectroscopy. Distribution coefficient were calculated from equations (1), were $A_{50mg(res.)}$ is the activity in 50 mg of the resin and $A_{50\mu L(sol.)}$ is the activity in 50 µL of solution.

$$K_D = \frac{C^{eq.}_{phase1}}{C^{eq.}_{phase2}} = \frac{A_{1g(res.)}}{A_{1mL(sol.)}} = \frac{A_{50mg(res.)}}{A_{50\mu L(sol.)}} \qquad (1)$$

Transfer of ^{90}Nb from AG 1x8 to UTEVA

Based on distribution coefficients determined in batch experiments, most appropriate mixtures of HCl and oxalic acid for the direct transfer are 0.2 M, 0.3, 0.4 M oxalic acid and consequently 9.2 M, 7.5 M, 6.9 M hydrochloric acid. These mixtures were tested for separation conditions of 300 mg AG 1x8 and 100 mg of UTEVA. Aliquots of Mo and Zr targets dissolved were loaded on the anion exchange column, washed with 5 mL of 28 M HF. Next the above described mixtures were applied. Fractions (200 µL) were collected from the anion exchanger until maximal activities of ^{90}Nb have been eluted. These fractions were directly transferred to the UTEVA resin.

Separation strategy

In the targets in case for the both materials (zirconium and molybdenum) wide range of tracers of other radionuclides from 1st up to 7th groups are presented. Most relevant radionuclides were isotopes of Tc^{VII} (in case of Mo target), Mo^{VI}, Nb^{V}, Zr^{IV}, Y^{III}, Sr^{II}, and Rb^{I}. Separation from all these radionuclides was monitored by γ-spectroscopy using the corresponding gamma emissions of the radionuclides.

Target dissolution

Zr target: The irradiated zirconium target, typically 260±3 mg was placed into a 15 mL plastic vial and water (500 µL) was added. For dissolution, 28 M hydrofluoric acid (500 µL) was portionally added and after full dissolution concentrated hydrofluoric acid (1 mL) was added.

Mo target: The irradiated molybdenum target, typically 760±6 mg, was placed into a 50 mL plastic via and water (1 mL) was added. For dissolution a mixture of 28 M HF and 16 M HNO_3 was applied. First 28 M hydrochloric acid (1.5 mL) was added and then 16 M HNO_3 (0.5 mL) dropwise was added. After complete target dissolution, the mixture was filled up to 5 mL with 28 M HF.

Crude separation on anion exchange column

2 mL of 21 M hydrofluoric acid containing the irradiated zirconium target were passed through the cation exchange resin (DOWEX 50x8, 100 mg, 200-400 mesh, 10x5 mm) resin in F^- form for removal of colloids, unsolved target particles and possible trace contamination of 2+ and 3+ charged metal cations, such as for example Cu^{2+} or Fe^{3+} from target holder. The column was additionally washed with concentrated hydrofluoric acid (1 mL). The solution (3 mL) which passed the cation exchange resin was transferred to an anion exchange column (300 mg, 25x5 mm) filled with AG 1x8 resin (200-400 mesh) in F^- form. Nb^{V} remained on this resin and the bulk amount of Zr^{IV} passed through. The column was washed with concentrated HF (4.5 mL) to elute traces of Zr^{IV}, while ^{90}Nb stays on the column.

Direct flow transfer ^{90}Nb target solution from AG 1x8 to UTEVA

A small plastic column filled with UTEVA resin (150 µm, 100 mg, 10x5 mm) was filled with UTEVA resin. Anion exchange column was directly connected with the UTEVA and 7 mL of 0.3 M oxalic acid/ 7.5 M HCl were passed through the both column

Purification of ^{90}Nb on UTEVA resin

The UTEVA was next washed with 5 M HCl (5 mL). Traces of *Zr^{IV} passed through the UTEVA, while Nb^{V} remains absorbed on the column. For elution of ^{90}Nb 0.1 M oxalic acid was applied. The column was washed with 200 µL and ^{90}Nb eluted with another 400 µL of 0.1 M oxalic acid. The decontamination factor Zr/Nb was measured by ICP-MS and γ-ray.

Results

Production of niobium and zirconium isotopes

^{92}Nb, ^{95}Nb and ^{88}Zr for distribution coefficients

After separation of the radionuclides, the corresponding fractions were evaporated to dryness and dissolved in 6 M HCl (2 mL). Stock solutions were made of: 8±3 kBq of ^{92m}Nb, 4±1 kBq of ^{95}Nb ($t_{1/2}$ = 35.0 d) and 7±2 kBq of ^{88}Zr

^{90}Nb production via ^{nat}Zr (p,n) process

The overall (p,n) irradiation yield of ^{90}Nb for 1 h and 5 µA irradiations was 720 ± 50 MBq, i. e. 145±10 MBq/µAh under the given irradiation parameters. The isotopic purity of ^{90}Nb after EOB was more than 97%. Minor isotopic impurities found were: ^{92m}Nb ($t_{1/2}$ 10.2 d) = 1.64%, ^{95}Nb ($t_{1/2}$ 35.0 d) = 0.08%, ^{95m}Nb ($t_{1/2}$ 3.6 d) = 0.29% and ^{96}Nb ($t_{1/2}$ 23.35 h) = 0.88%.

^{90}Nb and ^{90}Mo production by irradiation with high energy proton Zr and Mo via ^{nat}Zr/^{nat}Mo (p, xn) reactions

Three irradiations of natural molybdenum and zirconium targets were performed to determine i) production yield of ^{90}Mo and ^{90}Nb and to ii) monitor the simultaneous production of other radionuclides. In table 3 all radionuclides detected which are presented in the irradiated Mo target are listed with their activities are listed.

Table 3: Content for ^{nat}Mo target irradiated at the Phasotron facility with 100 MeV for 30 minutes with 4 µA at EOB.

Radionuclide	Half-life, $t_{1/2}$ (h)	Activity (MBq)
^{93}Tc	2.7	767
^{95m}Tc	1440	6
^{95g}Tc	20	92
^{96}Tc	103.2	41
^{90}Mo	5.7	423
^{93m}Mo	6.9	179
^{90}Nb	14.6	350
^{92}Nb	243.6	7
^{86}Zr	16.5	100
^{89}Zr	78.4	134
^{86}Y	14.6	209
^{87g}Y	80.3	45
^{87m}Y	3	449

The production yield of ^{90}Nb at the internal beam irradiation positron of the Phasotron facility was 258±40 MBq/µAh, that almost double higher than for cyclotron irradiation [32]. A second main advantage of this production route are the excellent purity of ^{90}Nb which is forming by decay of ^{90}Mo ($t_{1/2}$ = 5.56 h). This also gives additional time for transportation and handling to finally obtain during forming ^{90}Nb from ^{90}Mo decay. For ^{90}Mo, the production yield was 289±45 MBq/µAh. At 24 hours after end of irradiation 80% of ^{90}Nb originated from the decay of ^{90}Mo (Table 4).

Table 4: Content of ^{90}Nb in Mo irradiated target with time.

Time(days)	0 (EOB)	1st	3rd	5th
Activity of ^{90}Nb (MBq)	350	281	37	5

^{95}Zr/^{95}Nb

More than 1.5 GBq of ^{95}Zr was produced at the BERII reactor after 50 days of irradiation at a flux of thermal neutrons of 2×10^{14} s^{-1} cm^{-2}. The maximum daughter activity of ^{95}Nb as generated from ^{95}Zr was obtained at ~67 d after EOB.

Determination of distribution coefficients

Values of distribution coefficients provide us with understanding of behaviour of Zr^{IV} and Nb^{V} on anion exchange resin and UTEVA in HCl/ H_2O_2 HCl/ oxalic acid media in static system.

However, determination of K_d in HCl/H_2O_2 accompanied with some complicities. Incubation time is needed to setup equilibrium between tracers, resin and media, but this equilibrium is impossible because hydrochloric acid reacts with hydrogen peroxide and with time changes its concentration. Therefore 4 hours was founded to be optimum incubation time for radionuclides equilibrium from one hand and for the other hand not sufficient concentration change. Errors in samples with peroxide were up to 30%.

Zr^{IV} and Nb^{V} distribution coefficients in the system AG 1x8 and UTEVA - HCl/H_2O_2

Distribution coefficients in various hydrochloric acid concentrations and mixtures of HCl and hydrogen peroxide are illustrated in Table 6.

To allow effective transfer of Nb fraction from the anion exchanger AG1x8 to the UTEVA resin following conditions should be determined:

- distribution coefficients for AG1x8 should be as low as possible (≤10), that will allow easily elution of Nb fraction
- distribution coefficients for UTEVA should be as high as possible (≥ 1000), that will allow sorbtion of Nb fraction

Table 5 showed that just several mixtures of HCl/H_2O_2 satisfy the above described conditions.

The most appropriate mixture is 9 M HCl/1% H_2O_2. For anion exchange, the K_d value for Nb is 13 and for UTEVA 4674. Other options are 9 M HCl/0.75% H_2O_2 and 9 M HCl/ 1.18% H_2O_2 with K_d values for AG1x8 vs.UTEVA are 16 vs. 505 and 9 vs.728, respectively. However, these K_d values for the UTEVA resin are relative low, and may result in some Nb breakthrough in case of a dynamic column separation.

Table 5: Distribution coefficients for Nb^V in systems HCl/H_2O_2 for AG1x8 and UTEVA.

K_d ^{95}Nb	H_2O_2, %				
DOWEX 1x8/UTEVA	0.25	0.50	0.75	1.00	1.18
11 M HCl	-	745/466	113/755	259/2069	250/728
10 **M** HCl	632/143	510/1788	505/1367	36/1370	93/1247
9 M HCl	-	703/4103	16/505	13/4674	9/728
8 **M** HCl	13/89	5/179	5/42	1/47	4/46
7 **M** HCl	8/16	3/17	3/12	2/8	
6 **M** HCl	5/6	5/5	3/4	4/4	
5 **M** HCl	3/1				

In Table 6 K_d values for Zr^{IV} in HCl/H_2O_2 are presented for the AG1x8 and UTEVA. At 9 M HCl/1 % H_2O_2, the distribution coefficients for AG1x8 is 22 and for UTEVA 1706, that is very similar to Nb.

Table 6: Distribution coefficients for Zr^{IV} in systems HCl/H_2O_2 for AG1x8 and UTEVA.

K_d ^{95}Zr	H_2O_2, %				
DOWEX 1x8/UTEVA	0.25	0.50	0.75	1.00	1.18
11 M HCl	-	1363/898	198/654	149/1452	196/610
10 **M** HCl	148/136	114/1902	94/1139	36/284	45/1566
9 M HCl	-	29/1701	28/995	22/284	21/1566
8 **M** HCl	12/337	11/630	10/354	10/664	21/775
7 **M** HCl	8/158	11/109	17/287	18/303	
6 **M** HCl	8/39	14/7	15/75	19/77	
5 **M** HCl	9/22				

Some general dependencies can be formed from these distribution coefficients. An increasing of concentration of hydrochloric acid strongly increases K_d values for both Nb^V and Zr^{IV}, while increasing concentration of hydrogen peroxide does not. Thus, there is no significant difference between K_d values for Zr and Nb, which can allow additional separation.

Zr^{IV} and Nb^V distribution coefficients for AG1x8 and UTEVA - HCl/ oxalic acid

Oxalic acid is known for its very strong complexation with Nb^V [33]. Oxalate complexes elute NbV from the anion exchange column. The same time, the hydrochloric acid involved allows absorbing Nb on the UTEVA column.

Table 7 lists distribution coefficients at various combinations of HCl and oxalic acid for Nb^V.

Due to the strategy that high concentration of oxalic acid responsible for elution of Nb from anion exchange column and high concentration of hydrochloric acid will adsorb Nb on UTEVA appropriate combination of both components should be founded. However, maximal soluble and time stable

concentration of oxalic acid is 1 M and for HCl is 11.5 M (maximal 12 M), that make some restriction in samples preparation.

From the results presented in Table 7 several mixtures may satisfy the outline concept. Appropriate results was reached at concentrations of both components: 0.2 M oxalic acid/ 9.2 M HCl with K_d values for AG1x8 13±1 and for UTEVA 3334, 0.3 M oxalic acid/ 7.5 M HCl and 0.4 M oxalic acid/ 6.9 M HCl seems to be promising for direct flow transfer of Nb from anion exchanger to UTEVA.

Suitable mixture is also 0.005 M oxalic acid/ 6.28 M HCl distribution coefficients for anion exchanger is 11±1 and for UTEVA 747±10.

Table 7: Distribution coefficients for Nb^V in system HCl/ox. acid for AG1x8 and UTEVA.

K_d *Nb	oxalic acid, M								
DOWEX 1x8	0.005	0.01	0.02	0.05	0.10	0.20	0.30	0.40	0.45
UTEVA									
10.29 HCl	51±1	39±1	35±1	31±1	31±1				
	>10000	>10000	8065±76	>10000	>10000	>10000			
9.145 HCl	850±2	822±50	721±16	355±17	114±4	13±1			
	5835±663	9191±1332	4566± 47	6450±91	3101±360	3334±56			
7.995 HCl	418±8	186±5	93±3	10±3	7±1	5±1	12±1		
	5886±444	4759±441	2657±324	2025±45	609±22	159±1	1896±197		
6.845 HCl	32±1	10±1	5±1	3±1	5±1	5±1	2±1	2±1	
	1561±388	624±20	239±3	29±1	181±5	94±1	57±1	90±1	
6.28 HCl	11±1	4±1	4±1	4±1	6±1	4±1	2±1	4±1	4±1
	747±10	145±5	156±7	200±6	116±2	64±5	42±2	55±3	48±1

Zr^{IV} distribution coefficients on anion exchange and UTEVA resins in mixtures HCl/ oxalic acid presented in Table 8.

K_d values for Zr^{IV} are sufficiently lower for the anion exchanger and for UTEVA then for NbV in proposed above mixtures. That can be an additional advantage by direct flow separation strategy providing additional decontamination from zirconium target material.

Table 8: Distribution coefficients for Zr^{IV} in system HCl/ox. acid for AG1x8 and UTEVA.

K_d *Zr	oxalic acid, M								
DOWEX 1x8	0.005	0.01	0.02	0.05	0.1	0.2	0.3	0.4	0.45
UTEVA									
10,29 HCl	1080±21	534±13	610±17	164±5	79±5				
	>10000	>10000	>10000	>10000	>10000				
9,145 HCl	17±1	12±1	2387±53	<1	<1	<1			
	>10000	>10000	1021±34	7229±102	1926±224	1625±34			
7,995 HCl	<1	<1	<1	<1	<1	<1	<1		
	2801±318	128±12	560±68	296±3	61±2	15±1	48±6		
6,845 HCl	<1	<1	<1	<1	<1	<1	<1	<1	
	69±17	24±1	8±1	<1	2±1	<1	<1	4±1	
6,28 HCl	<1	<1	<1	<1	<1	<1	<1	<1	<1
	14±1	3±1	2±1	<1	<1	<1	<1	<1	2±1

Direct transfer of Nb from anion exchanger to UTEVA resin

Mixtures of 0.2 M oxalic acid/ 9.2 M HCl, 0.3 M oxalic acid/ 7.5 M HCl and 0.4 M oxalic acid/ 6.9 M HCl were tested in dynamic column to find the most appropriate solution for the direct transfer of the Nb fraction between two columns.

For 0.4 M oxalic acid/ 6.9 M HCl more than 99% of the $^{90/95}$Nb fraction was eluted (in 2 mL, however, a breakthrough of $^{90/95}$Nb (more than 90%) was measured after 1 mL loading on UTEVA.

7 mL of 0.2 M oxalic acid/ 9.2 M HCl were passed through the anion exchange column, however, ≤ 10% of $^{90/95}$Nb was eluted in first two milliliters.

Finally, a 7 mL mixture of 0.3 M oxalic acid/ 7.5 M HCl elutes ≥ 95% of $^{95/90}$Nb from the AG1x8 with of mixture and whole volume can be applied on UTEVA column.

Direct flow separation strategy

The overall separation proceeds with a yield 93-95% of $^{90/95}$Nb, collected in 400 µL 0.1 M oxalic acid. The whole separation procedure takes less than one hour, which is almost 4 times faster than the previously presented separation method [33]. Decontamination factor after anion exchange was $1 \cdot 10^5$ and after UTEVA purification $3 \cdot 10^8$. This decontamination factor equal 0.77 ng of zirconium presented in final fraction for a 260 mg zirconium target.

Discussion

^{90}Nb holds promise for application in immune-PET. Nuclear data are adequate, and labeling to proteins works very efficiently. A routine use of ^{90}Nb, however, would ask for a robust availability of this positron emmiter in terms of high-yield nuclear reaction process and the efficient isolation of the 90NB from irradiated target.

In this work we first compare the commonly utilized ^{nat}Zr(p, n) reaction with a ^{nat}Mo(p, xn)^{90}Mo$\rightarrow\beta^-\rightarrow^{90}$Nb process. The latter route gives almost double yields of 289±45 MBq/µAh compare 145 MBq/µAh to the Zr(p ,n) reaction. However radionuclide purity of ^{90}Nb is improved within the Mo(p, xn) process.

The second aim aim was to modify a previously developed separation strategy. The direct transfer of NbV eluted from an anion exchange column to the UTEVA column, allows sufficiently simplified automation and minimizes the separation time. Here, the optimum composition of mixtures of hydrochloric acid and hydrogen peroxide is required. According to the K_d data several combinations seem to be appropriate. However, due to the problems associated with the handling of peroxide solutions (bubbling, concentration instability with hydrochloric acid) an alternative system was evaluated, utilizing oxalic acid. In our previous study we used oxalic acid solution for elution of Nb^V from UTEVA column. Oxalate complexes of Nb^V can be eluted easily from the UTEVA column. The presence of hydrochloric acid can direct this behaviour and turn it into adsorption. K_d values measured for Nb^V and Zr^{IV} in mixtures of hydrochloric acid and oxalic acid. Identified several concentrations were a transfer is possible. Most suitable concentrations are 0.3 M oxalic acid/7.5 M HCl was founded most suitable. 7 mL of this solution provide a transfer of 95-97% of Nb^V from the anion exchange column to the UTEVA resin, no breakthrough of Nb^V via UTEVA column was measured. An important factor for the efficient transfer of

Nb^{V} is the time of contact eluent with resin. In case of fast (1 drop per second) transfer velocity up to 30% of losses of $^{90/95}Nb$ can be observed, occurs in terms of a breakthrough trough the UTEVA column. The overall separation time was not exceeding one hour not including preparation (solutions and columns preconditioning). The overall separation yield of ^{90}Nb was varied between 93-95% with a decontamination factor $\geq 10^{8}$ both for Mo and Zr targets. There is no significant difference in behaviour of zirconium and molybdenum as the target materials within separation processes. For the $^{nat}Mo(p, xn)^{90}Mo \rightarrow ^{90}Nb$ route, the other nca radionuclides present in the irradiated molybdenum target. No other radioisotopes of Rb^{I}, Sr^{II}, Y^{III}, Zr^{IV}, Tc^{VI} and Mo^{VII} were measured in final fraction contained ^{90}Nb.

Conclusions

In conclusion, the modified separation simplifies the handling, also for automation of the separation protocol. Similar results were obtained for separation of Mo and Zr targets. Just slight different procedures for dissolution were applied.

Separation time does not exceed 1 hour. Direct flow strategy was applied for two targets material and provides similar separation characteristic. Developed strategy allow separate Nb^{V} from other nca radionuclides from Ist to VIth groups of periodic table Rb^{I}, Sr^{II}, Y^{III}, Zr^{IV}, Tc^{VI}. Thus, this strategy provides a more reliable source of ^{90}Nb with appropriate purity and in appropriate conditions for subsequent labelling and medical application.

Acknowledgements

The authors thank the teams of TRIGA reactor Mainz and reactor BRII at Helmholtz Centrum Berlin, Germany, for production of ^{95}Zr and the teams of Phasotron operators at JINR for production of Nb and Zr isotopes from molybdenum target.

Thanks to VU University Medical Centre in Amsterdam, especially Danielle Vugts for providing of premodified antibody for testing labeling.

References

1. Fass, L. Imaging and cancer: A review. *Mol Oncol* 2008; 2(2); 115-152.
2. Nolting, D. D., Nickels, M. L., Guo, N., Pham, W. Molecular imaging probe development: a chemistry perspective. *Am J Nucl Med Mol Imaging* 2012; 2(3); 273-306.
3. Sinusas, A. J., Thomas, J. D., Mills, G. The future of molecular imaging. *J A C C Cardiovasc Imaging* 2011; 4(7); 799-806.
4. Bailey, D. L., Townsend, D. W., Valk P. E. and Maisey M. N. (Eds.), Positron Emission Tomography: Basic Sciences, *Springer-Verlag London Limited*; 2005.
5. Brush, J., Boyd, K., Chappell, F., Crawford, F., Dozier, M., Fenwick, E., Glanville, J., McIntosh, H., Renehan, A., Weller, D., Dunlop, M. The value of FDG positron emission tomography/computerised tomography (PET/CT) in pre-operative staging of colorectal cancer: a systematic review and economic evaluation*. Health Technol Assess* 2011*;* 15(35); 1-192.
6. Fletcher, J. W., Djulbegovic, B., Soares, H. P., Siegel, B. A., Lowe, V. J., Lyman, G. H., Coleman, R. E., Wahl, R., Paschold, J. C., Avril, N., Einhorn, L. H., Suh, W. W., Samson, D., Delbeke, D., Gorman, M., Shields, A. F. Recommendations on the use of ^{18}F-FDG PET in oncology. *J Nucl Med* 2008; 49(3); 480-508.
7. Fani, M., Maecke, H. R. Radiopharmaceutical development of radiolabelled peptides. *Eur J Nucl Med Mol Imaging* 2012; 39(1); 11-30.
8. Rösch, F., Baum, R. P. Generator-based PET radiopharmaceuticals for molecular imaging of tumours: on the way to THERANOSTICS. *Dalton Trans* 2011; 40(23); 6104-6111.
9. Zhao, H., Cui, K., Muschenborn, A., Wong, S. T. Progress of engineered antibody-targeted molecular imaging for solid tumors (Review). *Mol Med Rep* 2008; 1(1); 131-4.
10. Romer, T., Leonhardt, H., Rothbauer, U. Engineering antibodies and proteins for molecular *in vivo* imaging. *Curr Opin Biotechnol* 2011; 22(6); 882-7.
11. Knowles, S. M., Wu, A. M. Advances in immuno-positron emission tomography: antibodies for molecular imaging in oncology. *J Clin Oncol* 2012; 30(31); 3884-92.
12. van Dongen, G. A., Vosjan, M. J. Immuno-positron emission tomography: shedding light on clinical antibody therapy. *Cancer Biother Radiopharm* 2010; 25(4); 375-85.

13. van Dongen, G. A., Poot, A. J., Vugts, D. J. PET imaging with radiolabeled antibodies and tyrosine kinase inhibitors: immuno-PET and TKI-PET. *Tumour Biol* 2012; 33(3); 607-15.
14. Pecking, A. P., Bellet, D., Alberini, J. L. Immuno-SPET/CT and immuno-PET/CT: a step ahead to translational imaging. *Clin Exp Metastasis* 2012; 29(7); 847-52.
15. National Nuclear Data Center, Brookhaven National Laboratory, *last update: 12 January 2012, http://www.nndc.bnl.gov/.*
16. Bhattacharyya, S., Dixit, M. Metallic radionuclides in the development of diagnostic and therapeutic radiopharmaceuticals. *Dalton Trans* 2011; 40(23); 6112-28.
17. Rice, S. L., Roney, C. A., Daumar, P., Lewis, J. S. The next generation of positron emission tomography radiopharmaceuticals in oncology. *Semin Nucl Med* 2011; 41(4); 265-82.
18. Vugts, D. J., van Dongen, G. A. M. S. ^{89}Zr-labeled compounds for PET imaging guided personalized therapy. *Drug Discovery Today: Technologies* 2011; 8(2); 53-61.
19. Chang, A. J., De Silva, R. A., Lapi, S. E. Development and Characterization of ^{89}Zr-labeled panitumumab for immuno-positron emission tomographic imaging of the epidermal growth factor receptor. *Mol Imaging* 2013; 12(1); 17-27.
20. Chang, A. J., DeSilva, R., Jain, S., Lears, K., Rogers, B., Lapi, S. ^{89}Zr-radiolabeled trastuzumab imaging in orthotopic and metastatic breast tumors. *Pharmaceuticals* 2012; 5(1); 79-93.
21. Belov, V. V., Bonab, A. A., Fischman, A. J., Heartlein, M., Calias, P., Papisov, M. I. Iodine-124 as a label for pharmacological PET imaging. Mol. Pharm. 2011; 8(3); 736-47.
22. Koehler, L., Gagnon, K., McQuarrie, S., and Wuest, F. Iodine-124: A promising iodine radioisotope for positron emission tomography (PET). *Molecules* 2010; 15; 2686-718.
23. Thieme, S., Walther, M., Pietzsch, H. J., Henniger, J., Preusche, S., Mäding, P., Steinbach, J. Module-assisted preparation of ^{64}Cu with high specific activity. *Appl Radiat Isot* 2012; 70(4); 602-8.
24. Chen, K., Ma, W., Li, G., Wang, J., Yang, W., Yap, L. P., Hughes, L. D., Park, R., Conti, P. S. Synthesis and evaluation of ^{64}Cu-labeled monomeric and dimeric NGR peptides for MicroPET imaging of CD13 receptor expression. *Mol Pharm* 2013; 10(1); 417-427.
25. Anderson, C. J., Ferdani, R. Copper-64 radiopharmaceuticals for PET imaging of cancer: advances in preclinical and clinical research. *Cancer Biother Radiopharm* 2009; 24(4); 379-93.
26. Rösch, F., Qaim, S. M., Stöcklin, G. Production of the positron emitting radioisotope ^{86}Y for nuclear medical application. *Int J Appl Radiat Isot* 1993; 44(4); *677-81.*

27. Nayak, T. K., Brechbiel, M. W. ^{86}Y based PET radiopharmaceuticals: radiochemistry and biological applications. *Med Chem* 2011; 7(5); 380-8.

28. Tolmachev, V. Bromine-labelled tracers for positron emission tomography: possibilities and pitfalls. *Curr Radiopharm* 2011; 4(2); 76-89.

29. Rossin, R., Berndorff, D., Friebe, M., Dinkelborg, L. M., Welch, M. J. Small-animal PET of tumor angiogenesis using a ^{76}Br-labeled human recombinant antibody fragment to the ED-B domain of fibronectin. *J Nucl Med* 2007; 48(7); 1172-9.

30. Busse, S., Roesch, F., Qaim, S. M. Cross section data for the production of the positron emitting niobium isotope ^{90}Nb *via* the ^{90}Zr(*p, n*)-reaction. *Radiochim Acta* 2002; 90; 1-5.

31. Busse, S., Brockmann, J., Roesch, F. Radiochemical separation of no-carrier-added radioniobium from zirconium targets for application of ^{90}Nb-labelled compounds. *Radiochim Acta* 2002; 90; 411-415.

32. Radchenko, V., Hauser, H., Eisenhut, M., Vugts, J. D., van Dongen, G. A. M. S., Roesch, F. ^{90}Nb – a Potential PET Nuclide: Production and Labeling of Monoclonal Antibodies. *Radiohim Acta* 2012; 100(11); 857-865.

3.4 Desferrioxamine as an appropriate chelator for ^{90}Nb: Comparison of its complexation proprieties for M-Df-Octreotide (M = Nb, Fe, Ga, Zr).

Desferrioxamine as an appropriate chelator for ^{90}Nb: Comparison of its complexation proprieties for M-Df-Octreotide (M = Nb, Fe, Ga, Zr).

V. Radchenko, S. Busse and F. Roesch*

Institute of Nuclear Chemistry, Johannes Gutenberg-University Mainz, Fritz-Strassmann-Weg 2, D-55128 Mainz, Germany

Abstract

The nuclide ^{90}Nb, due to its decay parameters half-life of 14.6 hours, positron branching of 53% and β^+-energies of E_{mean} = 0.35 MeV and E_{max} = 1.5 MeV holds promise to become an effective positron emitter for *immuno*-PET. Different chelators were tested to identify the most appropriate one to conjugate ^{90}Nb to biological relevant molecules. As analog of ^{90}Nb, reactor produced ^{95}Nb ($T_{1/2}$ = 35 days) was chosen. Desferrioxamine (*N'*-{5-[acetyl(hydroxy)amino]pentyl}-*N*-[5-({4-[(5-aminopentyl) (hydroxy)amino]-4-oxobutanoyl} amino)pentyl]-*N*-hydroxysuccinamide) (Df) showed the best complexation proprieties with ^{95}Nb at room temperature and at various pH values. A fast kinetics of ^{95}Nb-Df complex formation and excellent *in vitro* stability of the complex in human serum (less than 7% degradation over 7 days) proved the potential of Df.

Df conjugated to a proof-of-principle compound, Df-succinyl-(D)Phe^1-Octreotide (Df-Octreotide), retained fast labeling kinetics at various pH values with more than 90% after 1 hour incubation at room temperature for tested pH values. For this compound, competition studies with different metals (Zr, Fe and Ga), that could be present in the labeling mixture and compete for niobium, were performed. In equimolar concentrations niobium showed the strongest complex formation with Df-Octreotide among all metals tested.

Furthermore, *in vitro* stability studies in serum revealed 87±2% of the unaltered product even after 7 days of incubation at 37 ºC. All these results prove the high potential and advantages of using desferrioxamine as chelator of choice for the synthesis of biomolecules labeled with Nb radioisotopes.

Keywords: positron emitter ^{90}Nb / desferroxamine / chelators / stability / Df-Octereotide

Introduction

Developments in nuclear medicine over the last decades both directed towards diagnosis and therapy call for investigation of adequate radinuclides which meet certain requirements. One attractive example of new directions in cancer diagnosis is *immuno*-PET [1]. *Immuno*-PET employs monoclonal antibodies and antibody fragments *in vivo*. Those targeting vectors enable a very precise visualization of tumors at earlier

stages and at later stages, and metastases can be comprehensively detected. Standard PET radionuclides such as ^{18}F ($T_{1/2}$ = 110 min), ^{15}O ($T_{1/2}$ = 2.04 min) and ^{11}C ($T_{1/2}$ = 20.4 min) are practically useless for applications in *immuno*-PET because of the slow pharmacokinetics of monoclonal antibodies and antibody fragments, which can last for several days (unless pretargeting concepts are not established).

Consequently, positron emitting radionuclides should be chosen according to the biological half-life of the biomolecules. Recently, several radioisotopes with long half-life became commercially available and have been introduced in the clinic such as ^{89}Zr ($T_{1/2}$ = 78.4 h) [2] and ^{124}I ($T_{1/2}$ = 100.2 h) [3].

For engineered antibody fragments [4, 5] the molecular weight is lower and correspondingly, the kinetics for tumor accumulation are faster. Thus, radionuclides with long half-life would create an extra dose burden for patients. Therefore, nuclides with intermediate half-lives (from several hours up to one day) would better correlate with the time necessary for achieving optimal imaging conditions.

Accordingly, positron emitters such as ^{64}Cu ($T_{1/2}$ = 12.7 h) [6], ^{86}Y ($T_{1/2}$ = 17.74 h) [7, 8] and ^{76}Br ($T_{1/2}$ = 16.2 h) [9] have been investigated with ^{86}Y and ^{64}Cu becoming involved even for human application.

Further important factors to qualify radinuclides for *immuno*-PET are: i) a high positron branching with no or only weak accompanying other types of radiation (β^-,γ) to offer high-sensitive PET imaging while reducing the radiation burden of the patient, ii) a preferable low β^+-energy to allow high-resolution PET-imaging; and iii) the option to (commercially) distribute the radionuclide. In addition, long-term imaging with chosen nuclide asks for robust labeling chemistry and sufficient *in vivo* stability of the labeled compounds [10].

In a recent study, we proposed ^{90}Nb as a new potential nuclide for *immuno*-PET. Its intermediate half-life of 14.6 hours is appropriate for antibody fragments as well as for antibodies. Its positron branching is as high as 53% at a rather low β^+-energy of E_{mean} = 350 keV (E_{max} = 1.5 MeV), which should allow high quality and high resolution images even at low activity of ^{90}Nb. We showed that ^{90}Nb can be produced in large batches and can sufficiently be separated from the irradiated zirconium target with appropriate purity for follow labeling of biomolecules [11, 12, 13]. In the present study, we investigated different chelators for niobium and present systematic labeling of a proof-of-principle peptidic targeting vector, namely desferrioxamine-Octreotide.

Materials and Methods

Materials

Reagents purchased from Sigma-Aldrich (Germany) and were used without further purification unless otherwise stated. Deionized water (18 MΩ cm^{-1}) and ultrapure HCl solution were used. No other special measures were taken regarding working under strict metal-free conditions. Different ligands were applied: Ethylenediaminetetraacetic acid (EDTA) (Fluka, Germany), 1,2-cyclohexylenedinitrilotetraacetic acid (CDTA), diethylene triamine pentaacetic acid (DTPA) (Fluka, Germany), triethylenetetraaminehexaacetic acid (TTHA) (Fluka, Germany), 1,4,7,10-tetraazacyclododecane-1,4,7,10-tetraacetic acid (DOTA) (Strem Chemicals, Germany), 1,4,8,11-tetraazacyclo tetradecane-1,4,8,11-tetraacetic acid (TETA) (Sigma-Aldrich, Germany), desferrioxamine mesylate (Df) (Sigma-Aldrich, Germany), and 4-(2-pyridylazo)resorcinol (PAR) (Merck, Germany) (Fig.1).
The octapeptide Df-succinyl-(D)Phe^1-Octreotide (SDZ 216-927) (Df-Octreotide) was kindly provided by Novartis AG Basel.

Production of ^{95}Nb

^{95}Nb ($T_{1/2}$ = 35 days, main photon emission 765.8 keV (100%)) was applied as analog of ^{90}Nb. ^{95}Nb was produced via the $^{94}Zr(n, \gamma)\rightarrow{}^{95}Zr(\beta^-, T_{½}$ = 64 d)$\rightarrow{}^{95}Nb$ process from natural zirconium granules of 1-3 mm/99.8% (ChemPur, Germany). Neutron capture reactions were performed at the TRIGA reactor at the Institute of Nuclear Chemistry of the Johannes Gutenberg-University Mainz, Germany, and at the research reactor BER II at the Helmholtz Centre Berlin, Germany. At a neutron flux of $2 \cdot 10^{14}$ $s^{-1} \cdot cm^{-2}$ (BER II) a 50 days irradiation of a 300 mg target generated more than 1.5 GBq of ^{95}Zr. Production of both nuclides, ^{95}Zr and ^{95}Nb, was monitored by gamma spectroscopy, *via* emission at 724.2 keV (44.2%) and 756.7 keV (54.0%) for ^{95}Zr and *via* the 765.8 keV (100%) for ^{95}Nb, respectively. The maximum activity of ^{95}Nb as a daughter of the $^{95}Zr/^{95}Nb$ generator pair appeared at ~67 d after EOB.

Radiochemical separation of ^{95}Nb

The separation protocol was described earlier by Busse *et al.*. [12] In short, the zirconium metal target (260±3 mg) was transferred into a 50 mL vial and water (2 mL) was added. Under ice-cooling, 48% HF (0.63 mL) was added in small portions. After a complete dissolution, 10 M HCl (6 mL) and saturated boric acid (3.4 mL) were added. The ^{95}Nb fraction was extracted with 0.02 M of *N*-benzoyl-*N*-phenylhydroxylamine (BPHA) (Merck, Germany) in $CHCl_3$ (5 mL) by vigorous stirring of the two phases in a 50 mL vial for 20 min. The aqueous phase was additionally washed with $CHCl_3$ (3 mL). The organic phases were combined and washed with a mixture of 9 M HCl/0.001 M HF (2 mL) and with 9 M HCl (2 mL). Re-extraction was carried out with aqua regia (5 mL).

For a final purification of ^{95}Nb from trace amounts of zirconium, an anionic exchange method was employed. After re-extraction, the aqueous phase was evaporated to dryness. The residue was dissolved in a mixture of 0.25 M HCl/0.1 M oxalic acid (0.5 mL) and adsorbed on a small Aminex A27 (Bio-Rad, Germany) 15 ± 2 µm anionic exchange column (20 x 1.5 mm). Elution was performed under slight overpressure of 0.3 bars. After loading, the column was washed with 10 M HCl (100 µL). Residues of Zr were removed by washing with a mixture of 9 M HCl/0.001 M HF (200 µL). ^{95}Nb was eluted by of a mixture of 6 M HCl/0.01 M oxalic acid (200 µL).

Evaluation of Nb-chelate complexes in aqueous solutions

The following chelating ligands, were tested to find an optimal complexation agent for niobium isotopes: EDTA, CDTA, DTPA, TTHA, DOTA, TETA, Df, PAR, cf . Fig. 1.

Complexation of niobium with the different chelators was analyzed in terms of distribution of radioactivity of ^{95}Nb between a cation exchange resin (Chelex, Bio-Rad, Germany) and the complex according to Pueschel *et al.* [14]. Chelex is a chelating resin with iminodiacetic acid groups attached to a styrene-divinylbenzenecopolymer matrix, which was preconditioned with acetate buffer (0.1 M NaOAc, pH 4.7). Portions of 100 mg of resin were placed in eight plastic vials and acetate buffer (1.8 mL) and mixed with 0.01 M chelating solution (200 µL) in each vial. Finally, ^{95}Nb solution in 6 M HCl/0.01 M oxalic acid, 1 µL (50 kBq) was added to each vial. Mixtures were shaken and incubated for 24 hours at room temperature. Aliquots (1 mL) were taken and radioactivity was measured by gamma spectroscopy. For DOTA and TETA, due to their cyclic structure, kinetics of complex formation is generally slower than for

the other open chain chelators. For this reason the corresponding solutions were heated for 3 hours at 60 ºC during the 24 hours incubation.

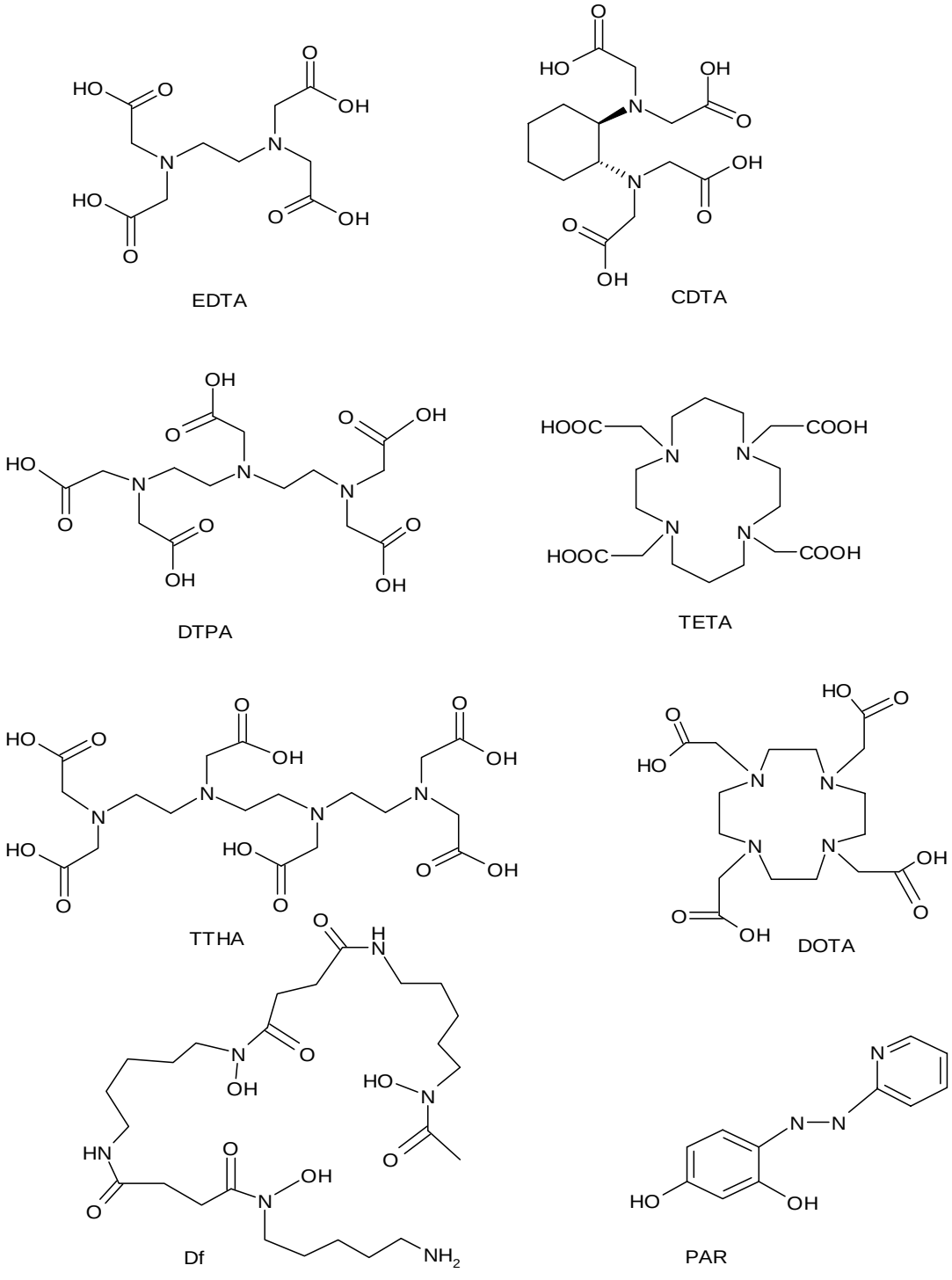

Figure 1: Different chelators, candidates for a Nb-complexation agent.

Influence of the pH on Nb-ligand complex formation

For EDTA, TTHA and Df the influence of different pH values for ^{95}Nb-ligand complex formation was tested. The experimental setup was similar to the one used in the previous chapter, but for the precondition of the Chelex resin and as a buffer solution, two different buffers were employed, namely, 0.1 M NaOAc buffer (pH 4.7) and 0.1 M tris(hydroxymethyl)aminomethane (TRIS, pH 7.4). After preconditioning, the resin was placed in polyethylene tubes and mixed with a solution of the chelator and ^{95}Nb (1 µL) (10-50 kBq) solution. After 24 hours incubation, aliquots (1 mL) of the solution were taken and analyzed by gamma spectroscopy.

Kinetics of the formation of Nb-Df complexes

To investigate the formation kinetics of ^{95}Nb-Df complexes, the following procedure was applied. In 1 mL reaction vials, to a solution of 0.1 µM Df (200 µL) in 0.1 M acetate buffer (pH 4.7) 6 M NaOH (1 µL) the ^{95}Nb solution (1 µL) (10-50 kBq) was added sequentially under stirring. Samples were taken for TLC analysis at appropriate time points (1, 5, 10, 20 and 30 min). Two different systems of TLC analysis were employed. As solid phase for both systems, C-18 modified silica gel on aluminum support (Merck, Germany) were used, and as mobile phases, a 0.25 M oxalic acid solution and a mixture of 0.07 M KH_2PO_4/MeCN (40/60), respectively.

Stoichiometry of the Nb-Df complexes

Different stoichiometric proportions of Nb/Df were examined using a ^{95}Nb + ^{nat}Nb$^{(V)}$ mixture. Aliquots of 10, 20 ,40 and 200 µL of 10^{-3} M Nb$^{(V)}$ standard solution (Alfa Aesar, Germany) spiked with ^{95}Nb in 0.1 M HCl/0.1 M oxalic acid were mixed with 0.02 µM Df in 0.1 M NaOAc (pH 4.7) in a 3 mL reaction vial. As a result, Nb$^{(V)}$ concentrations were $5\cdot10^{-6}$, 10^{-5}, $2\cdot10^{-5}$ and 10^{-4} M which equaled the Nb/Df proportions 1/1, 1/2, 2/1, 10/1, respectively. Reaction mixtures were filled-up to 2 mL with acetate buffer (pH 4.7) and were incubated at room temperature for 24 hours.

Synthesis and *in vitro* stability of Nb-Df Octreotide

A solution of 1 µM of Df-Octreotide (Fig. 2.) in 0.1 M NaOAc (pH 6) with an addition of 0.1 µM NaN_3 was used. This solution can be stored for days at -20 ºC.

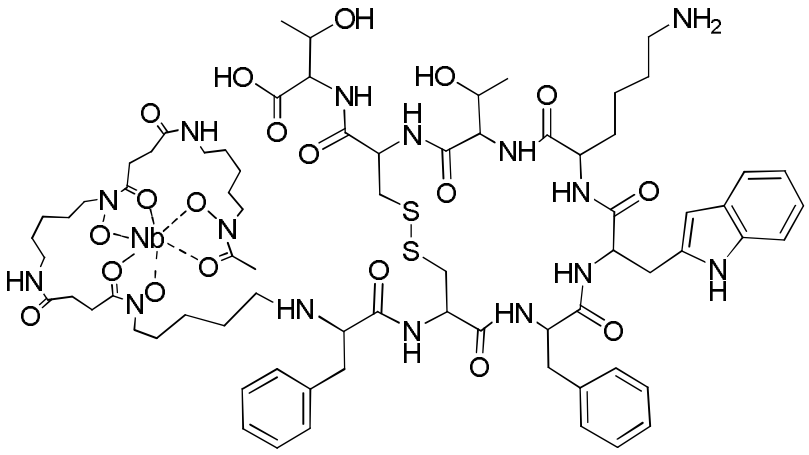

Figure 2: Structure of ^{95}Nb-Df-Octreotide complex.

7 µl (7 nmol) of the Df-Octreotide solution was mixed with 6 M NaOH (1 µL) and ^{95}Nb solution (1 µL) (10-50 kBq) and filled-up with 500 µL of buffer ammonium acetate (pH 5.0), KH_2PO_4/Na_2HPO_4 (pH 7.4) or TRIS (pH 8.6) buffer solutions. Aliquots were taken at different time points and the kinetics of ^{95}Nb-Df-Octreotide formation was monitored *via* TLC. As solid phase cellulose and as mobile phase a mixture of NaOAc/MeCN (55/45) were applied.

Competitive stability studies of Nb-Df

Competitive complexation experiment was carried out for EDTA and Df. A solution of 1 µM EDTA spiked with ^{95}Nb in acetate buffer (pH 4.7) was mixed with 0.01 µM Df. The ^{95}Nb-Df complex formation was measured by thin layer chromatography. As mobile phase 0.25 M oxalate solution (pH 8.5), as solid phase silica gel on aluminum plates RP-18 (Merck, Germany) was used.

Stability studies of Nb-Df and Nb-Df-Octreotide in serum

To examine the applicability of Nb-Df and Nb-Df-Octreotide complexes for medical purposes, stability tests in serum were performed. 120 mg of lyophilized human serum albumin (Sigma Aldrich, Germany) were dissolved in water (2 mL). 290 µL of 0.1 M NaOAc (pH 4.7) were mixed with of 1 µM Df solution (5 µL), 6 M NaOH (3 µL) and ^{95}Nb solution (3 µL) (30-150 kBq), and incubated at room temperature for 1 hour under gentle stirring.

In case of Df-Octreotide, a 0.1 M NaOAc (290 µL) solution (pH 4.7) was mixed with 5 nM Df-Octreotide (5 µL), 6 M NaOH (3 µL) and finally a ^{95}Nb solution (3 µL) (30-150 kBq) was added. The mixture was incubated for 1 hour at room temperature under intensive stirring. For both samples, TLC analysis was performed after 1 hour. In another test, the ^{95}Nb-Df (7 µL) and the ^{95}Nb-Df-Octreotide (6 µL) solutions were combined with serum (200 µL) and incubated under gentle stirring at 37 ºC. At different time points, aliquots were taken and analyzed by TLC. As solid phase, cellulose was used and as mobile phase NaOAc.

Stability studies of Nb-Df-Octreotide using competing metals such as Zr, Fe and Ga

Standard solutions (1 µM) for inductively coupled plasma mass spectrometry (ICP-MS) of $Zr^{(IV)}$, $Fe^{(III)}$, $Ga^{(III)}$ and $Nb^{(V)}$ in 0.09 M oxalic acid solution were applied (Alfa Aeasr, Germany).

In the first experimental setup, in four 3 mL reaction vials solutions of 0.1 M NaOAc (pH 4.7) (1.84 mL), Df-Octreotide (20 µL) and 0.1 M oxalic acid (100 µL) (pH 8.5), ^{95}Nb solution (1 µL) (10-50 kBq) and a 1 µM stable $Nb^{(V)}$ standard solution (20 µL) were added. The mixtures were incubated under gentle stirring. After 24 hours, 1 µM standard solutions (20 µL) of $Zr^{(IV)}$, $Fe^{(III)}$, $Ga^{(III)}$ or $Nb^{(V)}$ were added to one of the prepared vials with $^{95+nat}$Nb-Df-Octreotide. At appropriate time points, aliquots (3 µL) were taken and analyzed by TLC. A mobile phase 0.25 M oxalate solution (pH 8.5) and as solid phase RP-18 silica gel on aluminum plates were used.

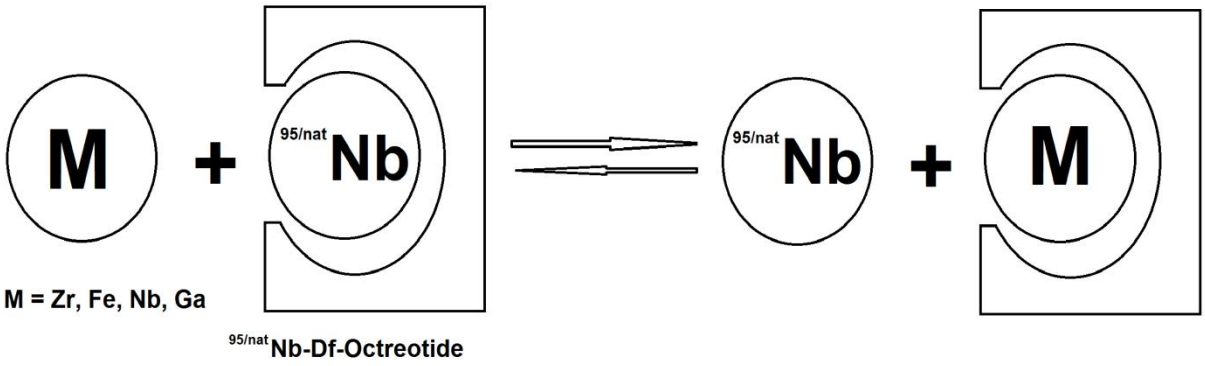

Figure 3: Scetch of the studies on the stability $^{95+nat}$Nb-Df-Octreotide using competing metals (Zr, Fe, Nb and Ga).

In an additional experimental setup the test was conducted in an opposite direction. To each of the four polyethylene 3 mL reaction vials, 0.1 M NaOAc (1.84 mL), Df-Octreotide (20 µL) (pH 4.7) and 0.1 M oxalic acid (100 µL) (pH 8.5) were added. 1 µM standard solutions (20 µL) of the metals Zr, Fe, Ga and Nb were added. The mixtures were then incubated under gentle stirring. After 24 hours a 1 µM standard solution (20 µL) of $Nb^{(V)}$ and the ^{95}Nb solution (1 µL) were added. At appropriate time points, aliquots (3 µL) were taken and analyzed by TLC, as mobile phase 0.25 M oxalate solution (pH 8.5) and as solid phase RP-18 silica gel on aluminum plate were used.

Results

Evaluation of Nb-chelate-complexes in aqueous solutions

The individual ligands showed different capability for ^{95}Nb complex formation (Fig. 4). Desferrioxamine shows the best results with 82±3% of complex formation at room temperature, pH 4.7, at 24 hour time point in comparison with all tested chelators. TTHA, DTPA and EDTA showed good complexation properties with niobium too (73±2%, 54±4% and 53±3% respectively). For the cyclic chelators DOTA and

TETA, in spite of 3 hours heating at 60 ºC during the conjugation process, less than 20% of complex formation were observed.

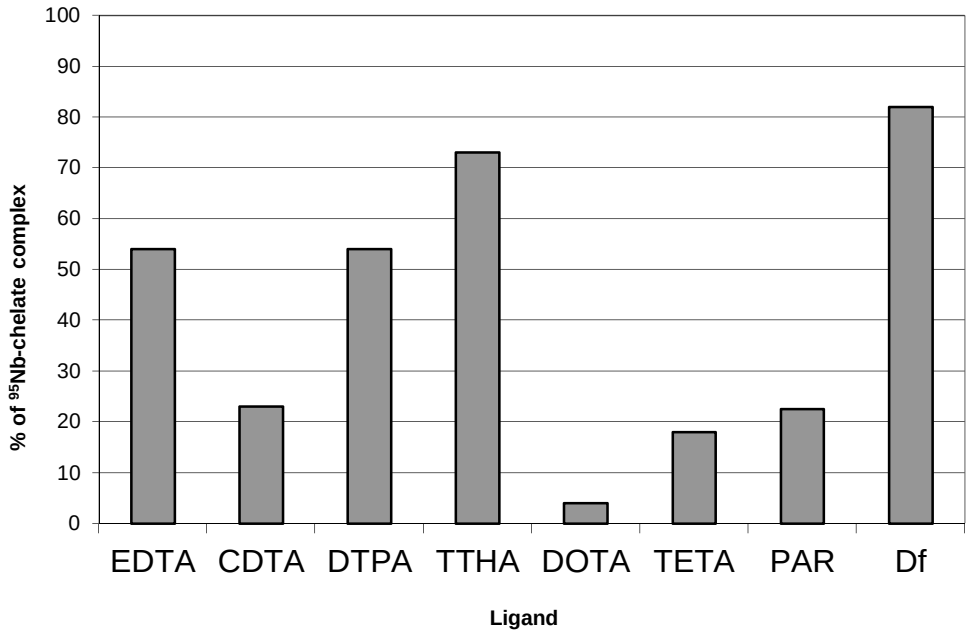

Figure 4: Percentage of the ^{95}Nb-chelate-complex formation using different chelators at pH 4.7 (24 hours, RT, 0.01 M ligand-concentration).

Influence of the pH on the Nb-chelate-complex formation

For EDTA and TTHA, increasing the pH to 7.4 caused a very strong decreased in complex formation with ^{95}Nb. In case of EDTA, between pH 4.7 and 7.4 a difference of 32±2% was observed, for TTHA the difference was even higher (64±3%). In case of Df, no significant difference was found between the two pH values.

Kinetics of the formation of Nb-Df complexes

The kinetics of the formation of ^{95}Nb-Df complexes was monitored at various time points during incubation of mixture for half an hour at room temperature in acetate buffer (pH 4.7). Already after the first minute of reaction, more than 70% of complex formation was observed. At 5 and 10 min of incubation high yield of 86±5% and 95±3%, respectively, can be achieved. At later time points between 20 and 30 min the labeling yields approach ≥ 98% of product formation. Results allow us to conclude that for appropriate labeling 15 to 20 minutes of reaction period is sufficient.

Stoichiometry of Nb-Df complexes

Results of the stoichiometry tests showed for a stoichiometric ratio of Df/$^{95+nat}$Nb = 2/1 and also 1/1 an almost quantitative $^{95+nat}$Nb-Df complex formation (Tab. 1). An increasing content of $Nb^{(V)}$ of a 1/2 and 1/10 ratio led to an Nb-Df complex formation of 49±2% and 13±3%, respectively. Both values correlate very well with the results of a ratio of 1/1. These results show that for an efficient and high yield complexation of niobium with desferrioxamine a 1/1 ratio already gives excellent results and a 2-fold excess of Df over $Nb^{(V)}$ allows for a quantitative Nb-Df complexation.

Table 1: Experimental and theoretically calculated $^{95+nat}$Nb-Df complex formation yields at different Df/Nb ratios (24 hours, RT, pH 4.7 NaOAc).

Ratio of Df/Nb	Nb-Df complex formation yields (%)	Theoretically calculated yields for Df/Nb-1/1 (%)
2/1	≥ 99	100
1/1	96±5	100
1/2	49±3	50
1/10	13±4	10

Synthesis of Nb-Df Octreotide

For a first testing of the application of ^{90}Nb as a potential candidate for PET imaging, labeling of ^{95}Nb with Df-Octreotide was performed. Here, the simple chelate Df turns into a bifunctional derivate, yielding Df-succinyl-(D)Phe^{1}-Octreotide. However, this conjugation creates a different structure of the chelate (one amino group replaced on succinyl linker to attach Octreotide) compared to initial Df. Therefore it is important to prove that the stability of the derivate forms complexes with Nb not significant weaker than for the initial desferrioxamine. However, labeling kinetics showed that already after 30 min at room temperature, for all tested pH values, labeling yields are more than 90% and for pH 5.0 are >99% (Fig. 5). After 1 hour at different pH values the labeling yields varied from 97% to 100%. These results show that one hour incubation is efficient to reach a maximal labeling yield and an optimal pH for labeling is 5.0. However, pH 7.4 and 8.6 also showed good kinetics of complex formation and might be preferred in case of very pH sensitive molecules as targeting vectors different to octreotide. Thus, even after bifunctionalization and the loss of one NH_2-functionality, the bifunctional Df-derivative retains excellent complex formation properties for $Nb^{(V)}$.

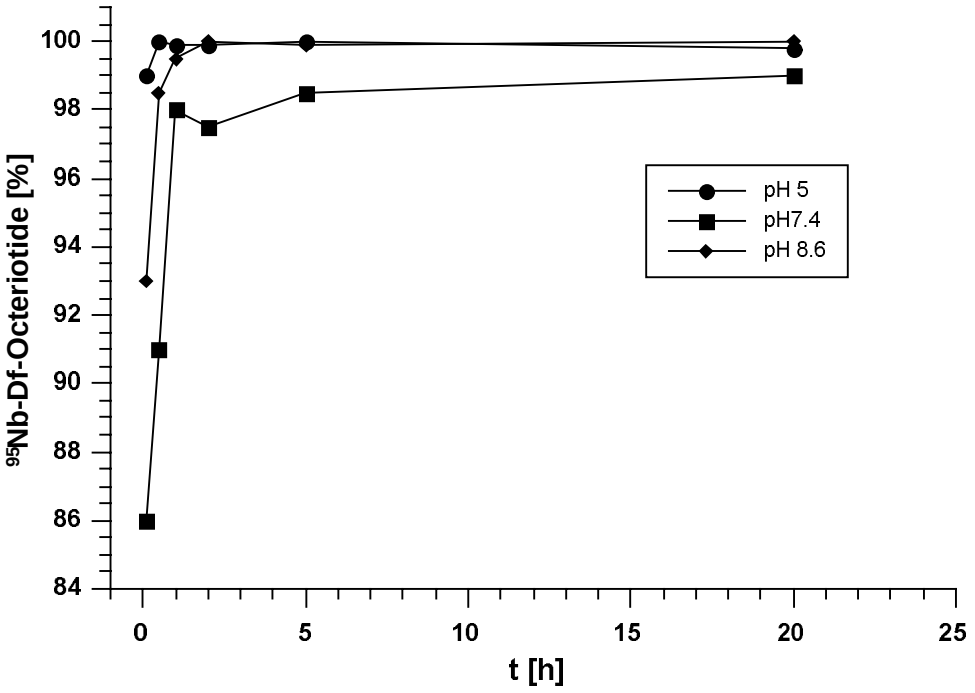

Figure 5: Kinetics of the formation of ^{95}Nb-Df Octreotide at various pH values (RT, 7 nmol Df-Octreotide).

Comparative studies of the *in vitro* stability of Nb-Df with EDTA and Nb-Df-Octreotide *versus* analogue M-Df-Octreotide (M= Zr, Fe and Ga) complexes

A competitive experiment of ^{95}Nb-EDTA versus desferrioxamine showed a relatively fast transchelation of ^{95}Nb from EDTA to ^{95}Nb-Df. At 30 min of incubation, the ratio of ^{95}Nb-EDTA/^{95}Nb-Df was 1/1. After 120 min less than 10% of the ^{95}Nb-EDTA was left and at 180 min more than 95% of ^{95}Nb-Df was found.

Competitive studies with other metals that can be present in the labeling mixture (Fe, Zr and Ga) and can act as a competitor of Nb during of labeling procedure or *in vivo* (Fe) showed that the complex formation of Nb-Df is more preferred than with all other tested metals (Fig 6.).

For a first experimental setup, the ^{95}Nb solution was added to M-Df-Octreotide (M= Zr, Fe, Ga, Nb) to test if $Nb^{(V)}$ will displace the other metals in the complex.

As a result, the capacity of Df-Octreotide complex formation for niobium is higher than for all the other metals evaluated. After addition of the ^{95}Nb solution, more than 50% of $^{95+nat}$Nb-Df-Octreotide complex was formed for Zr, Fe and Ga already after 30 min. After three days, the Zr sample contained already 80±2% of $^{95+nat}$Nb-Df-Octreotide. In case of Fe and Ga, the percentages of $Nb^{(V)}$ displacing the Me-Df-Octreotide complexes were 86±2% and 89±3%, respectively. In the case of ^{95}Nb versus ^{nat}Nb-Df-Octreiotide complexation, a 50±4% value was approached as expected.

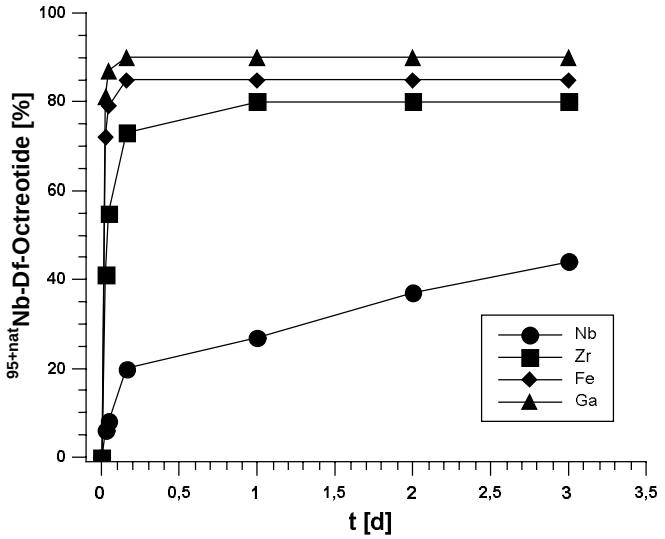

Figure 6: Kinetics of the formation of $^{95+nat}$Nb-Df-Octreotide in a system of M-Df-Octreotide (M= Zr, Fe, Nb, Ga) after addition of $^{95+nat}$Nb.

To prove the results, the experimental setup was performed the other way around. $Nb^{(V)}$ was complexed with Df-Octreotide first and then all other metals (Zr, Fe, Ga and Nb) were added to check if they can displace $^{95+nat}Nb$ from the Nb-labeled Octreotide (Fig. 7).

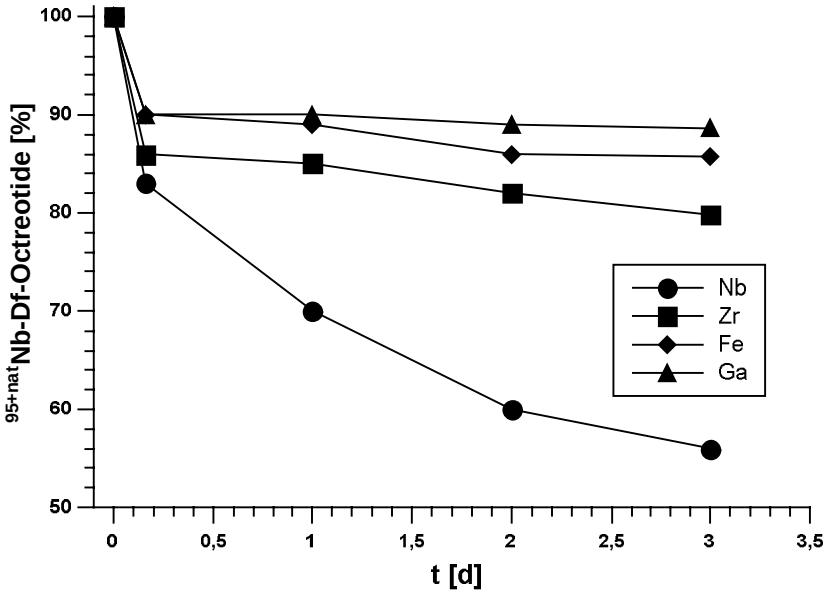

Figure 7: Stability of the $^{95+nat}Nb$-Df-Octreotide after addition of Zr, Fe, Nb and Ga.

After three days of incubation of the mixture with Zr and $^{95+nat}Nb$-Df-Octreotide, the solution showed only 20±1% of Df-Octreotide displaced by Zr. For Fe and Ga, the percentages of Df-Octreotide complex formation after three days incubation were even less, only 14±2% and 11±1%, respectively.

The results clearly demonstrate that $Nb^{(V)}$ presents the best capacity for complexation with desferrioxamine in comparison to all other evaluated metals.

Stability studies of Nb-Df and Nb-Df-Octreotide in serum

The ^{95}Nb-Df complex incubated in serum at 37 ºC showed excellent *in vitro* stability. Over two days, less than 4% and after seven days less than 6% of free ^{95}Nb was found. Slightly increasing degradation of the complex with 11±1% free ^{95}Nb was observed after ten days.
A slightly decreased *in vitro* complex stability was detected after two days of incubation for the ^{95}Nb-Df-Octreotide complex in comparison to the ^{95}Nb-Df complex. After seven days 9±2% of free ^{95}Nb was found and at day ten this amount increased to 13±2%.

Discussions

In present experiments it was shown that desferrioxamine is the most appropriate ligand for formation complexes with $Nb^{(V)}$ isotopes among the other common chelators tested. In addition, desferrioxamine preferens complex formation with $Nb^{(V)}$ compared with other metals involved (Zr, Fe and Ga). Desferrioxamine thus is identified as chelator of choice to synthesize ^{90}Nb labeled biomoleclues (antibody, antibody fragments or peptides) for *immuno*-PET. Bifunctionalization of Df as needed for covalently attaching Df to a targeting vector does not decrease its potential for $Nb^{(V)}$ complex formation and stability. As proof-of-principle the Df-succinyl-(D)Phe^{1}-Octreotide was successfully labeled with ^{95}Nb for 30 minutes at pH 5 at room temperature in more than 99% yield. The *in vitro* stability of this product was excellent over days in HSA at 37°C. The potential of bifunctional derivates of Df should retain also in the case of other bifunctional derivatives of Df such as *N*-Succinyl-desferrioxamine (N-suc-Df) and p-Isothiocyanato- benzyl-desferrioxamine (NCS-Bz-Df) [15, 16].

Conclusions

In summary, fast and almost quantitative complex formation of $Nb^{(V)}$ with desferrioxamine can be performed at a wide range of pH (4-7) and at room temperature, which opens a broad field for applications of Nb-Df for biomolecules. Bifunctionalisation does not affect the complex formation parameters of Df. Radiolabeled *Nb-Df-Octreotide remains stable *in vitro* and *in vivo*. With this Nb-

specific bifunctional chelate in hands, the use of ^{90}Nb for *immuno*-PET may now be evaluated in adequate applications.

Acknowledgements

The authors thank the teams of the TRIGA reactor in Mainz and the research reactor BERII at the Helmholtz Centre Berlin for production of ^{95}Nb as well as Novartis Pharma AG, Basel for providing Df-succinyl-(D)Phe^{1}-Octreotide.

References

1. van Dongen, G. A. M. S., Visser, G. W. M., Lub-de Hooge, M. N., de Vries, E. G., and Perk, L. R. Immuno-PET: a navigator in monoclonal antibody development and applications. *Oncologist* 2010; 12; 1379–89.
2. Perk, L. R., Visser, O. J., Stigter-van Walsum, M., Vosjan, M. J. V. D., Visser, G. W. M., Zijlstra J., Huygens P. C., and van Dongen G. A. M. S. Preparation and evaluation of ^{89}Zr-Zevalin for monitoring of ^{90}Y-Zevalin biodistribution with positron emission tomography. *Eur J Nucl Med Mol Imaging* 2006; 33; 1337–45.
3. Koehler, L., Gagnon, K., McQuarrie, S., and Wuest, F. Iodine-124: A promising iodine radioisotope for positron emission tomography (PET). *Molecules* 2010; 15; 2686–718.
4. Wu, A. M., and Yazaki, P. J. Designer genes: recombinant antibody fragments for biological imaging. *Q J Nucl Med* 2000; 44; 268–83.
5. Deffar, K. Hengliang, S., Liang, L., Xingzhi W., and Xiaojuan Z. Nanobodies—the new concept in antibody engineering. *African J Biotechnology* 2009; 8; 2645–52.
6. Cai, W., Chen, K., He, L., Cao, Q., Koong, A., and Chen, X. Quantitative PET of EGFR expression in xenograftbearing mice using ^{64}Cu-labeled cetuximab, a chimeric anti-EGFR monoclonal antibody. *Eur J Nucl Med Mol Imaging* 2007; 34; 850–58.
7. Roesch, F., Qaim, S. M., and Stöcklin, G. Production of the positron emitting radioisotope ^{86}Y for nuclear medical application. *Appl Radiat Isot* 1993; 44; 677–81.

8. Jamar, F., Barone, R., Mathieu, I., Walrand, S., Labar, D., Carlier, P., De Camps, J., Schran, H., Chen, T., Smith, M. C., Bouterfa, H., Valkema, R., Krenning, E. P., Kvols, and L. K., Pauwels, S. (2003) ^{86}YDOTA^{0}-D-Phe^{1}-Tyr^{3}-octreotide (SMT487) - a phase 1 clinical study: pharmacokinetics, biodistribution and renal protective effect of different regimens of amino acid co-infusion. *Eur J Nucl Med Mol Imaging* 2003; 30; 510–18.
9. Bruehlmeier, M., Roelcke, U., Blauenstein, P., Missimer, J., Schubiger, P. A., Locher, J. T., Pellikka, R., and Ametamey S. M. Measurement of the extracellular space in brain tumors using ^{76}Br-bromide and PET. *J Nucl Med* 2003; 44; 1210–18.
10. Zeglis, B. M., and Lewis, J. S. A practical guide to the construction of radiometallated bioconjugates for positron emission tomography. *Dalton Trans* 2011; 40(23); 6168–95.
11. Busse, S., Roesch, F., and Qaim, S. M. Cross section data for the production of the positron emitting niobium isotope ^{90}Nb via the ^{90}Zr(p, n)-reaction. *Radiochim Acta* 2002; 9; 1–5.
12. Busse, S., Brockmann, J., and Roesch, F. Radiochemical separation of no-carrier-added radioniobium from zirconium targets for application of ^{90}Nb-labelled compounds. *Radiochim Acta* 2002; 90; 411–15.
13. Radchenko, V., Hauser, H., Eisenhut, M., Vugts, J. D., van Dongen, G. A. M. S., and Roesch, F. ^{90}Nb – a Potential PET Nuclide: Production and Labeling of Monoclonal Antibodies. *Radiohim Acta* 2012; 100(11); 857-64.
14. Pueschel, R., and Lassner, E., Das Sorptionverhalten von Titan, Niob und Tantal an Dowex A-1 in Gegenwart von Wasserstoffperoxid und von verschiedenen Chelonen. *Z Anorg Anal Chem* 1964; 326; 317-22.
15. Verel, I., Visser, G. W. M., Boellaard, R., van Walsum, S. M., Snow, G. B., and van Dongen, G. A. M. S. ^{89}Zr immuno-PET: comprehensive procedures for the production of ^{89}Zr-labeled monoclonal antibodies. *J Nucl Med* 2003; 44; 1271–81.
16. Perk, L. R., Vosjan, M. J., Visser, G. W., Budde, M., Jurek, P., Kiefer, G. E., and van Dongen G. A. M. S. p-Isothiocyanatobenzyl-desferrioxamine: a new bifunctional chelate for facile radiolabeling of monoclonal antibodies with zirconium-89 for immuno-PET imaging. *Eur J Nucl Med Mol Imaging* 2009; 37; 250–9.

3.5 Conjugation, labeling and initial *in vivo* assessment of an anti-VEGF monoclonal antibody labeled with Niobium isotopes.

Conjugation, labeling and initial *in vivo* assessment of an anti-VEGF monoclonal antibody labeled with Niobium isotopes.

V. Radchenko[1], P. Bouziotis[2], G. Loudos[3], S. Xanthopoulos[2], H. Hauser[4], M. Eisenhut[4], B. Ponsard[5], F. Roesch[1]

[1]Institute of Nuclear Chemistry, Johannes Gutenberg University, Mainz, Germany

[2]Institute of Radioisotopes and Radiodiagnostic Products, N.C.S.R. "Demokritos", Athens, Greece

[3]Department of Medical Instruments Technology, Technological Educational Institute of Athens, Athens, Greece

[4] Radiopharmaceutical Chemistry, German Cancer Research Center, Im Neuenheimer Feld 280, D-69120 Heidelberg, Germany

[5] Radioisotopes and Silicon Production, Belgian Nuclear Research Centre, Boeretang 200, BE-2400 Mol, Belgium

Abstract

The application of radionuclide-labeled biomolecules such monoclonal antibodies or antibody fragments for imaging purposes is called *immunoscintigraphy*. More specifically, when the nuclides used are positron emitters, such as Zirconium-89, the technique is referred to as *immuno-PET*. Currently, there is an urgent need of radionuclides with a half-life which correlates well with the biological kinetics of biomolecules under question. ^{90}Nb is a promising candidate due its half-life of 14.6 hours and rather low β^+ energy of E_{mean} = 0.35 MeV. In this work, the monoclonal antibody bevacizumab (Avastin®) was labeled with $^{90/95}$Nb with two different specific activities and *in vitro* and *in vivo* stability was evaluated in normal Swiss mice and in tumor-bearing SCID mice. Biodistribution of ^{95}Nb-oxalate, ^{95}Nb-chloride and ^{95}Nb-Df was conducted to prove stability of *Nb-labeled biomolecules and also to understand the behavior of *Nb compounds *in vivo*.

Results showed that high concentration of bevacizumab gives adequate tumor uptake, however at the same time high uptake in the liver, spleen and kidneys. Injection of low concentration of bevacizumab with higher specific activity did not show high uptake in the liver, spleen, kidneys and also in the bones. Biodistribution of ^{95}Nb-oxalate, ^{95}Nb-chloride and ^{95}Nb-Df did not show any specific uptake, apart from bone accumulation for ^{95}Nb-oxalate and ^{95}Nb-chloride, which can be an "indicator" for the detection of release of ^{90}Nb from the labeled biomolecules. Results proved promise of application of ^{90}Nb for the purposes of *immuno*-PET.

Keywords: $^{90/95}$Nb / bevacizumab / labeling / VEGFR / biodistribution / PET imaging

Introduction

Targeted imaging of cancer is crucial to modern-day cancer management. Targeting radionuclides are an exciting strategy for tumor diagnosis and therapy [1]. An attractive feature of this strategy is the ability to select radionuclides and targeting vehicles with characteristics which are best suited for a particular application.

Angiogenesis is the development of new blood vessels from pre-existing ones. Angiogenesis is regulated by chemical signals of the organism, which function as an "angiogenesis switch", regulating the formation of new vasculature. Bevacizumab is a humanized monoclonal antibody (mAb) which binds all VEGF-A isoforms [2].

Currently many studies were concentrating on labeling of bevacizumab with radionuclides for it in vivo behavior evaluation [3-6].

An important criterion for application of radionuclides with mAb is the half-life of the radionuclide which should favorably correlate to the biological kinetic of large-size biomolecules. Due to the long circulation of intact antibodies, optimal tumor-to-non tumor ratios can be reached from 5 to 7 days post injection. Therefore, radionuclides with appropriate half-life should be chosen. Several positron-emitting radionuclides with long and medium-long half-lives of interest for PET-imaging with antibodies and antibody fragments are, for example, ^{89}Zr ($t_{1/2}$ = 78.4 h) [7, 8], ^{64}Cu ($t_{1/2}$ = 12.7 h) [9, 10], ^{86}Y ($t_{1/2}$ = 14.7 h) [11, 12], ^{76}Br ($t_{1/2}$ = 16.0 h) [13].

Several crucial factors and characteristics apply to radionuclide candidates for *immuno*-PET. The most important ones are: i) a physical half-life paralleling the biological half-life of the mAb or antibody fragment; ii) a high positron branching with no or weak accompanying other radiation (β^-, γ) to offer high-sensitivity PET imaging while reducing the radiation burden of the patient; iii) a preferably low β^+-energy to allow for high-resolution PET imaging; and iv) the availability of the radionuclide, i. e. an efficient production and radiochemical separation route.

In previous reports we have proposed ^{90}Nb as a promising candidate for application in *immuno*-PET [14-16]. Its intermediate half-life of 14.6 hours and a high positron branching of 53% may make ^{90}Nb an ideal candidate for application with antibody fragments, monoclonal antibodies, drug delivery systems and nanoparticles.

In recent work we have evaluated the *in vit*ro and *in vivo* stability of $^{90/95}$Nb radiolabeled bevacizumab. Influence of concentrations and specific activity of the radiolabeled product was studied. *In vivo* evaluation of ^{95}Nb-oxalate, ^{95}Nb-chloride and ^{95}Nb-Df in healthy mice was performed.

Materials and Methods

Materials

Reagents were purchased from Sigma-Aldrich (Germany) and used without further purification, unless otherwise stated. Deionized water (18 MΩ cm^{-1}) and ultra pure HCl solution were used. No further special measures were taken regarding working under strict metal-free conditions. The mAb Bevacizumab (Avastin®, Roche) directed against the VEGF-A family of isoforms was bought from Roche Ellas S. A. (Greece). For the purification of conjugated and labeled antibodies, PD-10 columns (GE Healthcare Life Science) were applied, for ion exchange separation Aminex A27, 15 ± 2 μm and AG1x8, 200-400 mesh anionic exchange resins and DOWEX50x8, 200-400 mesh (BioRad) were used. For solid extraction, UTEVA® resin (Triskem Int., France) was applied.

The production yield, radionuclidic purity, radiochemical purity and separation yield of $^{90/95}$Nb were determined by *γ*-ray spectroscopy using an Ortec HPGe detector system and Canberra Genie 2000 software. The dead time of the detector was always kept below 10%. The detector was calibrated for efficiency at all positions with the certified standard solution QCY48, R6/50/38 (Amersham, UK).

Production of ^{90}Nb and ^{95}Nb

^{90}Nb was produced via the ^{90}Zr(p,n)^{90}Nb reaction at the cyclotron MC32NI of the German Cancer Research Center, Heidelberg. For irradiation, a stack of three discs of natural zirconium (natural abundance: 51.45% ^{90}Zr) foils of 10 mm diameter and a thickness of 0.25 mm each was used. Irradiation was performed at 20 MeV proton energy and a current of 5 μA for 1 hour. This initial proton energy decreased, by using an aluminum holder cover of 0.5 mm thickness, to 17.5 MeV while entering the first foil of Zr. Twenty-four hours after end of irradiation (EOB), production yield and impurities were measured by gamma ray spectroscopy. The absolute activity of ^{90}Nb was calculated as average of its two gamma-lines at 141.2 keV (66.8% abundance) and 1129.2 keV (92.7%).

^{95}Nb ($T_{1/2}$ = 35 d) was employed for the biodistribution experiments and also to clarify the separation chemistry. ^{95}Nb was produced via the ^{94}Zr(n, γ)→^{95}Zr(β^-, $T_{1/2}$ = 64 d)→^{95}Nb reaction from natural zirconium granules (1-3 mm, 99.8% ChemPur, Germany). Neutron irradiation was performed at the BR2 reactor at

the Belgian Nuclear Research Centre, Belgium and at BERII reactor at Helmholtz Centre in Berlin, Germany.

The production of the radionuclides ^{95}Zr / ^{95}Nb and ^{90}Nb was monitored by gamma ray spectroscopy, via emissions at 724.2 keV (44.2%) and 756.7 keV (54.0%) for ^{95}Zr, and at 765.8 keV (100%) for ^{95}Nb and 1129 KeV (92%) for ^{90}Nb.

Separation and purification of n.c.a. $^{90/95}$Nb

First separation strategy

The first separation strategy was applied for biodistribution studies in tumor-bearing mice.

The separation procedure was modified following the procedure described by Busse *et al.* [19]. In short, the zirconium metal target (260±3 mg) was transferred into a 50 mL vial and 2 mL of water were added. Under ice-cooling, 48% HF (0.63 mL) was added in small portions. After complete dissolution, 10 M HCl (6 mL) and saturated boric acid (3.4 mL) were added. The $^{90/95}$Nb fraction was extracted with 0.02 M *N*-benzoyl-*N*-phenylhydroxylamine (BPHA) in $CHCl_3$ (5 mL) by vigorous stirring of the two phases in a 50 mL vial for 20 min. The aqueous phase was additionally washed with $CHCl_3$ (3 mL). The organic phases were combined and washed with a mixture of 9 M HCl/0.001 M HF (2 mL) and with 9 M HCl (2 mL) and finally extracted with aqua regia (5 mL).

For a final purification of $^{90/95}$Nb from remaining trace amounts of zirconium, an anionic exchange method was employed. After the aforementioned back extraction, the aqueous phase was evaporated to dryness. The residue was dissolved in a mixture of 0.25 M HCl/0.1 M oxalic acid (0.5 mL) and adsorbed onto a small Aminex A27 (15 ± 2 μm) anionic exchange column (20 x 1.5 mm). Elution was performed under slight overpressure of 0.3 bars. After loading, the column was washed with 10 M HCl (100 μL). Residues of Zr were removed by washing with a mixture of 9 M HCl/0.001 M HF (200 μL). $^{90/95}$Nb was eluted by a mixture of 6 M HCl/0.01 M oxalic acid (200 μL).

Alternative separation strategy

A second separation strategy was applied to obtain high specific activity product for biodistribution studies involving a lower mAb concentration in healthy mice, as well as for biodistribution studies of ^{95}Nb-oxalate, ^{95}Nb-chloride and ^{95}Nb-Df in healthy mice, as well.

Crude separation from the Zr target was applied following a published protocol [32]. In short,
2 mL of 21 M hydrofluoric acid containing the irradiated zirconium target were passed through the cation exchange resin (DOWEX 50x8, 100 mg, 200-400 mesh, 10x5 mm) resin in F^- form for the removal of colloids, unsolved target particles and possible trace contamination of 2+ and 3+ charged metal cations, such as for example Cu^{2+} or Fe^{3+} from the target holder. The column was additionally washed with concentrated hydrofluoric acid (1 mL). The solution (3 mL) which passed through the cation exchange resin was transferred to an anion exchange column (300 mg, 25x5 mm) filled with AG 1x8 resin (200-400 mesh) in the F^- form. Nb^V remained on this resin and the bulk amount of Zr^{IV} passed through. The column was washed with concentrated HF (4.5 mL) to elute traces of Zr^{IV}, while ^{90}Nb stays on the column.
A small plastic column was filled with UTEVA resin (150 µm, 100 mg, 10x5 mm). The aforementioned anion exchange column was directly connected with the UTEVA column and 7 mL of 0.3 M oxalic acid/ 7.5 M HCl were passed through both columns.
The UTEVA column was next washed with 5 M HCl (5 mL). Traces of $*Zr^{IV}$ passed through the UTEVA, while Nb^V remains absorbed on the column. For elution of ^{90}Nb 0.1 M oxalic acid was applied. The column was washed with 200 µL and ^{90}Nb eluted with another 400 µL of 0.1 M oxalic acid.

Synthesis of ^{95}Nb-oxalate, ^{95}Nb-chloride, ^{95}Nb-Dessferrioxamine (Df)

^{95}Nb-oxalate. Preparation of ^{95}Nb-oxalate (10 mM) consists of 10 mM ^{95}Nb-oxalate was prepared by dilution of purified ^{95}Nb fraction with saline.
^{95}Nb-chloride. ^{95}Nb-chloride was prepared by evaporation of an aliquot (50 µL) of the oxalate fraction obtained after ^{95}Nb purification, and addition of several portions (3x 100 µL) of 30% HCl, after which the mixture was dried again at 100 °C. The resulting preparation was dissolved in saline.
^{95}Nb-Df. For the preparation of ^{95}Nb-Df, 50 mM of Dessferioxamine B in saline (1.45 mL) were mixed with ^{95}Nb-oxalate (50 µL) and incubated for 30 min at room temperature. The formation of ^{95}Nb-Df was monitored by thin layer chromatography at RP-18 TLC plates in 0.25 M oxalic acid solution as mobile phase.

Monoclonal antibody modification with Df-Bz-NCS

Bevacizumab was pre-modified with Df-Bz-NCS [2]. In short, while gently shaking, a threefold molar excess of Df-Bz-NCS (in 20 µL DMSO) was added to the mAb (3 mg/mL in 1 ml 0.1 M $NaHCO_3$ buffer, pH 9.0), and incubated for 30 min at 37 °C. Non-conjugated chelator was removed by size exclusion chromatography (SEC) using a PD-10 column and 0.9% sodium chloride solution as the eluent.

Labeling of Bevacizumab with $^{90/95}$Nb

Df-Bz-NCS-bevacizumab was labeled with $^{90/95}$Nb following two different labeling protocols. For the first protocol, to a $^{90/95}$Nb solution in 6M HCl/0.01M oxalic acid solution (200 µL), 6M NaOH (180 µL) and 1M NaOH (230 µL) were added. After 3 min, 0.5M HEPES buffer (pH 7.0) (390 µL) and Df-Bz-NCS-mAb (1.5 mg/mL) (1.0 mL) were added. The total volume of the mixture was 2 mL.
For the second labeling protocol, a purified $^{90/95}$Nb fraction in 0.1 M oxalic acid (20 µL) was mixed with 300 µL of normal saline and then the mixture was adjusted to pH 6-7 with 0.1 M Na_2CO_3 (50-60 µL). The modified mAb (300 µg, 120 µL) was then added to this mixture and then the volume of the mixture was adjusted to 1 mL with normal saline. Both mixtures were incubated at room temperature for 60 min. Analysis of product formation was monitored by ITLC (0.02 M citric acid/MECN, 90/10) at 10, 30 and 60 min and by HPLC at 60 min post-incubation. Finally, $^{90/95}$Nb -Df-Bz-NCS-bevacizumab was purified by using a PD-10 column, with 0.9% sodium chloride solution as the mobile phase.

In vitro metabolic stability

Metabolic stability of $^{95/90}$Nb-Bevacizumab was studied in two setups, first in normal saline at room temperature and in fresh human plasma at 37°C. For preparation of human plasma, human blood was collected in heparinized polypropylene tubes and centrifuged at 5000 rpm at 4°C for 5 min. The plasma was collected and three fold excess (300 µL) was incubated with $^{95/90}$Nb-Bevacizumab (100 µL) at 37°C. Aliquots of the sample were withdrawn at 60 min, 3 h, 3 d, 5 d and 7 d, and analyzed by ITLC and HPLC.

Biodistribution studies

Female athymic SCID mice (average weight 20 g, 5 weeks) as well as normal Swiss mice were obtained from the breeding facilities of the Institute of Biology of the NCSR "Demokritos". The SCID mice were inoculated subcutaneously into the right front leg with M165 cells (1 x 10^7 cells/animal) in 100 μL fetal bovine serum-free medium. When tumors reached a size of 0.2 to 1 g (i.e. 10 to 15 days for all cell lines involved), biodistribution studies were performed.

Tumor-bearing mice were injected via the tail vein with (270 kBq/100 μg) and healthy mice received an injection of higher specific activity product (300 kBq/ ~ 10 μg). Groups of three animals were sacrificed at 4, 24, 48 and 72 hours after injection of radiolabeled antibody.

To prove specific binding of the radiolabeled mAb to the tumor, blocking experiments were performed in the tumor-bearing SCID mice. Group of animals was treated with 100 fold excess of the cold bevacizumab and sacrified at 24, 48 and 72 hours post injection.

Biodistribution of ^{95}Nb-Df, ^{95}Nb-chloride and ^{95}Nb-oxalate were performed in healthy mice. Each animal received an injection of 100 μL of substance with 300±30 kBq of ^{95}Nb. Groups of three animals were sacrificed at 4, 24, 48 and 72 hours after injection of the compounds.

Tumors (in the case of SCID mice) and tissues and organs (blood, heart, liver, stomach, intestines, spleen, muscle, lungs, pancreas, muscle and bones) were excised, blotted dry and weighed. Samples were counted in a gamma counter (NaI gamma counter, Packard). Standards were prepared from the injected material and were counted each time simultaneously with the tissues excised, allowing for calculations to be corrected for physical decay of the radioisotope. Radiolabeled antibody distribution over time was expressed as injected dose per gram (%ID/g). All animal studies were performed in compliance with European legislation. Hellenic authorities approved of all animal protocols.

PET Imaging Studies

PET imaging was performed on an experimental, small field-of-view PET camera, designed and assembled by the "Detector and Imaging Group" of the "Thomas Jefferson National Accelerator Facility, USA, in collaboration with the Medical Instruments Department of the Technological Educational Institute of Athens. The high performance of the system is archived by using the very fast LSO crystal, the Hamamatsu

H8500 PSPMTs, fast amplification electronics, an FPGA system and USB 2 data transfer protocol. Image reconstruction is performed with JAVA in the Kmax environment.

Tumor-bearing SCID mice were injected with 200 kBq/100 µg of ^{90}Nb-bevacizumab (volume 100 µL) and were anaesthetized by i.p. injection of 100 µl/10 g mouse body weight of a cocktail solution of ketamine/xylazine. Dynamic imaging was not performed, due to the low specific activity of the radiolabeled species.

Results

Production of Nb isotopes

^{90}Nb. The overall irradiation yield of ^{90}Nb for three 1 h and 5 µA irradiations was 720± 50 MBq, i. e. 145±10 MBq/µAh under given irradiation parameters. The radionuclidic purity of ^{90}Nb after EOB was more than 97%. Minor isotopic impurities found were: ^{92m}Nb ($T_{1/2}$ = 10.2 d) = 1.64%, ^{95}Nb ($T_{1/2}$ = 35.0 d) = 0.08%, ^{95m}Nb ($T_{1/2}$ = 3.6 d) = 0.29% and ^{96}Nb ($T_{1/2}$ = 23.35 h) = 0.88%.

^{95}Nb. At a neutron flux of $2 \cdot 10^{14}$ $s^{-1} \cdot cm^{-2}$ (BER II), a 50 days irradiation of 300 mg target produced more than 1.5 GBq of ^{95}Zr. The maximum daughter activity of ^{95}Nb generated from ^{95}Zr was obtained at ~67 d, EOB.

Separation and purification of no-carrier added ^{90}Nb

First separation strategy

The extraction steps provided crude separation of ^{90}Nb from the target material with the organic phase collecting more than 99% of ^{90}Nb. After the back extraction procedure, the 5 mL aqueous phase contained 90-95% of the ^{90}Nb activity. After both extractions this corresponds to a high reduction of Zr mass by a factor of 10^4. Subsequent anionic exchange separation further removed traces of Zr. The final separation yield of ^{90}Nb was 60-65% and the decontamination factor for Zr/Nb was $\geq 10^7$, representing ≤ 26 ng of Zr present in the final ^{90}Nb fraction.

Second separation strategy

The overall separation proceeds with a yield of 93-95% of $^{90/95}$Nb, collected in 400 µL 0.1 M oxalic acid. The whole separation procedure takes less than one hour, which is almost 4 times faster than the first separation method. Decontamination after UTEVA purification is $3x10^8$.This decontamination factor equals 0.77 ng of zirconium present in the final fraction for a 260 mg zirconium target.

Preparation of ^{90}Nb-labeled Df-Bz-NCS-mAb

The ^{90}Nb labeling yield was >90% (96% ITLC, 95% HPLC) after 1 hour. Labeling kinetics indicate that the labeling yields reached ≥ 80% already at 15 min and increased to more than 90% after 50 min. After SEC separation on a PD-10 column, the two ^{90}Nb-Df-mAb derivatives had a99.0% purity. Specific activity for first separation strategy was 270 kBq/100 µL of mAb and for alternative separation strategy was 3 MBq/100 µL.

In vitro stability

After 3 days of incubation in saline at RT, more than 99% (≥ 99% HPLC, ≥ 99% ITLC) and after 7 days ≥95% (99% HPLC, 97% ITLC) of ^{95}Nb-Df-Bevacizumab was detected. Stability testing in in fresh human serum at 37°C showed higher product degradation. After 3 days of incubation ≥94% (97% HPLC, 94% ITLC) of labeled product was available, while at 7 days ≥ 86% (89% HPLC, 86% ITLC) of the product was still intact.

Biodistribution experiments

Biodistribution of ^{95}Nb-oxalate, ^{95}Nb-chloride in healthy mice

Biodistribution of ^{95}Nb-oxalate and ^{95}Nb-chloride showed similar results, with no specific organ uptake observed (Figure 1). However for ^{95}Nb-chloride, higher uptake in all organs was detected in comparison to ^{95}Nb-oxalate. The highest observed uptake was in the blood, lungs and bones. Slight bone accumulation was measured for both substances. Uptake for liver, kidneys and spleen was approximately 1% at 1 day p.i. for oxalate and below 3% for chloride compounds. After 7 days p. i. for ^{95}Nb-oxalate and ^{95}Nb-chloride, all organs uptakes except for bone were below 1% and 2% respectively, apart from the bone uptake,

which was ≥ 2 % for the oxalate and ≥ 4 % for the chloride product. ^{95}Nb-Df showed very fast clearance from the body (Figure 1). At 1 day p.i., no single organ uptake above 0.5 % was observed. After 4 hours uptake in kidneys, stomach and intestines was still detected and all other organs were almost negligible. After 7 days p.i. the radiolabeled products had almost completely cleared from the organism.

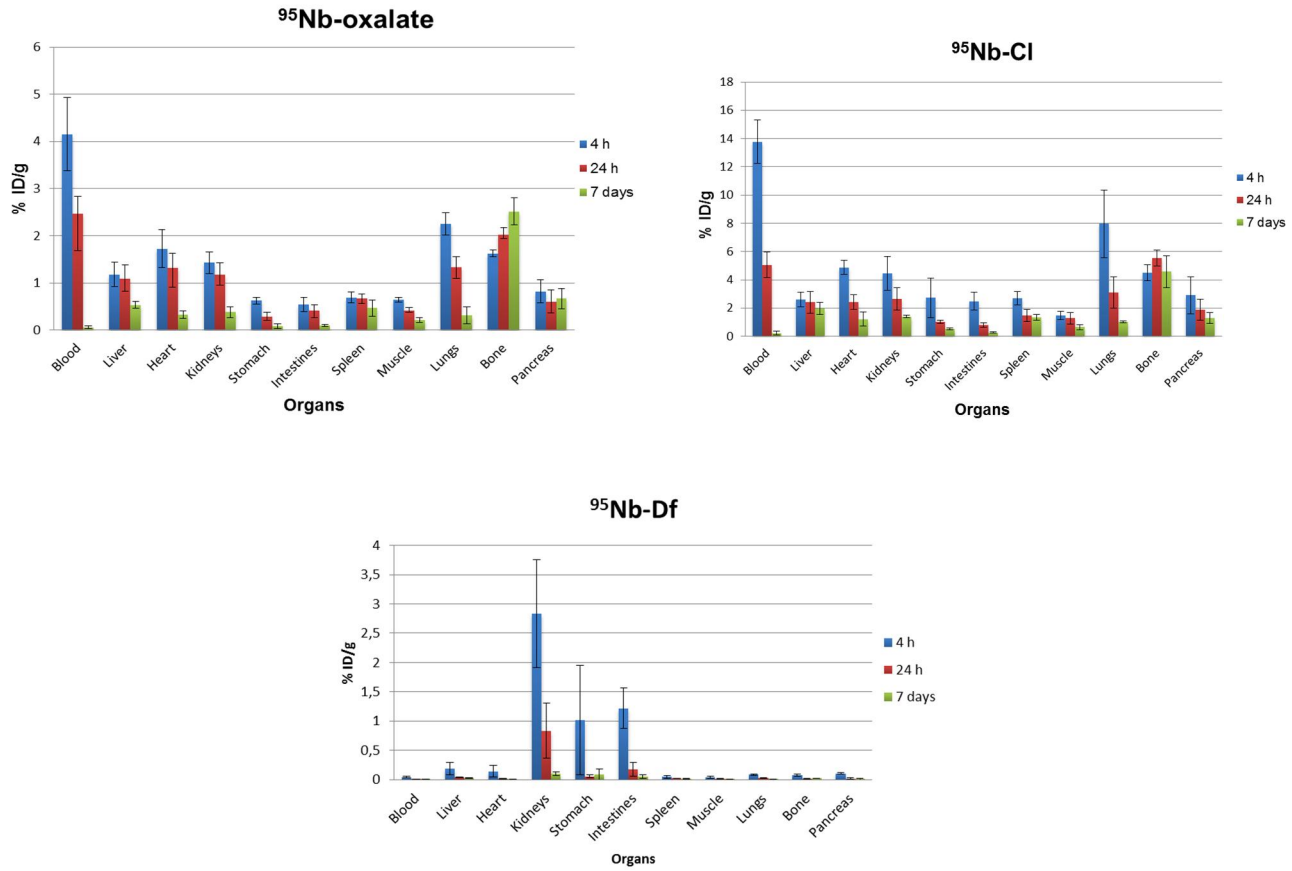

Figure 1: Biodistribution of ^{95}Nb-oxalate, ^{95}Nb-chloride and ^{95}Nb-Df in healthy mice.

Biodistribution of ^{95}Nb-bevacizumab in tumor-bearing and healthy mice

Biodistribution of the labeled product, at an injected dose of 270 kBq/100 µL/mouse showed a relatively low accumulation in the tumor (≤ 3%) at 1 day p.i., which decreased in time (Figure 2). On the other hand, a high accumulation in the liver (> 30%), spleen (>10%) and kidneys (> 5%) was detected. Blocking experiments showed specific uptake of the radiolabeled mAb in the tumor at all time points, since injection of a large quantity of cold antibody resulted in sufficiently lower tumor uptake (Table 1).

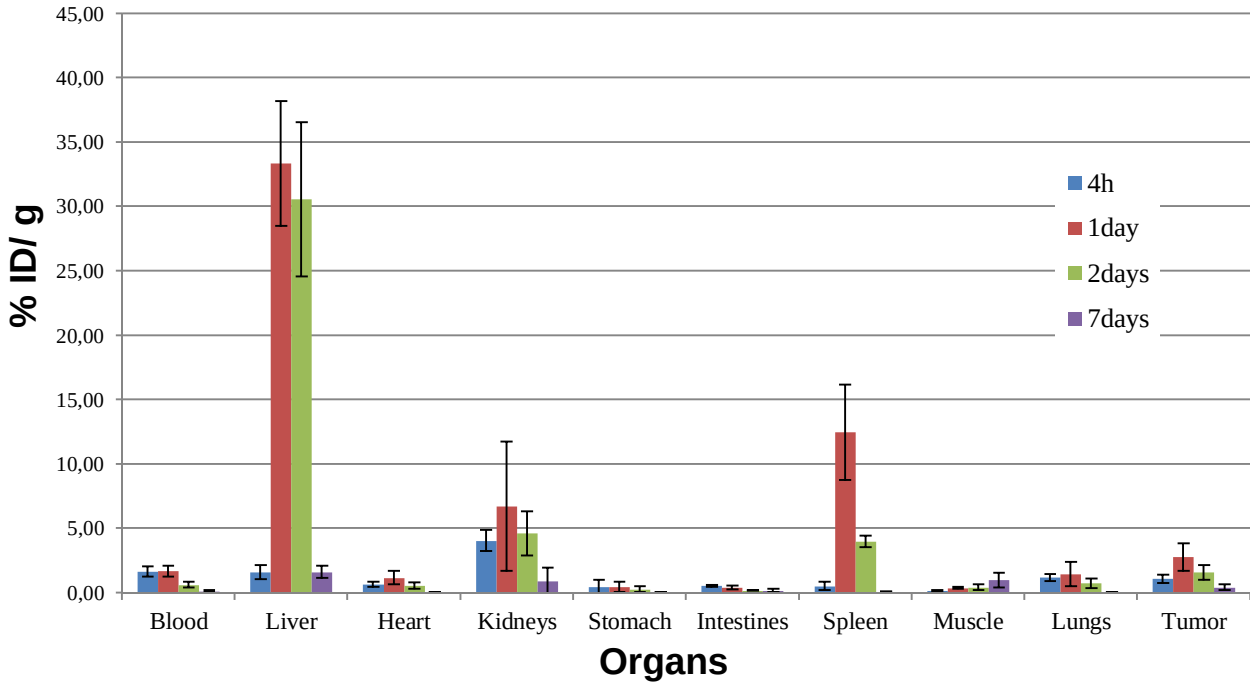

Figure 2: Biodistribution of ^{95}Nb-bevacizumab (270 kBq/100 µg/mouse) in tumor-bearing mice.

Table 1: Tumor uptake for blocked and unblocked experiments.

	4 h	1 day	2 days	7 days
Unblocked	1.08±0,34	2.77± 1,07	1.57± 0.57	0.40± 0.22
blocked	-	1,25± 0.35	0,62± 0.17	0,22± 0.09

To prove that the previous biodistribution data, i.e high liver, lung and spleen uptake, were a result of the antibody concentration and not of the instability of the labeled product, another biodistribution study was conducted, where normal Swiss mice were injected with a higher specific-activity product.

The results presented in Figure 2 show a much less uptake in liver (< 5%), as well as in the kidneys and spleen at 1 day p.i. , which rapidly decrease in time. After 7 days, the uptake in these organs was less than 2%. On the other hand, a much higher uptake in blood (> 15%) and lungs (> 5%) was detected, which at 7

days p.i. is significantly decreased. A constant bone uptake (approx. 2% ID/g) was observed over the 7 days of the experiment.

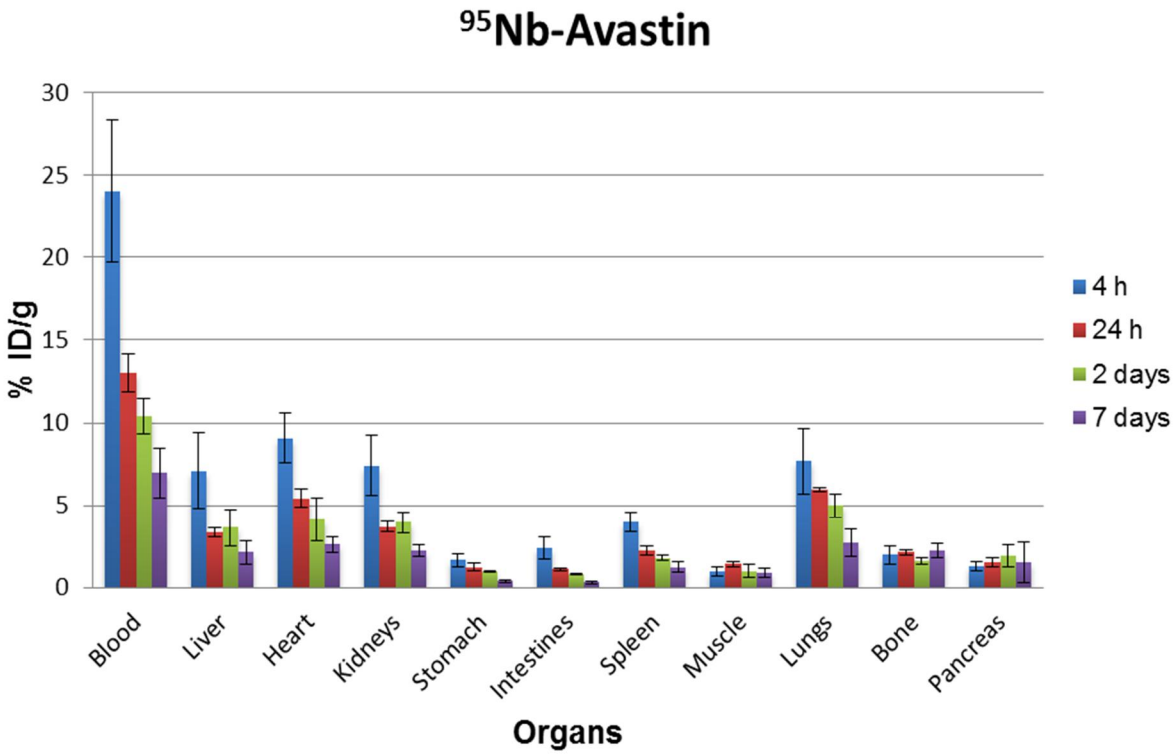

Figure 3: Biodistribution of ^{95}Nb-labeled bevacizumab (300 kBq/ ~10 µg/mouse) in normal Swiss mice.

PET imaging

Due to the low specific activity of ^{90}Nb-bevacizumab, single PET image 4 hours post injection was obtained (Figure 4.). However, even at this time point the tumor is clearly visible. This data provides the first image of a ^{90}Nb-labeled monoclonal antibody described in literature.

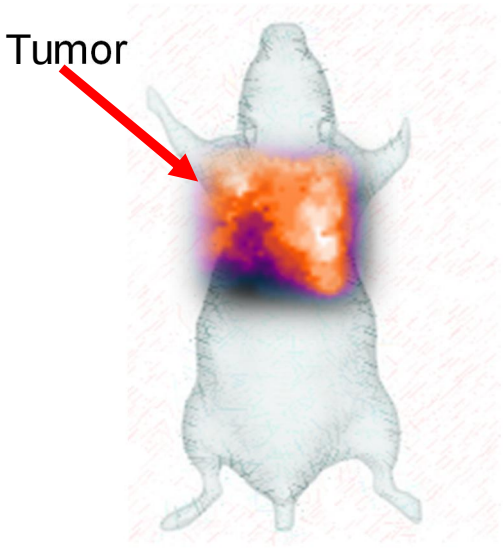

*Figure **4:** Static PET imaging 4 hours p.i. of ^{95}Nb-bevacizumab.*

Discussion

Two separation strategies were proceed and compared. Alternative separation strategy provides faster separation time, higher yield and higher decontamination factor that crucially reflect on specific activity of labelled product. Labeled product with maximal specific activity 2.7 MBq of ^{95}Nb per mg of mAb was synthesized for first separation strategy that results specific activity 0.4 MBq/nmol. For alternative separation strategy more than 10 times higher specific activity can be achieved (30 MBq/mg or 4.5 MBq/nmol) for ^{95}Nb and even higher for ^{90}Nb (45 MBq/nmol).

Biodistribution of 100 µg of bevacizumab with low specific activity showed adequate tumor uptake (3%) which is comparable with previously obtained data for ^{89}Zr [3], however unusual high uptake in liver, spleen and kidneys was observed 1 day p.i.. To prove that this uptake is result of specific activity in couple with concentration of mAb, first in vivo evaluation of ^{95}Nb-oxalate, ^{95}Nb-chloride and ^{95}Nb-Df was conducted. These compounds can be formed by destruction of the labelled product. Biodistribution of these compounds in healthy mice did not showed specific uptake in any organs. For ^{95}Nb-oxalate and ^{95}Nb-chloride slight accumulation in the bone was occur, that can be future “indicator “ for relase of *Nb from labeled compounds. 95Nb-Df very fast cleared from the living organism almost quantitative already

one day p.i.. Next step was evaluating influence of specific activity and concentration of mAb, therefore in vivo study of low concentration of mAb in healthy mice was performed. Results did not showed increased uptake in liver, spleen and kidneys and also no bone accumulation. These data clearly prove high in vivo stability of Nb-labeled biomolecules and especially strengthens of Nb-Df bond.

Conclusions

Obtained data clearly showed excellent in vitro and in vivo stability of 95/90Nb-labeled mAb. That make ^{90}Nb promising for application for immune-PET.

Acknowledgments

The authors gratefully acknowledge financial support from the COST, actions TD1004 and D38 Action: Metal-Based Systems for Molecular Imaging Applications. Also teams of BR2 and TRIGA Mainz for production of ^{95}Nb and operator team of cyclotron of DKFZ Heidleberg for production of ^{90}Nb.

References

1. Maecke, H. R., Reubi, J. C. Somatostatin receptors as targets for nuclear medicine imaging and radionuclide treatment. *J Nucl Med* 2011; 52(6); 841-4.
2. Ellis, L. M., Hicklin, D. J. VEGF-targeted therapy: mechanisms of anti-tumour activity. *Nat Rev Cancer* 2008; 8; 579–91.
3. Nagengast, W. B., de Vries, E. G., Hospers, G. A., Mulder, N. H., de Jong, J. R., Hollema, H., Brouwers, A. H., van Dongen, G.A., Perk, L. R., Lub-de Hooge, M. N. In vivo VEGF imaging with radiolabeled bevacizumab in a human ovarian tumor xenograft. *J Nucl Med* 2007; 48; 1313–19.
4. Nagengast, W. B., de Korte, M. A., Oude, Munnink, T. H., Timmer-Bosscha, H., den Dunnen, W. F., Hollema, H., de Jong, J. R., Jensen, M. R., Quadt, C., Garcia-Echeverria, C., van Dongen, G. A., Lub-deHooge, M. N., Schroder, C. P., de Vries, E. G. ^{89}Zr-bevacizumab PET of early antiangiogenic tumor response to treatment with HSP90 inhibitor NVP-AUY922. *J Nucl Med* 2010; 51; 761–7.

5. Nayak, T. K., Garmestani, K., Baidoo, K. E., Milenic, D. E., Brechbiel, M. W. PET imaging of tumor angiogenesis in mice with VEGF-a-targeted ^{86}Y-chx-a″-DTPA-bevacizumab. *Int J Cancer* 2011; 128; 920–6.
6. Chang, A. J., Sohn, R., Lu, Z. H., Arbeit, J. M., Lapi, S. E. Detection of rapalog-mediated therapeutic response in renal cancer xenografts using **^{64}**Cu-bevacizumab *immuno*PET. *PLoS One* 2013; 8(3); e58949. doi: 10.1371
7. Vugts, D. J., Visser, G. W., van Dongen, G. A. ^{89}Zr-PET radiochemistry in the development and application of therapeutic monoclonal antibodies and other biologicals. *Curr Top Med Chem* 2013; 13(4); 446-57.
8. Severin, G. W., Engle, J. W., Barnhart, T. E., Nickles, R. J. ^{89}Zr radiochemistry for positron emission tomography. *Med Chem* 2011; 7(5); 389-94.
9. Pfeifer, A., Knigge, U., Mortensen, J., Oturai, P., Berthelsen, A. K., Loft, A., Binderup, T., Rasmussen, P., Elema, D., Klausen, T. L., Holm, S., von Benzon, E., Højgaard, L., Kjaer, A. Clinical PET of neuroendocrine tumors using ^{64}Cu-DOTATATE: first-in-humans study. *J Nucl Med* 2012; 53(8); 1207-15.
10. Anderson, C. J., Ferdani, R. Copper-64 radiopharmaceuticals for PET imaging of cancer: advances in preclinical and clinical research. *Cancer Biother Radiopharm* 2009; 24(4); 379-93.
11. Rosch, F., Herzog, H., Stolz, B., Brockmann, J., Kohle, M., Muhlensiepen, H., Marbach, P., Muller-Gartner, H. W. Uptake kinetics of the somatostatin receptor ligand [^{86}Y]DOTA-DPhe1-Tyr3-octreotide ([^{86}Y]SMT487) using positron emission tomography in non-human primates and calculation of of radiation doses of the ^{90}Y-labelled analogue. *Eur J Nucl Med* 1999; 26(4); 358-66.
12. Nayak, T. K., Brechbiel, M. W. ^{86}Y based PET radiopharmaceuticals: radiochemistry and biological applications. *Med Chem* 2011; 7(5); 380-8.
13. Tolmachev, V. Radiobromine-labelled tracers for positron emission tomography: possibilities and pitfalls. *Curr Radiopharm* 2011; 4(2); 76-89.
14. Busse, S., Rösch, F., Qaim, S. M. Cross section data for the production of the positron emitting niobium isotope ^{90}Nb *via* the ^{90}Zr(*p, n*)-reaction. *Radiochim Acta* 2002; 90; 1-5.
15. Busse, S., Brockmann, J., Roesch, F. Radiochemical separation of no-carrier-added radioniobium from zirconium targets for application of ^{90}Nb-labelled compounds. *Radiochim Acta* 2002; 90; 411-5.

16. Radchenko, V., Hauser, H., Eisenhut, M., Vugts, J. D., van Dongen, G. A. M. S., Roesch, F. ^{90}Nb – a Potential PET Nuclide: Production and Labeling of Monoclonal Antibodies. *Radiohim Acta* 2012; 100(11); 857-64.

4. Summary, conclusions and future perspectives

Currently in the field of the nuclear medicine hundreds of novel imaging agents become available every year. However, there is sufficient lack of radionuclides for imaging with half-lives longer than several hours which are required for novel molecules. Also a lack of appropriate radionuclides for radiotherapy is observed, where just several radionuclides are applied for all tumor sizes.

Groups of radionuclides with favorable intermediate half-lives which can be applicable with antibody fragments as well with some antibodies have been analyzed. There are some promising isotopes such as ^{76}Br (16.0 hours) [1], ^{86}Y (14.7 hours) [2, 3], ^{64}Cu (12.7 hours) [4, 5] and the proposed in this work ^{90}Nb (14.6 hours). ^{90}Nb is characterized by a high positron branching of 53%, which is comparable just to ^{76}Br (56 %), while for ^{86}Y it is 33 % and for ^{64}Cu 17.8 %. High positron branching allows for the acquisition of the same quality imaging by using less amount of isotope, which means less radiation burden. The mean β^+ energy of ^{90}Nb is 0.35 MeV, which is more than that of ^{86}Y (0.21 MeV) and ^{64}Cu (0.05 MeV) but sufficiently less than that of ^{76}Br (0.64 MeV). All four isotopes are also characterized by additional emissions (β^-,γ) which can affect the PET image and create additional dose burden for patients and medical personnel. For ^{90}Nb, several gamma emissions with relative high energies are presented in the decay scheme, and this is a similar problem observed with ^{86}Y and ^{76}Br. ^{64}Cu has a very low intensity gamma emission, however it has high β^- emission branch (38.4%) that will create additional dose burden.

All discussed “intermediate” isotopes can be produced by simple proton bombardment on low-energy cyclotrons (< 20 MeV,) that make production of these isotopes «in house» at clinical centers possible. One advantage of ^{90}Nb is the the use of a natural zirconium metal target for irradiation, in time when for all other discussed isotopes enriched target materials are necessary. Radioisotopic purity of ^{90}Nb produced by proton bombardment is 97% and can even be improved by conducting of additional studies with variations of energy and foil thickness.

From the point of separation of no carrier added ^{90}Nb from irradiated zirconium, a rapid separation strategy providing a high yield of 90-niobium (95%) with high purity appropriate for follow labeling application was developed. The labeling chemistry of the intermediate isotopes presented is primarily characterized by the use of bifunctional chelating agents, which allow the attachment of the metallic isotope to the biomolecules. The exception is ^{76}Br which is a halogen and can be attached to the biomolecules directly [4].

In previous studies with ^{86}Y and ^{64}Cu, two types of chelating agents have been proposed: acyclic agents and cyclic agents [5-7]. For complex formation of Y(III) and Cu(II) with DOTA high reaction temperatures are necessary, and this can be a limiting factor for applying this strategy for biomolecules due to the sensitivity of proteins to temperature cycling. For copper, the crucial factor is also that it exists in two oxidation states (I and II), that can make labeling chemistry difficult and decrease complex stability. Therefore, the search for optimal labeling strategies for both isotopes is still underway [8, 9].

For ^{90}Nb the chelator of choice is desferrioxamine (Df). Previous studies showed fast kinetics of complex formation (more than 95% at one hour at RT) and high stability of ^{90}Nb-Df-mAb complexes (less than 5% was dissociated after 5 days of incubation in FCS).

All the above mentioned parameters (half-life, decay scheme) as well as the promising results obtained (production, separation and labeling chemistry) allow to confirm, that ^{90}Nb is a promising isotope for *immuno*-PET and give reason to continue our study with *in vivo* evaluation of ^{90}Nb-labeled biomolecules for the purposes of *immuno*-PET.

4.1 Production of ^{90}Nb

The overall irradiation yield of ^{90}Nb for three 1 h and 5 μA irradiations was 720± 50 MBq, i. e. 145±10 MBq/μAh under given irradiation parameters. This production yield is high compared to the yield observed for other PET radionuclides (Table 1). However, our previous work indicate that the production yield can be even higher [10].

Table 1: Production yield of several PET radionuclides [11].

Radionuclide	Commonly used production route	Proton energy range (MeV)	Calculated yield (MBq/μAh)
^{124}I	^{124}Te(p, n)^{124}I	12→8	16
^{89}Zr	^{89}Y(p, n)^{89}Zr	12 →6	43
^{72}As	^{nat}Ge(p, xn)^{72}As	18 →8	93
^{55}Co	^{58}Ni(p, α)^{55}Co	15 →7	14

Another important parameter is the isotopic purity of ^{90}Nb. For the performed irradiations, the content of ^{90}Nb after EOB was more than 97%. Minor isotopic impurities found were: ^{92m}Nb ($T_{1/2}$ 10.2 d) = 1.64%, ^{95}Nb ($T_{1/2}$ 35.0 d) = 0.08%, ^{95m}Nb ($T_{1/2}$ 3.6 d) = 0.29% and ^{96}Nb ($T_{1/2}$ 23.35 h) = 0.88%. This isotopic content allows the application of ^{90}Nb within a few days (the content of ^{90}Nb will exceed 90%) for evaluation of slower *in vivo* processes without sufficient imaging contamination with other niobium radioisotopes.

For further clinical application, the purity of ^{90}Nb should be improved up to ≥99%, thus allowing the use of ^{90}Nb for patient imaging. Three different strategies can be applied to improve the radioisotopic purity of ^{90}Nb: The first strategy is by variation of existing parameters such as energy, target geometry and design. Variations of energies can decrease radioisotopic impurities. For example, from cross sections of ^{90}Nb and ^{92m}Nb the optimum energy ranges to decrease the content of ^{92m}Nb in irradiation target can be applied. Variation of foil thickness can also increase the radioisotopic purity of ^{90}Nb. For example, using a thin foil (0.1 mm thickness) will decrease production yield but will also sufficiently restrict the energy spectrum applied on the target by using a stack of three foils (0.25 mm thickness each).
Another strategy is the production of ^{90}Nb via the decay of ^{90}Mo. To produce ^{90}Mo, a high energy proton flux is required. Therefore, several related metal target materials (Zr, Nb, Mo, Rh, Ag and Pd) were irradiated with high energy protons (100 MeV) at the Phasotron facilities at Joint Institute for Nuclear Research (Russian Federation) to estimate the production yield of ^{90}Mo and the content of coproduced radionuclides. Rh and Pd targets can provide a sufficient yield of ^{90}Mo and a wide spectrum of other medical radionuclides which can be later extracted from the irradiated target material. However, application of these targets is limited due to their low thermal stability that can affect the production yield and limit its application. Rh and respectively Ru have great thermal stability and can also provide a sufficient yield of ^{90}Mo and several other medical radionuclides; however extraction of products is complicated due to the high chemical stability of the platinum group of metals. Therefore, the most convenient targets are Mo, Nb and Zr, since they provide a high yield of ^{90}Mo in comparison with the targets listed above, while showing high melting resistance. Also, regarding product extraction, several strategies were proposed and tested. Another advantage of these targets is co-production of other radionuclides which can be applied in nuclear medicine (such as ^{86}Y and ^{89}Zr). Such a multinuclide strategy can offer a future cost-safe opportunity to provide a source of *immuno*-PET radionuclides with excellent purity.
The main advantages of the production of ^{90}Nb via the decay of ^{90}Mo are:

- Excellent radionuclide purity, because ^{90}Nb will be formed by decay of ^{90}Mo, which will exclude presence of other Nb isotopes.
- Excellent radiochemical purity, because Nb and Mo have considerable differences in chemical proprieties, that give opportunities to develop a separation procedure allowing high separation factor between these both elements.
- Decay of ^{90}Mo will give additional time for transportation (10-20 hours) that is an important factor taking into account the decay of ^{90}Nb (14.6 hours).
- High production yield of ^{90}Nb will save irradiation cost that can otherwise be used to cover transportation expenses.

Another option to increase radioisotopic purity of ^{90}Nb is the application of enriched ^{90}Zr (≥99%) metal foil or oxide for irradiation, that will sufficiently increase the radioisotopic purity of ^{90}Nb after irradiation. However, the enriched target material is much more expensive than natural zirconium target. Therefore, the following separation strategy should be adopted and include a step for the recovery of the target material for repetitive usage. The disadvantage of this step is the additional time spent for recovering the target and consequent target preparation, but on the other hand, in case of using enriched Zr oxide or salt by target dissolution using of hydrofluoric acid can be avoided.

4.2 Separation of ^{90}Nb

The radiolabeling chemistry of $^{90}Nb^{V}$ appears to be quite similar to $^{89}Zr^{IV}$ [12, 13], though the almost complete removal of Zr from the cyclotron target is essential. A high decontamination factor is crucial, because zirconium also creates very stable complexes with desferrioxamine and competes with niobium, affecting labeling efficiency and causing purity and purification problems. The overall separation proceeds with a separation yield of more than 99% of $^{90/95}$Nb, after anion exchange. The final 1 M oxalic acid fraction contains more than 95% of $^{90/95}$Nb. The whole separation procedure takes around 1.5 hours, which is almost 4 times faster than the previous separation method. The decontamination factor after anion exchange was $1 \cdot 10^5$ and after UTEVA purification $3 \cdot 10^8$. This decontamination factor equals 0.77 ng of zirconium present in final fraction for a 260 mg zirconium target.

This procedure was adapted to a semi-automated separation module. Separation yields of $^{95/90}$Nb in the final fraction were somewhat lower (90%), which can be explained by losses on valves and tubes during

the separation procedure. However, this takes less time (only 1 hour) and allows remote operation, which is very important factor in the case of high activity irradiations.

Table 2: Comparison of developed and previous separation strategies.

Parameters	Developed separation strategy	Previous separation strategy
Separation time (h)	1-1.5	> 4
Separation yield (%)	90-95	79-81
Decontamination factor Zr/Nb	10^8	10^7
Automation	available	complicated
Final fraction	200 μL 1 M ox. acid	200 μL 6 M HCl/ 0.01 M ox. acid

Furthermore, the developed separation strategy was improved by the direct transfer of the Nb fraction from the anion exchange resin to UTEVA, thus avoiding additional heating and dilution steps. To find optimal conditions for direct transfer and also possibility of additional purification of ^{90}Nb the behaviour of Zr^{IV} and Nb^{V} were studied for an anion exchanger and UTEVA in HCl/H_2O_2 and HCl/oxalic acid. For HCl/H_2O_2, a mixture of 9M HCl/1% H_2O_2 seems to be most suitable for direct transfer of ^{90}Nb from the anion exchange column to UTEVA due the low K_d for Nb^{V} on the anion exchanger and the relatively high K_d value on the UTEVA resin. However, the HCl/H_2O_2 system is not stable system due to the reaction of hydrochloric acid with peroxide, which changes the initial concentration and also produces hydrogen as a result of peroxide destruction. These reasons can be a crucial limitation for future routine application and automation of this strategy. Therefore, another system with HCl and oxalic acid was evaluated, to provide direct flow transfer of ^{90}Nb. Results showed several possibilities to realize direct flow transfer in areas of concentrations. 0.2 M oxalic acid/ 9.2 M HCl with K_d values for AG1x8 13±1 and for UTEVA 3334, 0.3 M oxalic acid/ 7.5 M HCl and 0.4 M oxalic acid/ 6.9 M HCl seem to be promising for the direct flow transfer of Nb from the anion exchanger to UTEVA. In addition an interesting area of low concentration of both components was detected. At 0.005 M oxalic acid/ 6.28 M HCl, distribution coefficients for anion

exchanger is 11 and for UTEVA 747. Due to limiting of mixtures preparation by HCl (12 M) and oxalic acid maximal stable solution is 1 M, and results which indicate that more appropriate condition for direct transfer can be reached higher concentrations of HCl and oxalic acid another higher analogue of carboxylic acid can be applied. A preliminary study was conducted with tartaric acid. It remains stable at higher molarity values (5 M). Promising results were observed at 2 M tartaric acid/ 6.8 M HCl acid, where K_d values for anion exchange were below 10 and for UTEVA higher than 10000. More detailed studies in various carboxylic acids can provide even more suitable conditions for the direct transfer system.

The direct flow separation strategy based on the 0.3 M oxalic acid/ 7.5 M HCl was developed, which allows the transfer of more than 95% of ^{90}Nb in 7 mL of solution without sufficient breakthrough via UTEVA. The separation yield and separation factor are very similar to the strategy without direct flow, however the separation time is lower and the automation setup is sufficiently simplified.
Several separation strategies were evaluated for different target materials (Zr, Nb and Mo) for the alternative production of ^{90}Nb via the decay of ^{90}Mo. The main goal was the adaptation of the separation direct flow strategy developed for the zirconium target, for isolation of ^{90}Nb from the Mo target. For isolation of ^{90}Mo from the Nb target, additional experiments are required. Finally, a "triangle" concept has been planned to be developed. This concept is based on semi-automated isolation strategies; where each of three proposed targets can be irradiated and three no carrier added products can be isolated with high radiochemical and radionuclide purity. For example, in the case of Mo target irradiation, the extracted product will be ^{90}Nb and ^{89}Zr or ^{86}Zr/^{86}Y.

4.3 Labeling chemistry

Due to the fact that ^{90}Nb cannot be directly attached to biomolecules, a study on which is the most appropriate bifunctional chelator (BFC) was performed. It was shown that desferrioxamine is the most appropriate ligand for formation of complexes with $Nb^{(V)}$ isotopes, among the other common chelators tested. In addition, desferrioxamine showed a preference for complex formation with $Nb^{(V)}$ compared to other metals involved (Zr, Fe and Ga). Desferrioxamine is thus identified as a chelator of choice for the synthesis of ^{90}Nb labeled biomolecules (antibody, antibody fragments or peptides) for *immuno*-PET. Bifunctionalization of Df as needed for covalently attaching Df to a targeting vector does not decrease its potential for $Nb^{(V)}$ complex formation and stability. As proof-of-principle the Df-succinyl-(D)Phe^1-

Octreotide was successfully labeled with ^{95}Nb for 30 minutes at pH 5 at room temperature in more than 99% yield. The *in vitro* stability of this product was excellent over days in HSA at 37°C.

To attach Df to biomolecules such as monoclonal antibodies or engineered antibody fragments, two coupling strategies developed for ^{89}Zr were adopted for ^{90}Nb, such as *N*-Succinyl-desferrioxamine (N-suc-Df)[12] and p-Isothiocyanato- benzyl-desferrioxamine (NCS-Bz-Df)[13].

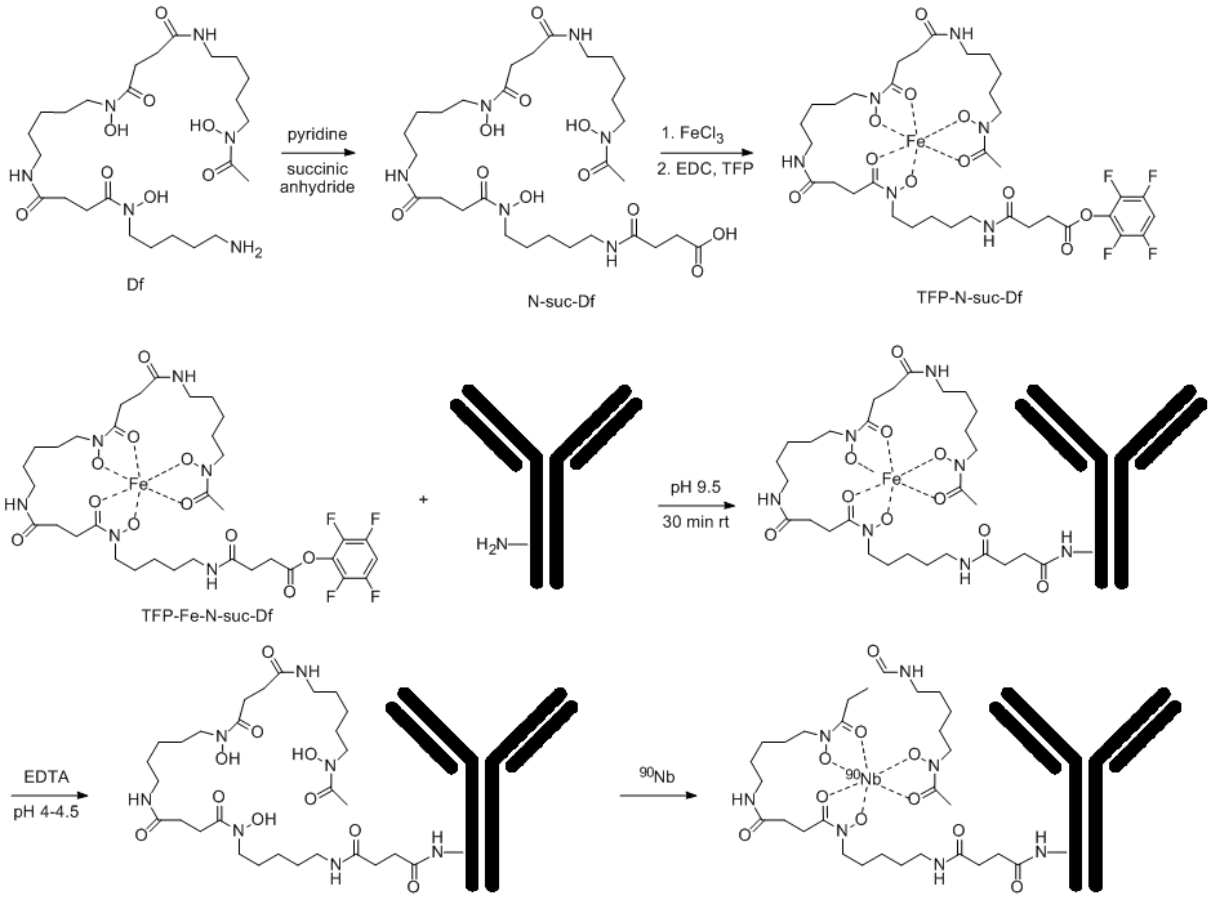

Figure 1: Df-conjugation via TFP-N-suc-Df-Fe and labeling with ^{90}Nb.

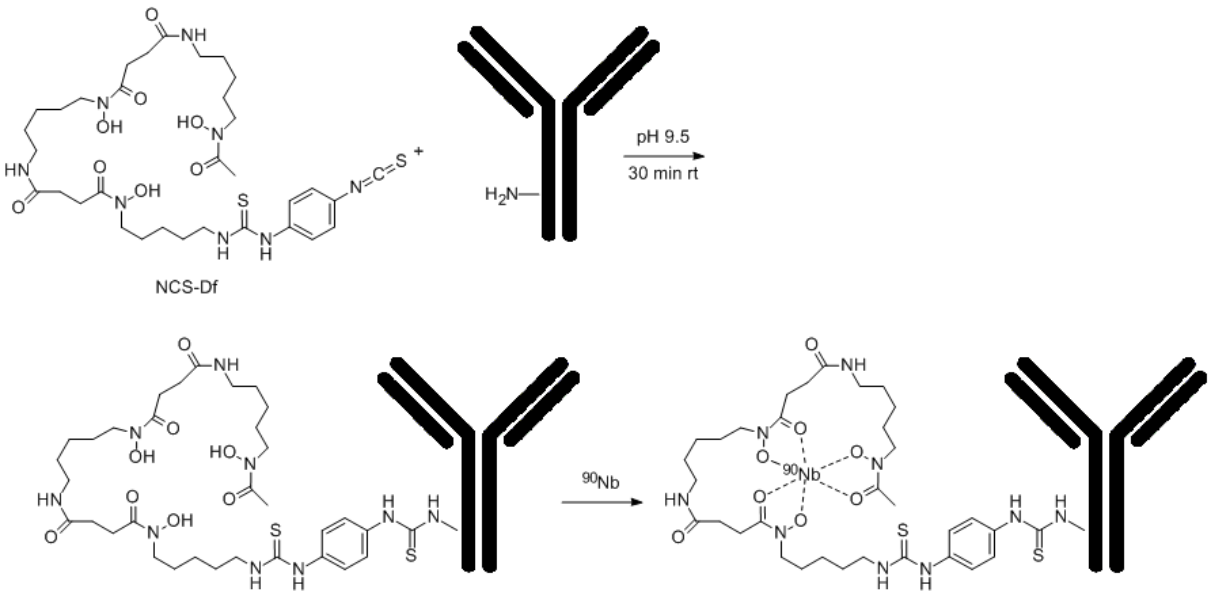

Figure 2: Df-conjugation via the bifunctional chelator Df-Bz-NCS and labeling with ^{90}Nb.

The molar ratio for the N-suc-Df method as well as for the Df-Bz-NCS method was 1.5 molecules of desferrioxamine per antibody molecule. Subsequent labeling with ^{90}Nb showed, for both modification strategies, the same high yield of more than 90%. *In vitro* stability studies in aqueous solutions as well as in the presence of fetal calf serum proved that the ^{90}Nb-desferal-antibodies are highly stable over several periods of half-life of ^{90}Nb, which allows their use in *immuno*-PET. For future labeling, the modification through the Df-Bz-NCS is preferable for reasons of simpler and faster preparation.

4.4 *In vitro* and *in vivo* stability of $^{90/95}$Nb-labeled compounds

$^{90/95}$Nb labeled monoclonal antibodies (Rituximab and bevacizumab) showed excellent *in vitro* stability at room temperature in saline as well in 37°C in human serum albumin (HSA) or fetal calf serum albumin (FSA). In saline after 7 days of incubation less of 5% of product degradation was detected and in second setup in HSA and FCS after 5 days more then 95% of product was stable and after 7 days more then 85% of product was detected.

In vivo evaluation of $^{95/90}$Nb labeled bevacizumab (100 µg/270 kBq of ^{95}Nb, 0.45 MBq/nmol) showed adequate tumor uptake (2.77%) after 1 day of post injection (p.i), that is comparable with previously obtained data of labeling bevacizumab with ^{89}Zr (7% after 1 day p.i.) [14]. However, parallel high uptake in other organs: liver (>35 %), spleen (>10 %) and kidneys (> 5%) was measured.

To find a reason for that i.e. whether this related to the biodistribution of bevacizumab, result of low specific activity or the instability of labeled compound, two additional experiments were realized.

First, biodistribution studies of ^{95}Nb-oxalate, ^{95}Nb-chloride and ^{95}Nb-Df were performed in healthy mice. These complexes were chosen as compounds which can be formed in case of labeled product instability. ^{95}Nb-oxalate and ^{95}Nb-chloride demonstrate a similar biodistribution. Not specific organs uptake was detected, except slight bone accumulation. Highest uptake in blood and lungs was observed. After 7 day p.i. no organs with uptake higher then 1% ID/g, except bone was detected. Bone accumulation can become a potential “indicator” for the relase of $^{95/90}$Nb from labeled complexes.

^{95}Nb-Df showed very fast clearance. After 4 hours most of it was found in stomach (1%), kidneys (2.7%) and intestines (1.3%), while the uptake in other organs was negligible (less then 0.3%). After 7 days p.i. no uptake higher then 0.1% was detected in any organ.

At second setup, biodistribution in healthy mice was peformed at higher specific activity product (3 MBq/100 µg of mAb, 4.5 MBq/nmol). Results did not show increased uptake in liver, spleen and kidneys (< 5% at 1 day p.i.). Highest uptake was detect in blood and lungs; however, uptake in all organs was decreasing rapidly with the time. An increasing bone uptake with the time was not observed that proved that $^{95/90}$Nb was not realse from labeled complex. In contract, current studies with ^{89}Zr [15] labeled monoclonal antibody, showed sufficient activity accumulation in bones (≥ 7%, at 7th day p.i.), that can dramatically influence on quality of obtained image. Following studies [16] proved that bone accumulation is result of relase ^{89}Zr from labeled complex. This fact is calling for improvement of labeling strategy and parallel investigation of more stable complexing agent for Zr^{IV}.

Obtained results showed excellent *in vitro* and *in vivo* stability of $^{95/90}$Nb labeled biomolecules and proved promise of use ^{90}Nb for purposes of *immuno*-PET.

4.5 Outlook

In this thesis separation and labeling chemistry for ^{90}Nb were evaluated systematically. A final product was successfully applied for first time to study its behavior *in vivo*.

^{90}Nb can have several applications in the future:

^{90}Nb can be applied for purposes of *immuno*-PET, for labeling of intact antibody and antibody fragments and their *in vivo* evaluation. Since the conjugation and labeling chemistry of ^{90}Nb is very similar to ^{89}Zr, its can be applied as a reference for each other for more deep evaluation of biomolecules behavior. Other radionuclides which can be also involved for *in vivo* imaging of antibody and their derivatives and coupled via Df are ^{68}Ga [17] and potentially ^{44}Sc. The half-lives of these four radionuclides will allow covering whole biological half-life range of all existing biomolecules. ^{68}Ga and ^{44}Sc are appropriate for molecules with small molecular weight (1-50 kDa), while ^{90}Nb and ^{89}Zr cover long kinetics sequence of molecular weights (50-150 kDa). Evaluation of such "tool box" will provide an unique instrument for evaluation of behavior existing biomolecules as well as novel drugs.

From point of view to personalized medicine ^{90}Nb can be also utilized for pre-therapy diagnostics with its therapeutic analogue ^{95}Nb. However, due to the relative long half-life of 35 days, ^{95}Nb is not an optimal radionuclide for radiotherapy. From the other side ^{90}Nb has a great potential to become a diagnostic radionuclide for therapy planning within 5th group radionuclides. In Table 3 some of the potential radionuclides for therapeutic purposes are listed.

Table3: Potential therapeutic radionuclides within 5th group of radionuclides.

Nuclide	$T_{1/2}$	Radiation type	Radiation characteristic	Other radiation and decays	Main γ lines KeV	Production routes
^{213}Bi	45.6 min	α	-	β^-	440 (26.1) 1100 (0.29)	generator
^{119}Sb	38.5 h	Conversion and auger electrons	*	EC	23.8 (16.1)	generator
^{77}As	38.8 h	β^-	E_{mean} 0.23 E_{max} 0.68	γ	239 (1.6) 521 (0.56)	Ge(n, γ)
^{239}Np	2.315 d	β^-	E_{mean} 0.11 E_{max} 0.71	γ	106 (27.2) 278 (14.4)	generator ^{238}U(n, γ)
^{32}P	14.26 d	β^-	E_{mean} 0.7 E_{max} 1.7	-	-	(p, n)
^{233}Pa	27.0 d	β^-	E_{mean} 0.06 E_{max} 0.27	γ	300 (6.62) 312 (38.6)	generator Th (n, γ)
^{95}Nb	35.0 d	β^-	E_{mean} 0.04 E_{max} 0.93	γ	765 (100) -	Zr(n, γ) generator

Very few studies was done concerning the evaluation of 5th group for purposes of nuclear medicine, however, there is a great resource of unique radionuclides which can far exceed the recently applied therapeutic radionuclides in terms of cost-effective and accurate tumor therapy. Theranostic systems can be base not similarities of isotopes of single element, but on similarities peculiar one group of elements. Therefore, ^{90}Nb can be a potential candidate for diagnostic radionuclide within such system.

References

1. Rossin, R., Berndorff, D., Friebe, M., Dinkelborg, L. M., Welch, M. J. Small-animal PET of tumor angiogenesis using a ^{76}Br-labeled human recombinant antibody fragment to the ED-B domain of fibronectin. *J Nucl Med* 2007; 48; 1172-9.
2. Herzog, H., Rösch, F., Stöcklin, G., Lueders, C., Qaim, S. M., Feinendegen, L. E.: Measurement of pharmacokinetics of yttrium-86 radiopharmaceuticals with PET and radiation dose calculation of analogous yttrium-90 radiotherapeutics. *J Nucl Med* 1993; 34; 2222-6.
3. Nayak, T. K., Brechbiel, M. W. ^{86}Y based PET radiopharmaceuticals: radiochemistry and biological applications. *Med Chem* 2011; 7(5); 380-8.
4. Cai, W., et al., Quantitative PET of EGFR expression in xenograf bearing mice using ^{64}Cu-labeled cetuximab, a chimeric anti-EGFR monoclonal antibody. *Eur J Nucl Med Mol Imaging* 2007; 34; 850–58.
5. Anderson, C. J., Ferdani, R. Copper-64 radiopharmaceuticals for PET imaging of cancer: advances in preclinical and clinical research. *Cancer Biother Radiopharm* 2009; 24(4); 379-93.
6. Tolmachev, V. Radiobromine-labelled tracers for positron emission tomography: possibilities and pitfalls. *Curr Radiopharm* 2011; 4(2); 76-89.
7. Wadas, T. J., Wong, E. H., Weisman, G. R., Anderson, C. J. Copper chelation chemistry and its role in copper radiopharmaceuticals. *Curr Pharm Des* 2007; 13(1); 3-16.
8. Anderson, C. J., Wadas, T. J., Wong, E. H., Weisman, G. R. Cross-bridged macrocyclic chelators for stable complexation of copper radionuclides for PET imaging. *Q J Nucl Med Mol Imaging* 2008; 52(2); 185-92.
9. Walrand, S., Flux, G. D., Konijnenberg, M. W., Valkema, R., Krenning, E. P., Lhommel, R., Pauwels, S., Jamar, F. Dosimetry of yttrium-labelled radiopharmaceuticals for internal therapy: ^{86}Y or ^{90}Y imaging? *Eur J Nucl Med Mol Imaging* 2011; 38(1); 57-68.
10. Busse, S., Rösch, F., Qaim, S. M.: Cross section data for the production of the positron emitting niobium isotope ^{90}Nb *via* the ^{90}Zr(*p, n*)-reaction. *Radiochim Acta* 2002; 90; 1-5.

11. Nayak, T. K., Brechbiel, M. W.: Radioimmunoimaging with longer-lived positron-emitting radionuclides: potentials and challenges. *Bioconj Chem* 2009; 20; 825-841.

12. Verel, I., Visser, G. W. M., Boellaard, R., van Walsum, S. M., Snow, G. B., van Dongen, G. A. M. S. ^{89}Zr *immuno*-PET: comprehensive procedures for the production of ^{89}Zr-labeled monoclonal antibodies. *J Nucl Med* 2003; 44; 1271-81.

13. Vosjan, M. J. W. D., Perk, L. R., Visser, G. V. M., Budde M., Jurek, P., Kiefer, G. E., van Dongen, G. A. M. S.: Conjugation and radiolabeling of monoclonal antibodies with zirconium-89 for PET imaging using the bifunctional chelate *p*-isothiocyanatobenzyl-desferrioxamine. *Nature Protocols* 2010; 5(4); 739-43.

14. Nagengast, W. B., de Vries, E. G., Hospers, G. A., Mulder, N. H., de Jong, J. R., Hollema, H., Brouwers, A. H., van Dongen, G. A., Perk, L. R., Lub-de Hooge, M. N. In vivo VEGF imaging with radiolabeled bevacizumab in a human ovarian tumor xenograft. *J Nucl Med* 2007; 48(8); 1313-9.

15. Holland, J. P., Divilov, V., Bander, N. H., Smith-Jones, P. M., Larson, S. M., Lewis, J. S. ^{89}Zr-DFO-J591 for *immuno*PET of prostate-specific membrane antigen expression *in vivo. J Nucl Med* 2010; 51(8); 1293-300.

16. Abou, D. S., Ku, T., Smith-Jones, P. M. *In vivo* biodistribution and accumulation of ^{89}Zr in mice. *Nucl Med Biol* 2011; 38(5); 675-81.

17. Vosjan, M. J., Perk, L. R., Roovers, R. C., Visser, G. W., Stigter-van Walsum, M., van Bergen En, Henegouwen, P. M., van Dongen, G. A. Facile labelling of an anti-epidermal growth factor receptor Nanobody with ^{68}Ga via a novel bifunctional desferal chelate for immuno-PET. *Eur J Nucl Med Mol Imaging* 2011; 38(4); 753-63.

5. Appendices

5.1 Abbreviations

immuno-PET immuno positron emission tomography
Mw weight average molecular weight
NMR Nuclear Magnetic Resonance
mAb monoclonal antibody
Df desferrioxamine
OI optical imaging
d day
DMSO dimethyl sulfoxide
SPECT single photon emission computed tomography
g gram
RCY radiochemical yield
HPLC high pressure liquid chromatography
sec second
SEC size exclusion chromatography
kDa kilo Dalton
SPECT single photon emission computed tomography
MBq megabequerel
TLC thin layer chromatography
min minute
MRI magnetic resonance imaging
NaCl sodium chloride
CT computed tomography
BFC bifunctional chelator
MI molecular imaging
US ultra sound
PBS phosphate buffered saline
PET positron emission tomography
FCS fetal calf serum
GBq gigabequerel
h hour
HSA human serum albumin
ID injected dose
kBq kilobequerel
L liter
M molar
MeCN acetonitrile
MeOH methanol
μPET small animal PET

5.2 Curriculum Vitae

Personal dates:

Name: Radchenko Valery

Date of birth: 8th of July 1984

Marital status: married (one son)

Place of birth: Penzenskaya obl. (Russian Federation)

Nationality: Russian

Education:

02/2008 PhD studies at the Institute of Nuclear Chemistry, Johannes Gutenberg University of Mainz, Germany

09/2001-02/2007 Sankt-Petersburg University of Technology, MSc. in Chemical Technology of modern energetic materials, Russian Federation
(Graduation work: excellent)

09/1998-07/2001 Gymnasium specialization “Chemistry and Biology”, Sankt- Petersburg, Russian Federation

Employment history:

02/2007-02/2008 Assistant in Laboratory of Nuclear Problems, Join Institute of Nuclear Research, Dubna, Russian Federation

SKILLS:

Particularly knowledge and experience in:

- Radiochemistry of metallic and semi-metallic radionuclides.
- Wide spectrum of separation and purification methods such as ion-ecxchange chromatography, extraction, precipitation, distillation.
- Modification of biomolecules such as antibodies, antibody fragments and peptides for follow labeling with radionuclides.
- Labeling of biomolecules with different radionuclides such as ^{90}Nb, ^{74,72}As, ^{89}Zr, ^{68}Ga and ^{44}Sc with main focus on *immuno-PET.*
- *In vitro* and *in vivo* evaluation of labeled biomolecules.
- Proteomics and radioiodine-labeling (^{125}I and ^{131}I) of proteins.

Teaching experience:

10/2008 - 06/2012 Manager of nuclear chemistry seminars at Johannes Gutenberg University Mainz, Germany

Invited talks

01/2011 Invited Lecture "Base of the molecular imaging", State University of Technology Sankt-Petersburg, Russian Federation

10/2012 Invited talk "Alternative rapid separation strategy for isolation of no-carrier added ^{90}Nb from Zr target, for application in *immuno*-PET", Triskem user meeting, Munich, Germany

12/2012 Invited Lecture "Base of the nuclear medicine", Joint Institute for Nuclear Research (JINR), Dubna, Russian Federation

12/2012 Invited Seminar at Dzelepov Laboratory of Nuclear Problem, Joint Institute for Nuclear Research, Dubna, Russian Federation

Contributed talks/presentations (selected):

- International Symposium on Radiopharmaceutical Sciences (ISRS) 2011, Amsterdam, the Netherlands

Radchenko V., Busse S., Hauser H., Eisenhut M., Vugts D., van Dongen G. A. M. S., Roesch F. Procedures for the production of ^{90}Nb-labeled monoclonal antibodies and stability studies (oral)

Radchenko V., Vugts D., van Dongen G. A. M. S., Wozny W., Schrattenholz A., Roesch F. Labeling of neuroregulin 1 β extracellular domain with ^{89}Zr and stability studies (poster)

Radchenko V., Jahn M., Filosofov D. V., Hauser H., Eisenhut M., Jennewein M., Rösch F., Development of alternative methods for separation and purification of no-carrier-added arsenic-77/72/74 from bulk amounts of natural germanium (poster)

- Annual Meeting Society of Nuclear Medicine (SNM) 2012 Miami Beach, FL, USA

Radchenko V., Filosofov D. V., Bochko O. K., Lebedev, Roesch F.: Alternative rapid separation strategy for isolation of no-carrier added ^{90}Nb from Zr target, for application in *immuno*-PET (oral)

Radchenko V., Roesch F. Evaluation of an appropriate chelator for ^{90}Nb and *in vitro* stability studies of ^{95} Nb-desferrioxamine complexes (poster)

Jahn M., Radchenko V., Hauser H., Eisenhut M., Rösch F. and Jennewein M. Separation of nca ^{77}As from reactor irradiated Ge dioxide targets via liquid-liquid extraction and HBr and subsequent labeling of monoclonal antibodies

Languages:

English –advance (certificate University of Mainz (B2))

German –advance (certificate University of Mainz (C2))

Russian -mother language

French –basic (School and University program (good))

Contact details:

Address: Eichendorffstrasse 51-53, 55122, Mainz, Germany
email: radchenk@uni-mainz.de
phone: +49 6131 392 5319
Fax: +49 6131 392 4692

5.3 List of Publications

Peer reviewed:

1. Radchenko, V., Hauser, H., Eisenhut, M., Vugts, J. D., van Dongen, G. A. M. S., Roesch, F. ^{90}Nb – a Potential PET Nuclide: Production and Labeling of Monoclonal Antibodies. *Radiohim Acta* 2012; 100(11); 857-65.
2. Jahn, M., Radchenko V., Filosofov, D. V.,Hauser H., Eisenhut M., Roesch, F. and Jennewein, M. Separation and purification of no-carrier-added arsenic from bulk amounts of germanium for use in radiopharmaceutical labelling. *Radiochim Acta* 2010; 98(12); 807-12.
3. Inoyatov, A. Kh., Perevoshchikov, L. L., Gorozhankin, V. M., Kovalik, A., Radchenko, V. I., Filosofov D. V. Searching for influence of the "atomic structure effect" on the KLL and LMM Auger transition energies of Zn (Z = 30) and Gd (Z = 64) *J El Spectr Rel Phen* 2011; 184: 457-62.
4. Aksenov, N. V., Bozhikov, G. A., Starodub, G. Ya., Dmitriev, S. N., Filosofov, D. V., Sun, J. J., Radchenko, V. I., Lebedev, N. A., Novgorodov, A. F. Anion Exchange Behavior of Ti, Zr, Hf, Nb and Ta as Homologues of Rf And Db In Mixed HF-acetone solutions. Preprint of the Joint Institute for Nuclear Research. Dubna (2009)

In preparation:

1. Radchenko, V., Filosofov, D. V., Bochko, O. K., Lebedev, N. A., Rakhimov, A., Aksenov, N. V., Bozhikov, G. A., Roesch, F.: Rapid strategy for separation of no-carrier-added ^{90}Nb from zirconium target for application in *immuno*-PET. in preparation for submission to *Radiocm Acta* (2013)

2. Radchenko V., Busse S., Roesch F. Desferrioxamine as an appropriate chelator for ^{90}Nb: Comparison of its complexation proprieties for M-Df-Octreotide (M = Nb, Fe, Ga, Zr). submitted *J Nucl Med Biol* (2013)
3. Radchenko, V., Filosofov, D. V, Dadakhanov, J., Roesch, F. Direct flow separation strategy, to isolate no-carrier-added ^{90}Nb from irradiated Mo or Zr target in preparation (2013)
4. Radchenko, V., Bouziotis, P., Loudos, G., Xanthopoulos, S., Roesch, F. Conjugation, labeling and initial *in vivo* assessment of an anti-VEGF monoclonal antibody labeled with Niobium isotopes. in preparation (2013).
5. Radchenko, V., Jahn, M., Hauser, H., Eisenhut, M., Roesch, F., Jennewein, M. Separation of no-carrier-added ^{77}As from reactor irradiated GeO_2 target via liquid-liquid extraction and HBr and subsequent labeling of monoclonal antibodies. in preparation (2013)

Conferences proceedings:

1. Radchenko, V., Busse, S., Hauser, H., Eisenhut, M., Vugts, D., van Dongen, G. A. M. S., Roesch, F. Procedures for the production of ^{90}Nb-labeled monoclonal antibodies and stability studies. J. Label. Compd. Radiopharm. 2011; 54 supp. 1: 16.
2. Radchenko, V., Filosofov, D. V., Bochko, O. K., Lebedev, N. A., Roesch F.Alternative rapid separation strategy for isolation of no-carrier added ^{90}Nb from Zr target, for application in *immuno*-PET. J. Nucl. Med. 2012; 53 Suppl. 1: 135.
3. Radchenko, V., Roesch, F. Evaluation of an appropriate chelator for ^{90}Nb and *in vitro* stability studies of ^{95} Nb-desferrioxamine complexes. J. Nucl. Med. 2012; 53 Suppl. 1: 1454.
4. Radchenko, V., Bouziotis, P., Loudos, G., Xanthopoulos, S., Roesch, F. Conjugation, labeling and initial *in vivo* assessment of an anti-VEGF monoclonal antibody labeled with Niobium isotopes. 2011; abstract final COST D38 meeting, Oxford (UK).

5. Radchenko, V., Vugts, D., van Dongen, G. A. M. S., Wozny, W., Schrattenholz A., Roesch F. Labeling of neuroregulin 1 β extracellular domain with ^{89}Zr and stability studies. J Label. Compd. Radiopharm. 2011; 54 supp. 1: 360.

6. Radchenko, V., Jahn, M., Filosofov, D. V., Hauser, H., Eisenhut, M., Jennewein, M., Roesch, F., Development of alternative methods for separation and purification of no-carrier-added arsenic-77/72/74 from bulk amounts of natural germanium. J Label. Compd. Radiopharm. 2011; 54 supp. 1: 361.

7. Jahn, M., Radchenko, V., Hauser, H., Eisenhut, M., Roesch, F. and Jennewein, M. Separation of nca ^{77}As from reactor irradiated Ge dioxide targets via liquid-liquid extraction and HBr and subsequent labeling of monoclonal antibodies. J. Nucl. Med. 2012; 53 Suppl. 1: 1453.

8. Aksenov, N. V., Bozhikov, G. A., Starodub, G. Ya., Dmitriev, S. N., Filosofov, D. V., Sun, J. J., Radchenko, V. I.; Lebedev, N. A.; Novgorodov, A. F. Anion Exchange Behavior of Ti, Zr, Hf, Nb and Ta as Homologues of Rf And Db In Mixed HF-acetone solutions. INTERNATIONAL SYMPOSIUM ON EXOTIC NUCLEI. AIP Conference Proceedings. 2010; 1224: 279-84.